Chapter 4
Massive Stars and Their Supernovae

Friedrich-Karl Thielemann, Roland Diehl, Alexander Heger, Raphael Hirschi, and Matthias Liebendörfer

Stars more massive than about 8–10 solar masses evolve differently from their lower-mass counterparts: nuclear energy liberation is possible at higher temperatures and densities, due to gravitational contraction caused by such high masses, until forming an iron core that ends this stellar evolution. The star collapses thereafter, as insufficient pressure support exists when energy release stops due to Fe/Ni possessing the highest nuclear binding per nucleon, and this implosion turns into either a supernova explosion or a compact black hole remnant object. Neutron stars are the likely compact-star remnants after supernova explosions for a certain stellar mass range. In this chapter, we discuss this late-phase evolution of massive stars and their core collapse, including the nuclear reactions and nucleosynthesis products. We also include in this discussion more exotic outcomes, such as magnetic

F.-K. Thielemann (✉)
Department of Physics, University of Basel, Basel, Switzerland
GSI Helmholtz Center for Heavy Ion Research, Darmstadt, Germany
e-mail: f-k.thielemann@unibas.ch

R. Diehl
Max Planck Institut für extraterrestrische Physik, Excellence Cluster 'Universe', Garching, Germany
e-mail: rod@mpe.mpg.de

A. Heger
Monash Centre for Astrophysics, School of Physics and Astronomy, Monash University, Clayton, VIC, Australia
Tsung-Dao Lee Institute, Shanghai, China

R. Hirschi
University of Keele, Keele, UK
e-mail: r.hirschi@keele.ac.uk

M. Liebendörfer
Department of Physics, University of Basel, Basel, Switzerland
e-mail: matthias.liebendoerfer@unibas.ch

R. Diehl et al. (eds.), *Astrophysics with Radioactive Isotopes*, Astrophysics and Space Science Library 453, https://doi.org/10.1007/978-3-319-91929-4_4

jet supernovae, hypernovae, gamma-ray bursts and neutron star mergers. In all cases we emphasize the viewpoint with respect to the role of radioactivities.

4.1 The Cosmic Significance of Massive Stars

Our understanding of stellar evolution and the final explosive endpoints such as supernovae or hypernovae or gamma-ray bursts relies on the combination of

(a) (magneto-) hydrodynamics
(b) nuclear reactions releasing energy and leading to changes of composition
(c) radiation transport
(d) thermodynamic properties (such as the equation of state of stellar matter).

Hydrodynamics is essentially embedded within the numerical schemes which implement the physics of processes (b)–(d). In early phases of stellar evolution, hydrodynamical processes can be approximated by a hydro*static* treatment. Nuclear energy production (b) includes all nuclear reactions triggered during stellar evolution and explosive end stages, also among unstable isotopes produced on the way. Radiation transport (c) covers atomic physics (e.g. opacities) for photon transport, but also nuclear physics and neutrino nucleon/nucleus interactions in late phases and core collapse. The thermodynamical treatment (d) addresses the mixture of *ideal gases* of (massless) photons, electrons/positrons and nuclei/ions. These are fermions and bosons, and in dilute media or at high temperatures the energies of non-massless particles can often be approximated by Maxwell-Boltzmann distributions. At very high densities, the *nuclear* equation of state is required for the relation between pressure, density, temperature, entropy, energy density, composition, etc... It exhibits a complex behavior, with transitions from individual nuclei to clusters of nucleons with a background neutron bath, homogeneous phases of nucleons, the emergence of hyperons and pions up to a possible hadron-quark phase transition.

The detailed treatment of all these ingredients and their combined application is discussed in more depth in textbooks (Kippenhahn and Weigert 1994; Maeder 2009; Arnett 1996; Iliadis 2007; Jose 2016; Branch and Wheeler 2017), and/or the preceding Chap. 3, where the evolution of low and intermediate mass stars is addressed. That chapter also includes the stellar structure equations in spherical symmetry and a discussion of opacities for photon transport. Chapters 8 and 9 (tools for modeling objects and their processes) go into more detail with regard to modeling hydro*dynamics*, (convective) instabilities and energy transport as well as the energy generation due to nuclear reactions and the determination of the latter. Here we want to focus on the astrophysical aspects, i.e. a description of the evolution of massive stars and their endpoints with a special emphasis on the composition of their ejecta (in their forms of stellar winds during the evolution, or of the explosive ejecta). This includes also aspects of metallicity, rotation, and binary evolution (see e.g. Eldridge et al. 2008; Langer 2012; Maeder and Meynet 2012; Yoon 2015; De Marco and Izzard 2017; Moe and Di Stefano 2017; Meynet and Maeder 2017).

Low and intermediate mass stars end their evolution as AGB stars, finally blowing off a planetary nebula via wind losses and leaving a white dwarf with an unburned C and O composition (see e.g. Karakas and Lattanzio 2014). In the range of 8–10 $M_\odot$, stars also undergo C-burning, but collapse due to electron capture on C-burning products in the O-Ne-Mg core, resulting in fast contraction and the formation of an Fe-core during collapse which causes finally supernova explosions, dubbed electron capture (EC) supernovae (Kitaura et al. 2006; Wanajo et al. 2009, 2011; Hüdepohl et al. 2010; Jones et al. 2013, 2016; Moriya et al. 2014; Woosley and Heger 2015b; Müller et al. 2017).

More massive stars in the mass range 10–90 $M_\odot$ evolve beyond further and experience all stellar burning stages from H over He, C, Ne, O and Si-burning, up to core collapse and explosive end stages. A major question is how the transition occurs from "regular" core-collapse supernovae (CCSNe), producing neutron stars, to the formation of a central black hole. This depends strongly on the properties of the stellar progenitor, among other properties the compactness, i.e. the central mass concentration is important (Heger and Woosley 2010; Chieffi and Limongi 2013; Karakas and Lattanzio 2014; Sukhbold et al. 2016; Ebinger et al. 2017, 2018; Nakamura et al. 2015; Pan et al. 2017). In case of fast rotation and strong magnetic fields so-called hypernovae/collapsars/long duration gamma-ray bursts (GRBs) possibly occur after black hole formation, otherwise this leads to a failed or faint supernova and "quiet" black hole formation. For the nucleosynthesis in GRBs/hypernovae, aspherical explosions are important. This is also the case if fast rotation and strong magnetic fields are present in core collapse, leading, however, finally to a central neutron star with magnetic fields as high as 10^{15} G, known as magnetar (Winteler et al. 2012; Mösta et al. 2014, 2015, 2017; Nishimura et al. 2015, 2017b; Halevi and Mösta 2018).

90–140 $M_\odot$ stars undergo pulsational nuclear instabilities at various nuclear burning stages, including O and Si-burning. 140–300 $M_\odot$ stars become pair-instability supernovae, if the mass loss is small enough to permit this final endstage. Very massive stars greater than 300 $M_\odot$ undergo core-collapse to form intermediate mass black holes. Detailed reviews and recent findings on the present understanding of end stages of such massive stars are given e.g. in Heger and Woosley (2010), Kasen et al. (2011), Nomoto et al. (2010, 2013), Woosley and Heger (2015a), and Georgy et al. (2017).

In this chapter we want to discuss the nucleosynthesis processes involved in massive stars and their explosions and the related production of radioactive nuclei[1] in more detail. This includes all hydrostatic nuclear-burning stages experienced by massive stars, the explosive burning stages when a shock wave moves outward after a successful explosion was initiated, and also final wind ejecta from the hot proto-neutron star which emerged in the collapse and explosion phase. All these ejecta

[1]We focus especially on long-lived radioactivities which can be observed with gamma-ray satellites, and refractory isotopes which can be observed in dust condensations included in meteorites.

will enter the interstellar medium in galaxies, initially appearing as gas and dust in wind bubbles and supernova remnants, later determining the evolution of the larger-scale gas composition. The interstellar gas composition will evolve with time, and the composition of newly formed stars will witness this composition at the time of their formation.

Massive stars play an important role as contributors to the gas composition of the interstellar medium via wind losses and/or explosions. In astronomical/observational terms they are the progenitors of blue supergiants (BSG), red supergiants (RSG), Wolf-Rayet (WR) and luminous blue variable (LBV) stars (Maeder and Meynet 2012) At the end of their life, they explode as core collapse supernovae (SNe), observed as SNe of type II or Ib,c (Woosley and Bloom 2006; Branch and Wheeler 2017) and also as long soft gamma-ray bursts (GRBs Piran 2004; Nakar and Piran 2017). After collapse, their cores become neutron stars or black holes. They are one of the main sites for nucleosynthesis, which takes place during both pre-SN (hydrostatic) burning stages and during explosive burning.

Neutron capture processes are mainly responsible for the heavy nuclei beyond the Fe-group, existing in the variety of a slow (s) and a rapid (r) process. A weak s-process occurs during core He-(and C-)burning (The et al. 2007; El Eid et al. 2009; Nishimura et al. 2017a), which can in case of fast rotation also be more powerful (Frischknecht et al. 2016). In past years it was also expected that an r-process occurs during the explosion (Woosley et al. 1994; Qian and Woosley 1996), but recent studies (essentially due to the neutrino interaction with the innermost ejecta, see e.g. Arcones and Thielemann 2013) indicate that only a weak r-process takes place in regular supernovae while a strong one might emerge in magnetar-producing supernovae (Winteler et al. 2012; Nishimura et al. 2017b; Halevi and Mösta 2018). A further option is the aftermath of two supernovae in binary systems, leading to neutron star mergers (see e.g. Thielemann et al. 2017b; Metzger 2017a), especially after the recent detection of GW170817 (Metzger 2017b).

Radioactive isotopes such as ^{26}Al and ^{60}Fe detected by the INTEGRAL (Diehl et al. 1997, 2006a,b; Wang et al. 2009) satellite are produced by massive stars (see e.g. Limongi and Chieffi 2006b), plus many more radioactivities from the final explosive ejecta (such as ^{44}Ti, ^{56}Ni, ^{56}Co etc., see Sect. 4.5.2 for more details). Chaps. 2 and 3 discussed also many long-lived heavy nuclei beyond Fe with half-lives larger than 10^7 and up to 10^{11}y. As massive stars are probably not the major origin of heavy s-process nuclei (see Chap. 3), we will address here those of these nuclei which are clearly identified with the r-process (^{232}Th, 1.4×10^{10} years, ^{235}U, 7×10^8 years, ^{236}U, 2.3×10^7 years, ^{238}U, 4.5×10^9 years, ^{244}Pu, 8×10^7 years, ^{247}Cm, 1.6×10^7 years) and where especially ^{232}Th and ^{238}U, with half-lives comparable to the age of the Galaxy/Universe, can also serve as chronometers (Cowan et al. 1999; Cayrel et al. 2001; Thielemann et al. 2002; Mashonkina et al. 2014)

Massive stars contribute significantly (about two thirds) to the integrated luminosity of galaxies, even though they are much less numerous than low mass stars. At high redshifts z, or low metallicities Z, they are even more important as drivers of characteristic phenomena and evolution. The first stars formed are

thought to be all massive or even very massive (Karlsson et al. 2013), and to be the cause of the re-ionisation of the universe. As discussed above, if the final core collapse leads to a black hole, the endpoint of this evolution can be the origin of the subset of (long, soft) gamma ray bursts (GRBs). GRBs can be used as new *standard candles* for cosmology at high redshifts, as they are visible from higher redshifts than usual SNe (of type I or II), and thus broaden the base to constrain cosmological models. Massive stars with their large energy output can be seen out to significant (cosmological) distances—either directly through their thermal photospheric emission, or indirectly through the impact on their surroundings (ionization, or heated dust). In their *collapsar* and GRB extremes, emission is beamed into a jet (Nakar and Piran 2017), which makes them visible even at greater distances. This can also give us information on the star formation history at a very early age of the universe ($z > 10$) beyond the reach of galaxy observations. Closer to home, recent surveys of metal poor halo stars provide a rich variety of constraints for the early chemical evolution of our Galaxy and thus the nucleosynthesis ejecta (see e.g. Nomoto et al. 2013) (*astro-archeology*).

4.2 Hydrostatic and Explosive Burning

Following this motivation for studying the evolution, final fate, and remnant aspects of massive stars (previous section), we now discuss the ingredients for modeling each of these aspects. Thermonuclear energy generation is one of the key processes: It shapes the interior structure of the star, thus its evolutionary time scales, and the generation of new chemical elements with their isotopes. Without understanding this, the *feedback* from massive stars as it determines the evolution of galaxies cannot be understood in astrophysical terms.[2] Thermonuclear burning, nuclear energy generation, and the resulting nuclear abundances are determined by thermonuclear and by weak interactions. The treatment of the required nuclear and plasma physics, and a detailed technical description of reaction rates, their determination, and the essential features of composition changes and reaction networks are presented in Chap. 9. Here we discuss the types of reactions that are specific to the evolution of massive stars, their collapse stage, and the compact remnants.

Nuclear burning can in general be placed into two categories:

1. hydrostatic burning stages on timescales dictated by stellar energy loss
2. explosive burning in a specific highly-dynamic event (collapse, explosion, compact-star collision).

Massive stars (as opposed to low and intermediate mass stars) experience explosive burning (2) as a natural outcome at the end of their evolution. They also undergo

[2]Empirical descriptions derived from observations of a multitude of galaxies are often used in cosmological simulations, as a substitute to such astrophysical models.

more extended hydrostatic burning stages (1) than their low- and intermediate-mass cousins. Therefore, we first address some aspects of these nuclear burnings in a general way, before describing evolution and explosions in more detail.

Nuclear burning and the resulting composition changes (i.e. nucleosynthesis) are fundamentally characterised by (1) strong interactions (hadron reactions) and photo-disintegrations, (2) weak interactions characterised by decay half-lives of electron or positron emissions and captures, and (3) neutrino-induced reactions. These will be discussed in the following sections.[3]

4.2.1 Nuclear Burning During Hydrostatic Evolution

Hydrostatic burning stages are characterised by temperature thresholds, above which thermal Maxwell-Boltzmann distributions of (charged) particles (nuclei) to penetrate increasingly larger Coulomb barriers of electrostatic repulsion. These are (two body) reactions as discussed in Eqs. (9.6) and (9.10) of Chap. 9, representing terms of the type ${}_ir_j$ in the network equation (9.1). H-burning converts ^{1}H into ^{4}He via pp-chains or the CNO-cycles. The simplest pp-chain is initiated by ^{1}H(p,$e^+\nu$)^{2}H(p,γ)^{3}He and completed by ^{3}He(^{3}He,2p)^{4}He. The dominant CNO-cycle chain ^{12}C(p,γ)^{13}N($e^+\nu$)^{13}C(p,γ)^{14}N(p,γ)^{15}O($e^+\nu$)^{15}N(p,α)^{12}C is controlled by the slowest reaction ^{14}N(p,γ)^{15}O. Thus, the important ashes of H-burning are ^{4}He and (metallicity-dependent, as acting on prior existing ^{12}C) ^{14}N.

The major reactions in He-burning are the triple-alpha reaction ^{4}He(2α, γ)^{12}C and ^{12}C(α, γ)^{16}O. The triple-alpha reaction, is essentially a sequence of two-body reactions with an extremely short-lived intermediate nucleus ^{8}Be. It is thus an example for the term ${}_i\hat{r}_j$ in Eq. (9.1) in Chap. 9, which includes the product of three abundances. The other H-burning product ^{14}N is processed to ^{22}Ne via ^{14}N(α, γ)^{18}F(β^+)^{18}O(α, γ) and can act as a neutron source for the s-capture process via ^{22}Ne(α, n)^{25}Mg.

The H- and He-burning stages are encountered in massive as well as in low and intermediate mass stars, the latter leaving white dwarfs as central objects. Mixing instabilities between the H- and He-burning zone can mix ^{12}C into proton-rich environments, causing the production of ^{13}C via ^{12}C(p, γ)^{13}N(β^+)^{13}C and in further CNO-type processing also ^{14}N. When being mixed back into He-rich environments they can act as the known neutron source ^{22}Ne (discussed above) and as well as via the reaction ^{13}C(α, n)^{16}O. The first one is important for massive stars, causing in case of rotation-induced mixing instabilities also the production of ^{14}N as a primary (not metallicity-dependent) neutron source (see e.g. Frischknecht et al. 2016). ^{13}C acts via He-shell flashes as the neutron source for the main s-

[3] A review of the sources for this microphysics input is given for (1) in Chap. 9 and for (3) in Chap. 8. We will review some of the required weak interaction rates (2) in the subsections on late phases of stellar evolution/core collapse and the description of the explosion.

Table 4.1 Burning stages of a $20\,M_\odot$ star

Fuel	ρ_c (g cm^{-3})	T_c (10^9 K)	τ (Years)	L_{phot} (erg s^{-1})
Hydrogen	5.6(0)	0.04	1.0(7)	2.7(38)
Helium	9.4(2)	0.19	9.5(5)	5.3(38)
Carbon	2.7(5)	0.81	3.0(2)	4.3(38)
Neon	4.0(6)	1.70	3.8(−1)	4.4(38)
Oxygen	6.0(6)	2.10	5.0(−1)	4.4(38)
Silicon	4.9(7)	3.70	2 days (2)	4.4(38)

Table 4.2 Major reactions in carbon burning

(a) Basic energy generation
$^{12}C(^{12}C,\alpha)^{20}Ne$ $^{12}C(^{12}C,p)^{23}Na$
$^{23}Na(p,\alpha)^{20}Ne$ $^{23}Na(p,\gamma)^{24}Mg$ $^{12}C(\alpha,\gamma)^{16}O$
(b) Fluxes $> 10^{-2}\times$*(a)*
$^{20}Ne(\alpha,\gamma)^{24}Mg$ $^{23}Na(\alpha,p)^{26}Mg(p,\gamma)^{27}Al$
$^{20}Ne(n,\gamma)^{21}Ne(p,\gamma)^{22}Na\ (e^+\nu)^{22}Ne(\alpha,n)^{25}Mg(n,\gamma)^{26}Mg$
$^{21}Ne(\alpha,n)^{24}Mg$ $^{22}Ne(p,\gamma)^{23}Na$ $^{25}Mg(p,\gamma)^{26}Al(e^+\nu)^{26}Mg$
(c) Low temperature, high density burning
$^{12}C(p,\gamma)^{13}N(e^+\nu)^{13}C(\alpha,n)^{16}O(\alpha,\gamma)^{20}Ne$
$^{24}Mg(p,\gamma)^{25}Al(e^+\nu)^{25}Mg$
$^{21}Ne(n,\gamma)^{22}Ne(n,\gamma)^{23}Ne(e^-\bar{\nu})^{23}Na(n,\gamma)^{24}Na(e^-\nu)^{24}Mg$ + s-processing

process in low and intermediate mass stars. They are discussed in much more detail with all minor reaction pathways in Chap. 3. Important features as well as the status of nuclear cross sections involved are discussed in reviews on hydrostatic burning stages (Haxton et al. 2006; Buchmann and Barnes 2006; Costantini et al. 2009; Wiescher et al. 2010; Adelberger et al. 2011; Xu et al. 2013; deBoer et al. 2017; Bao et al. 2000; Dillmann et al. 2006, 2014).

Massive stars, the subject of the present Chapter, undergo further burning stages up to those involving the production of Fe-group nuclei. Table 4.1 lists these burning stages and their typical central densities and temperatures, their duration and luminosity in photons (from Woosley and Weaver 1995; Woosley et al. 2002) (see Sect. 4.3 for more detail).

- *Heavy-ion fusion reactions:* In C-burning the reaction $^{12}C(^{12}C,\alpha)^{20}Ne$ dominates, in O-burning it is $^{16}O(^{16}O,\alpha)^{28}Si$. The corresponding reaction rates ${}_ir_j$ (after integrating over a Maxwell-Boltzmann distribution of targets and projectiles) have the form given in Eq. (9.10) of Chap. 9 and contribute to the second term in Eq. (9.1). Reactions going beyond these key reactions are provided in Tables 4.2 and 4.5. Important uncertainties of nuclear cross sections are discussed in Wiescher et al. (2012) as well as the publicly available reaction libraries Kadonis, JINA Reaclib, Starlib (Dillmann et al. 2014; Cyburt et al. 2010; Sallaska et al. 2013). Extended overviews on available (also theoretical) cross section predictions can be found in the data bases Bruslib, JINA Reaclib, Kadonis,

Table 4.3 Major reactions in neon burning

(a) Basic energy generation
^{20}Ne(γ, α)^{16}O ^{20}Ne(α, γ)^{24}Mg(α, γ)^{28}Si
(b) Fluxes $> 10^{-2}\times$(a)
^{23}Na(p,α)^{20}Ne ^{23}Na(α,p)^{26}Mg(α,n)^{29}Si
^{20}Ne(n,γ)^{21}Ne(α,n)^{24}Mg(n,γ)^{25}Mg(α,n)^{28}Si
^{28}Si(n,γ)^{29}Si(n,γ)^{30}Si
^{24}Mg(α,p)^{27}Al(α,p)^{30}Si
^{26}Mg(p,γ)^{27}Al(n,γ)^{28}Al($e^-\bar{\nu}$)^{28}Si
(c) Low temperature, high density burning
^{22}Ne(α,n)^{25}Mg(n,γ)^{26}Mg(n,γ)^{27}Mg($e^-\bar{\nu}$)^{27}Al
^{22}Ne left from prior neutron-rich carbon burning

and nucastro.org with their websites http://www-astro.ulb.ac.be/bruslib/, https://groups.nscl.msu.edu/jina/reaclib/db/, http://www.kadonis.org/, https://nucastro.org/reaclib.html. Further information is given in Chap. 9.

- *Photo-disintegrations:* The alternative to fusion reactions are photo-disintegrations which start to play a role at sufficiently high temperatures T when $30\,\mathrm{kT} \approx Q$ (the Q-value or energy release of the inverse capture reaction). This ensures the existence of photons with energies $> Q$ in the Planck distribution and leads to Ne-Burning [^{20}Ne(γ, α)^{16}O, ^{20}Ne(α, γ)^{24}Mg] at $T > 1.5 \times 10^9$ K (preceding O-burning), due to a small Q-value of $\approx$4 MeV, and Si-burning at temperatures in excess of 3×10^9 K [initiated like Ne-burning by photo-disintegrations]. Such photo-disintegrations (after integrating over a thermal (Planck) distribution of photons at temperature T) have the form given in Eq. (9.4) of Chap. 9 and act similar to decays with a temperature-dependent decay constant, contributing (like decays) to the first term ${}_i\lambda_j$ in Eq. (9.1). In Table 4.3 we provide some of the main reactions of Ne-burning, which is initiated by the photo-disintegration of Ne.
- *Electron capture reactions:* Massive stellar cores eventually evolve to degeneracy of their electron-gas, i.e. the Pauli exclusion principle for fermions determines the population of energy states, rather than the Boltzmann statistics which applies for lower densities/higher temperatures. The Fermi energy gives a useful estimate, and would be the highest energy occupied at zero temperature from the Pauli exclusion principle of identical electron states; it is (Chandrasekhar 1957)

$$E_F = \hbar^2/2m_e(3\pi^2)^{2/3}n_e^{2/3} \tag{4.1}$$

Here n_e is the density of the electron gas $n_e = \rho N_A Y_e$, ρ denotes the matter density and N_A Avogadro's number. In late stages of O-burning, in Si-burning (and during the later collapse stage) this Fermi energy of (degenerate) electrons increases to the level of nuclear energies (MeVs).In a neutral, completely ionized plasma, the electron abundance Y_e is equal to the total proton abundance $Y_e = \sum_i Z_i Y_i$ (summing over all abundances of nuclei, including protons/hydrogen)

Table 4.4 Electron capture

$p + e^- \rightarrow \nu_e + n$ or $\mathrm{p}(e^-, \nu_e)\mathrm{n}$	
$(A, Z) + e^- \rightarrow \nu_e + (A, Z-1)$ or	$^A\mathrm{Z}(e^-, \nu_e)^A\mathrm{Z\text{-}1}$
$E_F(\rho Y_e = 10^7 \mathrm{gcm}^{-3})$=0.75 MeV	
$E_F(\rho Y_e = 10^9 \mathrm{gcm}^{-3})$=4.70 MeV	

Table 4.5 Major reactions in oxygen burning

(a) Basic energy generation		
$^{16}\mathrm{O}(^{16}\mathrm{O},\alpha)^{28}\mathrm{Si}$	$^{16}\mathrm{O}(^{12}\mathrm{O},\mathrm{p})^{31}\mathrm{P}$	$^{16}\mathrm{O}(^{16}\mathrm{O},\mathrm{n})^{31}\mathrm{S}(e^+\nu)^{31}\mathrm{P}$
$^{31}\mathrm{P}(\mathrm{p},\alpha)^{28}\mathrm{Si}(\alpha,\gamma)^{32}\mathrm{S}$		
$^{28}\mathrm{Si}(\gamma,\alpha)^{24}\mathrm{Mg}(\alpha,\mathrm{p})^{27}\mathrm{Al}(\alpha,\mathrm{p})^{30}\mathrm{Si}$		
$^{32}\mathrm{S}(\mathrm{n},\gamma)^{33}\mathrm{S}(\mathrm{n},\alpha)^{30}\mathrm{Si}(\alpha,\gamma)^{34}\mathrm{S}$		
$^{28}\mathrm{Si}(\mathrm{n},\gamma)^{29}\mathrm{Si}(\alpha,\mathrm{n})^{32}\mathrm{S}(\alpha,\mathrm{p})^{35}\mathrm{Cl}$		
$^{29}\mathrm{Si}(\mathrm{p},\gamma)^{30}\mathrm{P}(e^+\nu)^{30}\mathrm{Si}$		
Electron captures		
$^{33}\mathrm{S}(e^-,\nu)^{33}\mathrm{P}(\mathrm{p},\mathrm{n})^{33}\mathrm{S}$		
$^{35}\mathrm{Cl}(e^-,\nu)^{35}\mathrm{S}(\mathrm{p},\mathrm{n})^{35}\mathrm{Cl}$		
(b) High temperature burning		
$^{32}\mathrm{S}(\alpha,\gamma)^{36}\mathrm{Ar}(\alpha,\mathrm{p})^{39}\mathrm{K}$		
$^{36}\mathrm{Ar}(\mathrm{n},\gamma)^{37}\mathrm{Ar}(e^-,\nu)^{37}\mathrm{Cl}$		
$^{35}\mathrm{Cl}(\gamma,\mathrm{p})^{34}\mathrm{S}(\alpha,\gamma)^{38}\mathrm{Ar}(\mathrm{p},\gamma)^{39}\mathrm{K}(\mathrm{p},\gamma)^{40}\mathrm{Ca}$		
$^{35}\mathrm{Cl}(e^-,\nu)^{35}\mathrm{S}(\gamma,\mathrm{p})^{34}\mathrm{S}$		
$^{38}\mathrm{Ar}(\alpha,\gamma)^{42}\mathrm{Ca}(\alpha,\gamma)^{46}\mathrm{Ti}$		
$^{42}\mathrm{Ca}(\alpha,\mathrm{p})^{45}\mathrm{Sc}(\mathrm{p},\gamma)^{46}\mathrm{Ti}$		
(c) Low temperature, high density burning		
$^{31}\mathrm{P}(e^-,\nu)^{31}\mathrm{S}$	$^{31}\mathrm{P}(\mathrm{n},\gamma)^{32}\mathrm{P}$	
$^{32}\mathrm{S}(e^-,\nu)^{32}\mathrm{P}(\mathrm{p},\mathrm{n})^{32}\mathrm{S}$		
$^{33}\mathrm{P}(\mathrm{p},\alpha)^{30}\mathrm{Si}$		

and limited by the extreme values 0 (only neutrons) and 1 (only protons) with typical values during stellar evolution close to 0.5 or slightly below. Such conditions permit electron captures on protons and nuclei, if the negative Q-value of the reaction can be overcome by the electron (Fermi) energy. The general features for typical conditions are presented in Table 4.4, example reactions were already given in Table 4.5. Thus, at sufficiently high densities, electron captures—which are energetically prohibited— become possible and lead to enhanced *neutronization* of the astrophysical plasma, in addition to the role of beta-decays and electron captures with positive Q-values (Nomoto and Hashimoto 1988; Woosley et al. 2002). In degenerate Ne-O-Mg cores (after core C-burning of stars with $8 < M/\mathrm{M}_\odot < 10$), electron captures on ^{20}Ne and ^{24}Mg cause a loss of pressure support. This introduces a collapse of the core, rather than only a contraction, which compresses all further burning stages on the short time scale of the collapse (Nomoto 1987; Kitaura et al. 2006; Wanajo et al. 2009; Jones et al. 2013). In Si-burning of more massive stars, electron capture on intermediate mass and Fe-group nuclei becomes highly important and determines

Table 4.6 Neutrino reactions

$\nu_e + n \leftrightarrow p + e^-$	or	$\mathrm{n}(\nu_e, e^-)\mathrm{p}$
$\bar{\nu}_e + p \leftrightarrow n + e^+$	or	$\mathrm{p}((\bar{\nu}_e, e^+)\mathrm{n}$
$\nu_e + (Z, A) \leftrightarrow (Z+1, A) + e^-$	or	${}^A\mathrm{Z}(\nu_e, e^-){}^A\mathrm{Z{+}1}$
$\bar{\nu}_e + (Z, A) \leftrightarrow (Z-1, A) + e^+$	or	${}^A\mathrm{Z}(\bar{\nu}_e, e^+){}^A\mathrm{Z{-}1}$
$(Z, A) + \nu \leftrightarrow \nu + (Z, A)^*$		

the neutronization (Y_e) of the central core. As discussed in Chap. 9, these electron captures contribute to the one-body reaction terms ${}_i\lambda_j$ in Eq. (9.1) with the effective decay constants in Eq. (9.5) being a function of T and $n_e = \rho N_A Y_e$, the electron number density, see e.g. Fuller et al. (1980, 1982), Oda et al. (1994), Langanke and Martínez-Pinedo (2001, 2003), Sampaio et al. (2003), Juodagalvis et al. (2010), and Sullivan et al. (2016).

- *Neutrino reactions:* Neutrino reaction cross section on nucleons, nuclei and electrons are minute, by comparison to above reactions, see e.g. Bruenn and Haxton (1991), Langanke and Martínez-Pinedo (2003), Kolbe et al. (2003), and Balasi et al. (2015), and for recent updates Burrows et al. (2018) and references therein. High densities of the order $\rho > 10^{12}\,\mathrm{g\,cm^{-3}}$ are therefore required for the inverse process to electron/positron capture (neutrino capture) to occur at significant rates on the relevant timescales (Table 4.6). The same holds for other processes, such as e.g. inelastic scattering, which leave a nucleus in an excited state that leads to emission of nucleons and alpha particles in exit channels. Such neutrino-induced reactions can be expressed in a similar way as photon and electron captures, integrating now over the corresponding neutrino distribution. The latter is, however, not necessarily in thermal equilibrium, therefore not just a function of temperature and neutrino densities. Neutrino energy distributions are rather the result of a variety of reactions (including scattering) with reaction rates much below those of particle collisions, and determined by (neutrino) radiation transport calculations (see Chap. 8, where also other neutrino scattering processes are discussed).

All the reaction types presented above occur at different times in the sequence of burning stages. They contribute to the three types of terms in the reaction network equation 9.1 of Chap. 9. As an illustration to show how nuclear abundances Y_i enter in this set of equations, it can also be written in the form[4]

[4]The formal difference to Eq. (9.1) is that one does not sum here over the reactions but rather over all reaction partners (see also the equation following Table 3.2 in Chap. 3). However, in total, all the terms which appear are identical. Due to the different summation indices, the P's have a slightly different notation, λ's stand for decay rates L of Chap. 9 and $< j, k >$ for $< \sigma^* v >$ of reactions between nuclei j and k, while $< j, k, l >$ includes a similar expression for three-body reactions (Nomoto et al. 1985). A survey of computational methods to solve nuclear networks is given in (Hix and Thielemann 1999a; Timmes 1999; Hix and Meyer 2006; Lippuner and Roberts 2017). (The abundances Y_i occurring in Eq. (4.2) are related—like electron abundances Y_e—to number densities $n_i = \rho N_A Y_i$ and mass fractions of the corresponding nuclei via $X_i = A_i Y_i$, where A_i is the mass number of nucleus i and $\sum X_i = 1$.)

$$\frac{dY_i}{dt} = \sum_j P^i_j \, \lambda_j Y_j + \sum_{j,k} P^i_{j,k} \, \rho N_A < j,k > Y_j Y_k + \sum_{j,k,l} P^i_{j,k,l} \, \rho^2 N_A^2 < j,k,l > Y_j Y_k Y_l. \quad (4.2)$$

Core Si-burning, the final burning stage during stellar evolution, which is initiated by the photo-disintegration $^{28}\mathrm{Si}(\gamma,\alpha)^{24}\mathrm{Mg}$ close to 3×10^9 K—and followed by a large number of fusion and photo-disintegration reactions—ends with nuclear reactions in a complete *chemical equilibrium*[5] (nuclear statistical equilibrium, NSE) and an abundance distribution centered around Fe (as discussed in Chap. 9 and Eq. (9.13)). These temperatures permit photo-disintegrations with typical Q-values of 8–10 MeV as well as the penetration of Coulomb barriers in capture reaction. In such an NSE the abundance of each nucleus Y_i is only dependent on temperature T, density ρ, its nuclear binding energy B_i, and via charge conservation on $\sum_i Z_i Y_i = Y_e$. Y_e is altered by weak interactions on longer timescales. *Quasi-equilibrium* can occur, if localised nuclear mass regions are in equilibrium with the background of free neutrons, protons and alphas, but offset from other regions of nuclei and thus their NSE values (Hix and Thielemann 1996, 1999b; Hix et al. 2007). Different quasi-equilibrium regions are usually separated from each other by slow reactions with typically small Q-values. Such boundaries between QSE groups, due to slow reactions, can be related to neutron or proton shell closures, like e.g. $Z = N = 20$, separating the Si- and Fe-groups in early phases of Si-burning.

The reactions discussed above occur during all stellar burning stages, and are essentially related to processing of nuclei from H to the Fe-group, but not much beyond. The major reaction sequences shown in the previous tables and the transition to quasi-equilibria and complete NSE have been discussed in detail in Thielemann and Arnett (1985); Woosley et al. (2002); Hix and Thielemann (1996, 1999b); Hix et al. (2007).

- *Neutron captures:* Neutron capture reactions open a chance to produce heavier nuclei also during regular stellar evolution. During core and shell He-burning specific alpha-induced reactions can liberate neutrons, which then are responsible for the slow neutron capture process (s-process). One such major neutron source is the reaction $^{22}\mathrm{Ne}(\alpha,n)^{25}\mathrm{Mg}$, from ^{22}Ne produced via successive α-captures on the products of H-burning in the CNO cycle $^{14}\mathrm{N}(\alpha,\gamma)^{18}\mathrm{F}(\beta^+)^{18}\mathrm{O}(\alpha,\gamma)^{22}\mathrm{Ne}$. If ^{12}C may be mixed into H-burning shells, this can produce an even stronger neutron source from $^{13}\mathrm{C}(\alpha,n)^{16}\mathrm{O}$ via $^{12}\mathrm{C}(p,\gamma)^{13}\mathrm{N}(\beta^+)^{13}\mathrm{C}$. In massive, rotating, low metallicity stars, mixing can lead to the production of "primary" ^{14}N and ^{22}Ne, i.e. a neutron source which does not depend on the initial metallicity of ^{14}N in the CNO-cycle, and can thus be much stronger, in particular at low

[5] All strong (thermonuclear) and photo-disintegration reactions are equilibrated, while weak interaction reactions, changing Y_e, may occur on longer timescales.

metallicity. The previous Chap. 3 discussed in detail the strong s-process via a combination of ^{13}C and ^{22}Ne in He-shell flashes of low and intermediate-mass stars. In a similar way, mixing processes can also occur in massive stars due to rotation or convective instabilities. Without such mixing processes only secondary (metallicity-dependent) ^{22}Ne is available for ^{22}Ne$(\alpha, n)^{25}$Mg and core He-burning as well as shell C-burning lead to a weak s-process (The et al. 2007; Käppeler et al. 2011). The s-process can in principle proceed towards elements up to Pb and Bi through a series of neutron captures and β^--decays, starting on existing heavy nuclei around Fe. Weak s-processing, based on *secondary* ^{22}Ne, does not reach beyond mass numbers of $A = 80$–90. The production of heavier nuclei is possible in massive stars if *primary* ^{14}N and ^{22}Ne are available (Pignatari et al. 2008; Frischknecht et al. 2016)

4.2.2 Nuclear Burning During the Explosion

Many of the hydrostatic nuclear-burning processes occur also under explosive conditions, at higher temperatures and on shorter timescales (see Fig. 4.1). Here, often the β-decay half-lives are longer than the explosive timescales, producing significant abundances of unstable isotopes, as the burning proceeds. This implies that additional knowledge of nuclear reactions for and among unstable nuclei is required. The fuel for explosive nucleosynthesis consists mainly of $N = Z$ nuclei such as ^{12}C, ^{16}O, ^{20}Ne, ^{24}Mg, or ^{28}Si (the ashes of previous hydrostatic burning). The results are heavier nuclei, again with $N \approx Z$. At high densities also electron captures on nuclei $e^- + {}^A Z \rightarrow {}^A (Z\text{-}1) + \nu$ can occur at substantial rates, due to high-energy electrons when Fermi energies are high in the degenerate gas (Fuller et al. 1980, 1982; Oda et al. 1994; Langanke and Martínez-Pinedo 2003; Sampaio et al. 2003; Juodagalvis et al. 2010); this was already discussed above for late hydrostatic burning stages.

Explosive Si-burning is very different than its hydrostatic counterpart. It can be divided into three different regimes: (1) incomplete Si-burning, and complete Si-burning with either (2) a normal (high density, low entropy) or (3) an α-rich (low density, high entropy) freeze-out of charged-particle reactions during cooling from NSE. At high temperatures, or during a *normal* freeze-out, all abundances remain in complete NSE. Then as temperatures and/or densities fall, the NSE can break up into smaller equilibrium clusters (quasi-equilibrium, QSE); for a detailed discussion see Hix and Thielemann (1996, 1999b) and Hix et al. (2007). An example for such QSE-behavior is an alpha-rich freeze-out, caused by the inability of the triple-alpha reaction ^{4}He$(2\alpha, \gamma)^{12}$C, and the ^{4}He$(\alpha\text{n},\gamma)^9$Be reaction to keep light nuclei such as n, p, and ^{4}He, and nuclei beyond $A = 12$ in NSE during declining temperatures, when densities are low. This leads to a large α-particle abundance after freeze-out of nuclear reactions. This effect, most pronounced for core collapse supernovae, depends on the entropy of the reaction environment, entropy being proportional to T^3/ρ in a radiation dominated plasma (see Fig. 4.2).

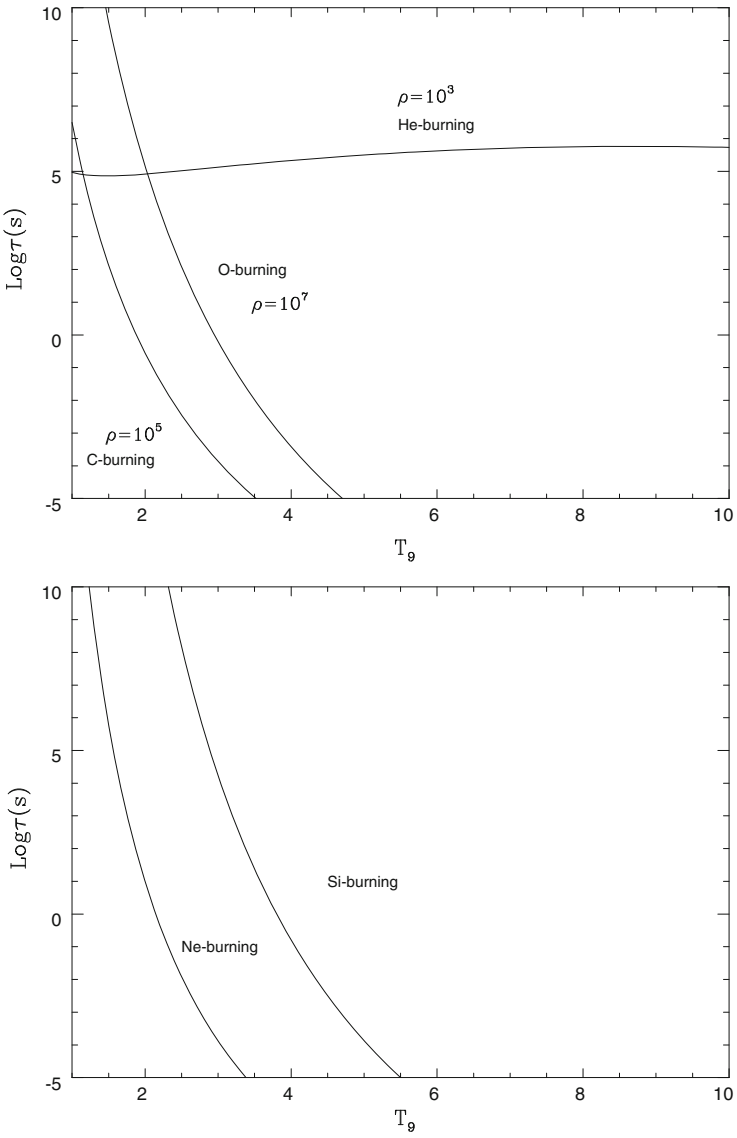

Fig. 4.1 Burning timescales τ in (log_{10}) seconds for fuel exhaustion of He-, C-, and O-burning (top) and Ne- and Si-burning (bottom), as a function of temperature, based on the expressions for dY_i/dt in Eq. (4.2) when equating this to $-1/\tau Y_i$, utilizing $Y_i = X_i/A_i = 1/A_i$ for the burning fuel. Thus, τ has no density dependence for decays and photo-disintegrations, a $1/\rho$ dependence for (two body) fusion reactions, and a $1/\rho^2$ dependence for (three body) fusion reactions. Density-dependent timescales are labeled with a chosen typical density (in g cm^{-3}). They scale with $1/\rho$ for C- and O-burning and $1/\rho^2$ for He-burning. Ne- and Si-burning, initiated by photo-disintegrations, are not density-dependent. The almost constant He-burning timescale beyond $T_9 = T/10^9\text{K} = 1$ permits efficient destruction on explosive timescales only for high densities

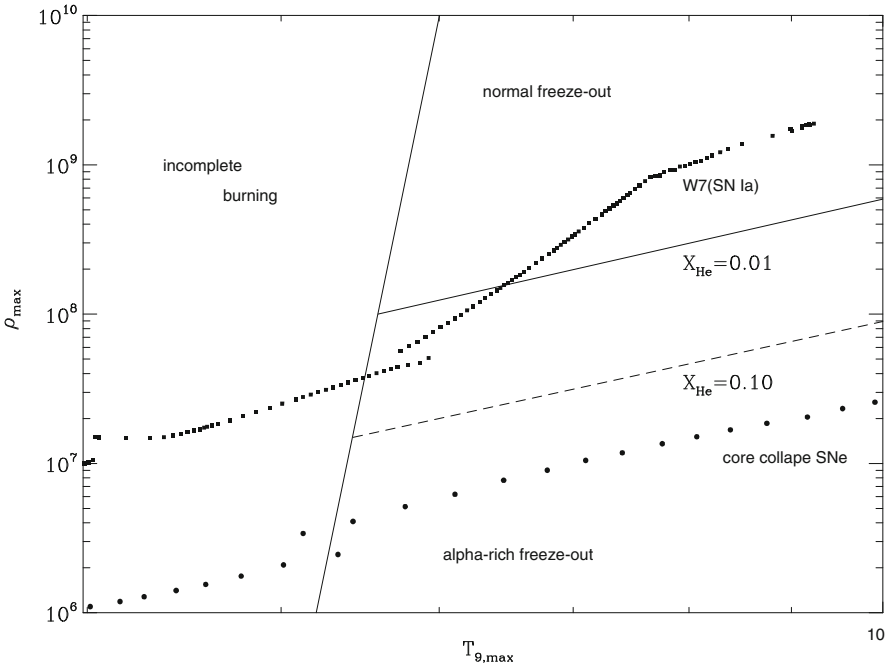

Fig. 4.2 Final results of explosive Si-burning as a function of maximum temperatures and densities attained in explosions before adiabatic expansion. For temperatures in excess of 5×10^9 K any fuel previously existing is photo-disintegrated into nucleons and alpha particles before re-assembling in the expansion. For high densities this is described by a full NSE with an Fe-group composition favouring nuclei with maximum binding energies and proton/nucleon ratios equal to Y_e. For lower densities the NSE breaks into local equilibrium groups (quasi-equilibrium, QSE) with group boundaries determined by reactions with an insufficiently fast reaction stream. Alpha-rich freeze-out (insufficient conversion of alpha-particles into nuclei beyond carbon) is such a QSE-behavior. Lines with 1% and 10% remaining alpha mass fraction are indicated as well as typical conditions in type Ia and core collapse supernovae. This division of the final outcome of explosive Si-burning goes back to Woosley et al. (1973), the type Ia and core-collapse supernova results shown here are taken from Thielemann et al. (1986, 1990) and represent still the current status (in case of type Ia supernovae for single degenerate systems)

Characteristics of the r-process (*rapid* neutron capture) relate to environments of explosive Si-burning as well. The requirement for r-process of a neutron to seed-nuclei ratio of 10 to 150 after freeze-out of charged particle reactions[6] translates into $Y_e = 0.12 - 0.3$ for a normal freeze-out. For a moderate Y_e >0.40, an extremely α-rich freeze-out is needed (see the discussion in Sect. 4.4). Under these conditions the large mass fraction in ^{4}He (with $N = Z$) permits sufficiently high ratios of remaining free neutrons to (small) abundances of heavier seed nuclei, so that r-

[6]Such neutron/seed ratio is required in order to produce all, including the heaviest, r-process nuclei via neutron capture from seed nuclei at their abundances before freeze-out.

process conditions are obtained. During the operation of the r-process, in many cases QSE-groups of neutron captures and photo-disintegrations are formed within the isotopic chains of heavy elements (see e.g. Freiburghaus et al. 1999a; Farouqi et al. 2010).

4.3 Evolution up to Core Collapse

Nuclear burning processes as relevant for massive stars have been discussed above in Sect. 4.2, including also specific individual reactions related to the main focus of this book, the production of (radioactive) nuclei in astrophysical environments. In the present section we will discuss the physics of stellar evolution and major related observational features; but we leave to review articles or textbooks a technical description of how mass, energy, and momentum conservations equations as well as energy transport (via radiation or convective motions) are treated (Maeder 2009; Maeder and Meynet 2012; Woosley et al. 2002; Heger et al. 2003; Limongi et al. 2000; Limongi and Chieffi 2003, 2006b, 2012; Umeda and Nomoto 2008; Ohkubo et al. 2008; El Eid et al. 2009; Paxton et al. 2011) (but see also the hydrostatic stellar structure/evolution equations in spherical symmetry, as presented in Chap. 3). Results of recent calculations are presented in the following subsection.

Massive star evolution is treated by a number of stellar evolution codes, a comparison to observational features has been undertaken by Martins and Palacios (2013) for the codes (MESA,STAREVOLV, GENEC, STERN, Padova, FRANEC). The main codes to follow the evolution through all burning stages until collapse are KEPLER (see e.g. Woosley et al. 2002), GENEC (Eggenberger et al. 2008; Ekström et al. 2012), FRANEC (Limongi and Chieffi 2012), and MESA (Paxton et al. 2011). A detailed comparison between predictions of MESA, KEPLER, and GENEC has recently been proved by Jones et al. (2015). There are differences in treating hydrodynamics/statics, surface layers, rotation and magnetic fields, opacities, mass loss, convection and overshooting, the equation of state, and nuclear reaction input, it is gratifying that there exists a quite good qualitative agreement, but there remain some (minor?) quantitative differences.

In the following we want to focus on results from the KEPLER and GENEC code, addressing topics like (1) adaptive reaction networks for the advanced burning stages, which are capable to follow the detailed evolution of Y_e and a large set of nuclei, (2) a discretization of the stellar-structure equations (and possible damping of instabilities occurring during the advanced stages of evolution, (3) the treatment of dynamical shear in addition to the other mixing processes (such as, e.g., horizontal turbulence, secular shear and meridional circulation), and (4) the treatment of convection/semiconvection, overshoot mixing. Both codes allow to follow the evolution of massive stars from their birth until the stage of Si-burning, including all nuclear burning stages discussed in Sect. 4.2, for a wide range of initial masses, metallicities and stellar rotation.

While there exist also first approaches to treat especially convective stages in multi dimensions (Meakin and Arnett 2007; Arnett et al. 2009; Cristini et al. 2015; Müller et al. 2016b; Edelmann et al. 2017), this can presently only be done for test cases rather than full stellar evolution calculations. Here the treatment of rotation and mixing effects is still based on spherical symmetry.

Finalizing this introduction to the further discussion on the evolution of massive stars, we want to emphasize that there have been many investigations with the FRANEC code (Limongi et al. 2000; Limongi and Chieffi 2003, 2006b, 2009, 2012; Chieffi and Limongi 2013, 2017, 2004), also with emphasis on the production of ^{26}Al, ^{44}Ti, ^{60}Fe, and ^{56}Ni, but in the discussion of the following subsection we summarize results from a large number of publications involving calculations with the KEPLER and GENEC codes (Woosley and Weaver 1995; Woosley et al. 2002; Heger and Woosley 2010, 2002; Heger et al. 2000, 2003, 2005; Woosley and Heger 2007; Jones et al. 2013, 2015, 2016, 2015; Pignatari et al. 2016, 2008; Hirschi et al. 2004, 2005, 2008; Meynet et al. 2008, 2016; Yusof et al. 2013; Georgy et al. 2013, 2017; Maeder et al. 2014; Frischknecht et al. 2016). The main emphasis lies on understanding (a) the composition of wind losses, and (b) the internal structure and composition of stars in their final stage before collapse, setting the stage for subsequent explosions.

4.3.1 Complexities of Post-Main-Sequence Evolution

The evolution of all stars is commonly visualised in the Hertzsprung-Russell (HR) diagram, which relates the stellar luminosity to the stellar surface temperature (color). Stellar evolution is initiated by core H-burning, during which the star is found on the so-called main sequence (MS) in the HR diagram. The release of nuclear binding energy mostly occurs in photons and kinetic energy, heating the star and thus producing thermal pressure against gravitational pressure. At stellar densities, photons undergo a multitude of scattering processes until they finally escape at the photosphere.[7] After the completion of core H-burning, the H-burning region continues to move outward as a burning shell. The He-core contracts and ignites core He-burning in the center, which produces C and O. In the HR diagram, this evolution is reflected by the star's position leaving the main sequence into the 'supergiant' region; the stellar radius increases due to the increased radiation pressure. Depending on the resulting surface temperature it becomes a blue or red supergiant (BSG or RSG). Radiation pressure can rise to such extreme values that stars blow off their outer parts through strong *stellar winds* of velocities up to 2000 km s^{-1}, exposing the more-interior parts of the star, the helium (or in some cases, the carbon) shell. In general, this occurs for stars more massive than

[7]It takes a photon about 10^5 years to reach the surface, after it has been launched in the hot core of, e.g., our Sun.

20–30 $M_\odot$. Such a Wolf-Rayet (WR) star loses between 10^{-6} and a few times 10^{-5} $M_\odot$ per year; for comparison, our Sun loses 10^{-14} of its $M_\odot$ per year through its solar wind. For non-rotating stars, the transition to the WR phase appears through the so-called 'Luminous Blue Variable' stars (LBVs). LBVs are massive, intrinsically bright stars which display different scales of light and color variability, ranging from rapid micro-variations to rare outbreaks of catastrophic mass loss. They represent a very short-lived (perhaps as little as 40,000 years) strongly mass-losing phase in the evolution of massive stars, during which they undergo deep erosion of the outer layers before they enter the Wolf-Rayet phase. Late burning phases progress much more rapidly than the H burning of the main sequence and He burning of the giant phase. The reason is that the energy loss, which drives the nuclear burning rate and hence the evolution, increases dramatically as neutrino production becomes a major part of the nuclear reactions; these escape immediately at the densities discussed here, and hence their share in the nuclear binding energy release is lost. The characteristics of late-burning stages are essentially identified by the size of a star's C+O-core after core He-burning.

In the following we discuss how the evolutionary phases depend on the initial properties of a star. In Fig. 4.3 we give a typical example of such an evolution for a 15 $M_\odot$ star.

The evolution of stars is governed mainly by three initial parameters: (1) its mass M (see Figs. 4.4 and 4.5), (2) its metallicity (Z, i.e. the mass fraction of pre-existing elements heavier than He from earlier stellar generations, see Fig. 4.6), and (3) the rotation rate or surface rotation velocity v_{rot} (see Figs. 4.7 and 4.8). Solar metallicity corresponds to[8] $Z = 0.02$. The evolution can also be influenced by interior magnetic fields, and by a close binary companion. Rotation significantly affects the pre-supernova state, through the impact it has on the H and He-burning evolution. Two mass groups are distinguishable: Either rotationally induced mixing dominates (for M <30 $M_\odot$), or rotationally increased mass loss dominates (for M >30 $M_\odot$). For massive stars around solar metallicity, mass loss plays a crucial role, in some cases removing more than half of the initial mass. Internal mixing, induced mainly by convection and rotation, also has a significant effect on the evolution of stars. An important result is the production of primary ^{14}N (via the CNO-cycle) and ^{22}Ne (via α-captures in He-burning), due to mixing of burning products (such as ^{12}C) with hydrogen or α's, respectively (see the discussion in Sect. 4.2).

The general impact of metallicity can be summarised in the following way: Lower metallicity implies a (slightly) lower luminosity due to the lack of CNO-cycling in hydrogen burning, which leads to slightly smaller convective cores. A lower metallicity also implies a lower opacity due to the lack of heavier elements with their many spectral lines, reducing therefore also radiation pressure and hence mass loss (as long as the chemical composition has not been changed by burning or

[8]The current value of solar metallicity is believed to be Z = 0.014, see Chap. 1; the value of Z = 0.02, which had been established before and was in common use till∼2005, remains a reference for comparisons, though.

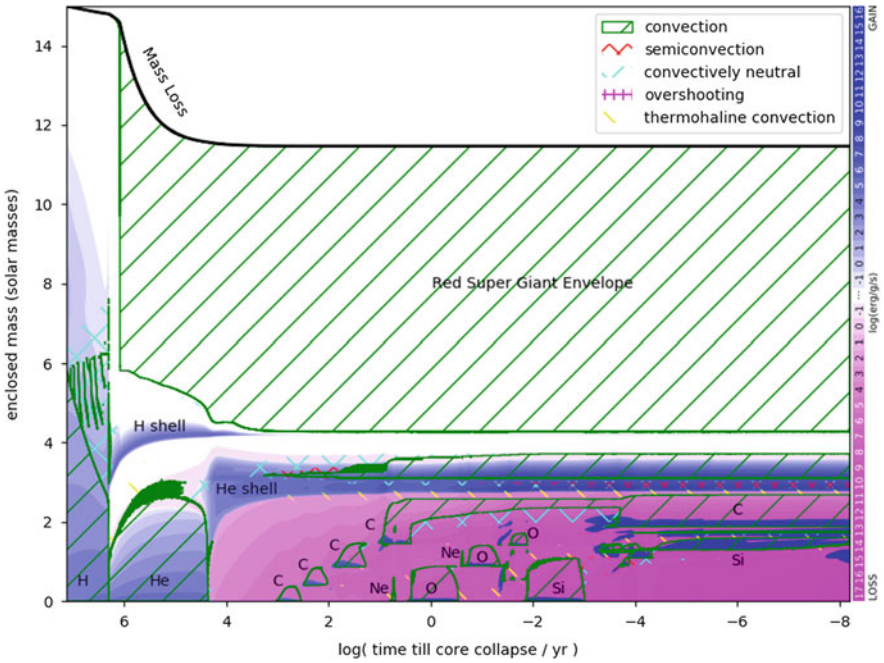

Fig. 4.3 Kippenhahn diagram of a $15\,M_\odot$ star of solar initial composition. The x-axis shoes the logarithm of the time till core collapse in years. The plots begins at about 10 million years before the star dies and ends a quarter of a second before core bounce is reached. The y-axis indicates enclosed mass relative to the center of the star, assuming a spherical symmetry. Blue and purple shading indicate net nuclear energy generation from burning minus neutrino losses. See scale on the right hand side. Green hatching indicates convection, which is the dominant mixing process. Convective regions are also outlined by a green line. Reed cross hatching indicates semi-convection, yellow hatching indicates thermohaline convection, and cyan indicates convectively neutral regions. Black labels indicate the different nuclear burning phases as a function in the core and in shells

mixing in the part of the star under consideration). This results in lower metallicity stars being more compact and experiencing less mass loss. Prescriptions for mass loss as used in the Geneva stellar evolution code are described in detail in Meynet and Maeder (2005). Mass loss rates depend on metallicity as $dM/dt \propto (Z/Z_\odot)^{0.5}$, where Z is the mass fraction of heavy elements at the surface of the star. The effects can be seen in Fig. 4.6 which shows the interior structure of stars through so-called *Kippenhahn diagrams* of $30\,M_\odot$ models for different metallicities of the stars. These diagrams indicate regions (in radial mass coordinates) where matter is unstable against convection; here the energy transport is dominated by transporting hot matter rather than through the propagation of photons. The implications of such a behavior

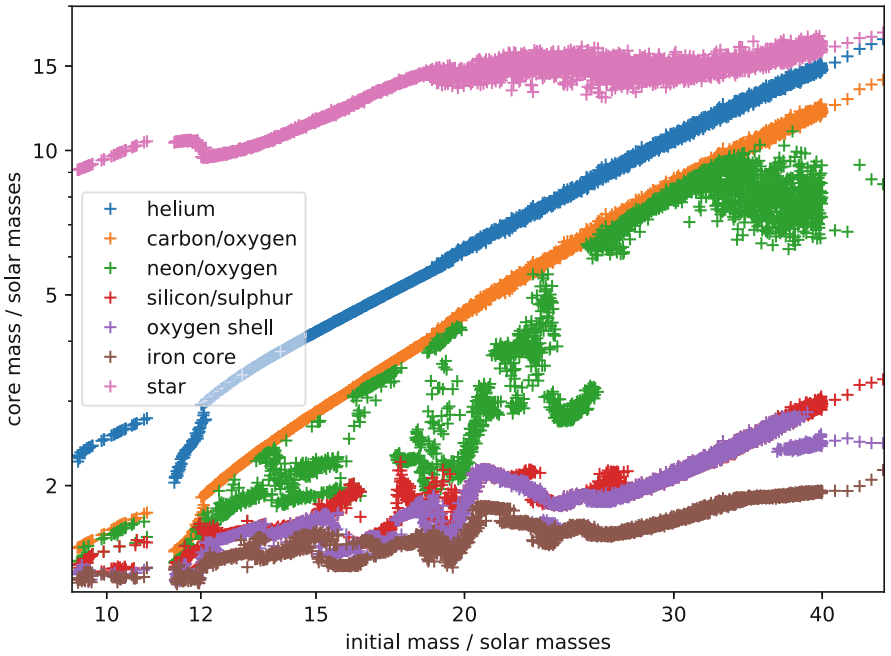

Fig. 4.4 Variation of core sizes as a function of initial mass (*y*-axis) for stars of solar metallicity. This is based on a compilation of 2910 pre-supernova models of solar initial composition from 9.45 $M_\odot$ to 45 $M_\odot$. Colored pluses indicate the outer edge of each core with a given composition (see figure legend). Below 9.45 $M_\odot$ stars did not undergo iron core collapse but ended up as O-Ne-Mg white dwarf stars. The mass gird is basically 0.01 $M_\odot$ solar mass resolution up to 40 $M_\odot$ and 1 $M_\odot$ above, but there are some gaps of varying size below about 11.5 $M_\odot$ due to non-convergence of the models; the stars in these gaps would still undergo iron core collapse and explode as supernova. We notice some scatter and many discontinuous changes, as well as the apparent existence of parallel branches in some cases. The discontinuous changes can be well understood due the onset of different convective shell burning stages, resulting in a non-linear behavior. Some of the noise indeed is due to numerical noise, largely seeded by semi-convection in hydrogen and helium burning, however, some of the wild variations in particular around 17–18 $M_\odot$ is due to the transition from convective to radiative carbon core burning, with many tiny shells causing an almost chaotic behavior with vastly different outcomes for small changes in initial mass (or other stellar parameters). This figure is based on models presented in Müller et al. (2016a). This is similar to results found by Sukhbold et al. (2017)

have already been described in the evolution of low and intermediate mass stars (Chap. 3), and the physical origin and treatment of these effects are addressed in Chap. 8.

With the exception of the outer convection zone, convective regions in most cases indicate *burning zones*, such as *core H-burning, core He-burning, core C-burning* etc. They testify also the ignition of outward moving burning shells of the same nuclear burning stages. When comparing models for decreasing metallicities (without rotation of Fig. 4.6) one notices only minute reductions of the core sizes,

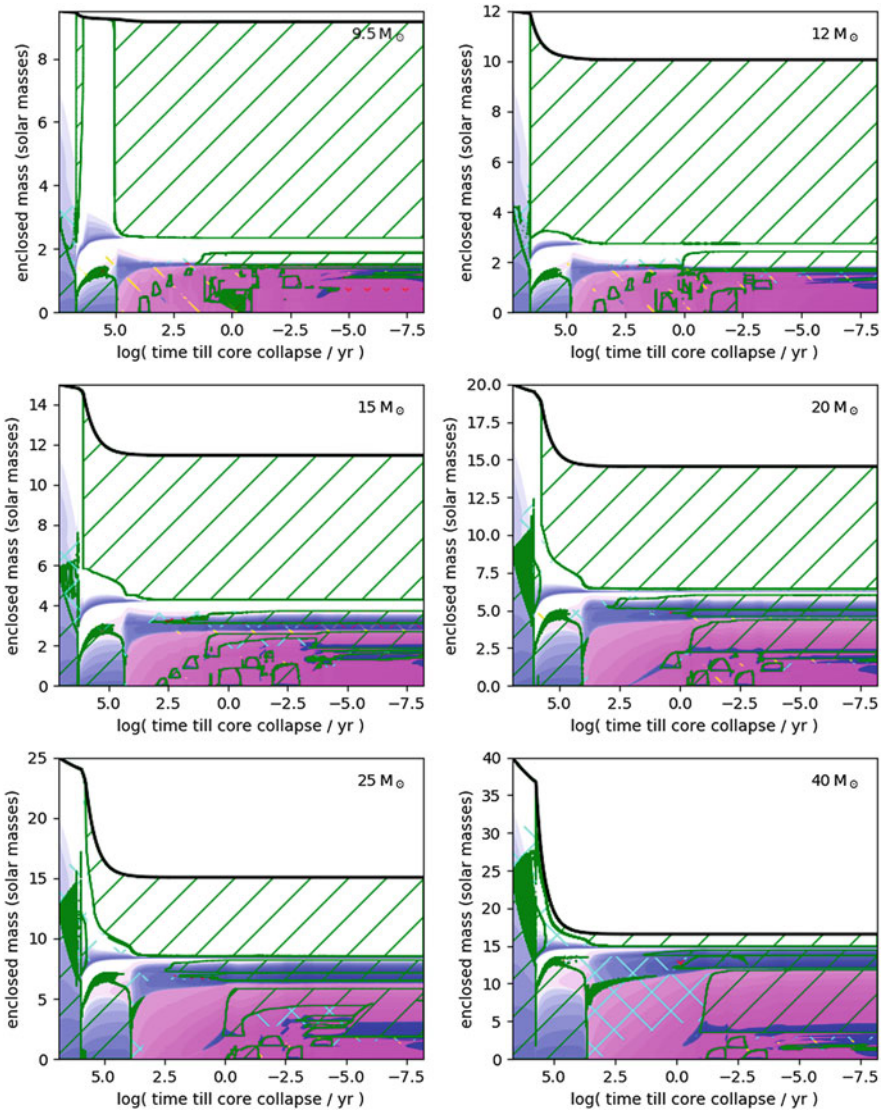

Fig. 4.5 Stellar structure (Kippenhahn) diagrams, which show the for 9.5, 12, 15, 20, 25, and 40 $M_{\odot}$ stars of solar composition. Coloring and axis are the same as in Fig. 4.3. For the more massive stars the mass loss form the surface significantly increases until almost all of the hydrogen envelope is lost for the 40 $M_{\odot}$ star. Between 15 and 20 $M_{\odot}$ central carbon burning transitions from convective to radiative

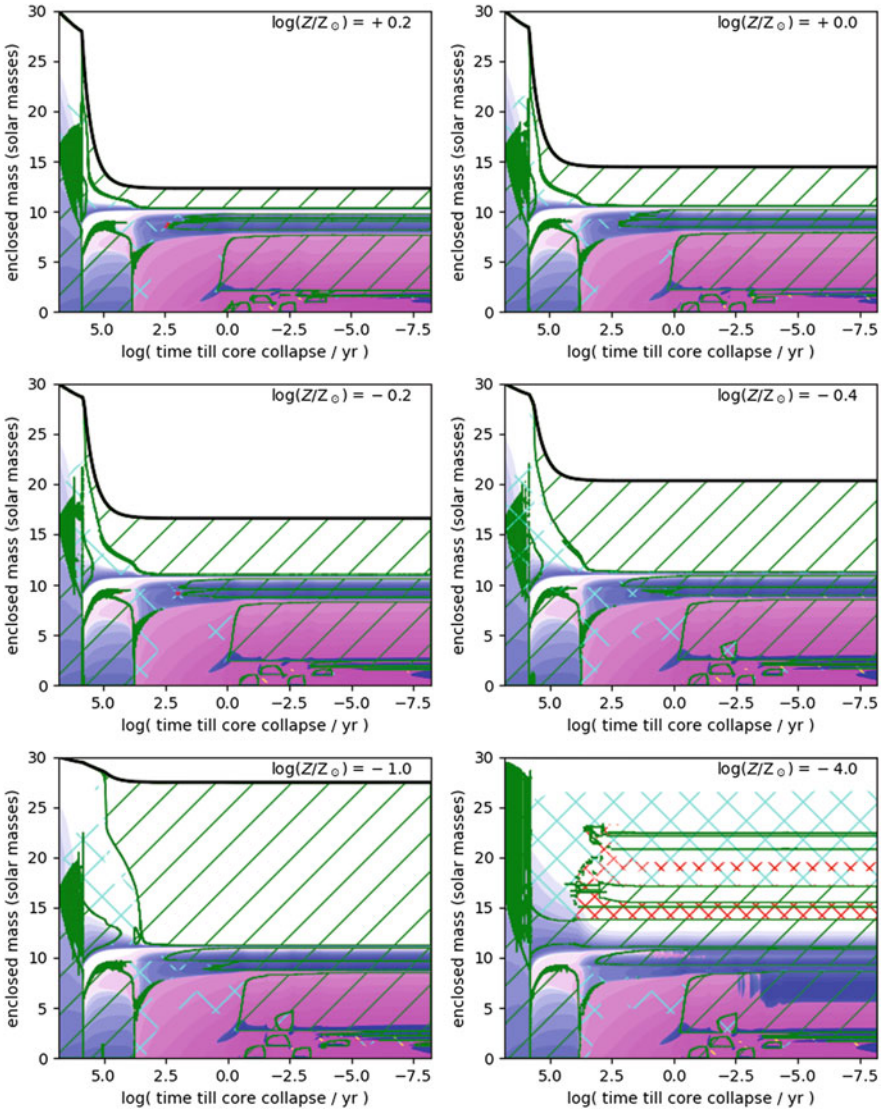

Fig. 4.6 Stellar structure (Kippenhahn) diagrams, which show the for different initial metallicities for a non-rotating 30 $M_{\odot}$ star. Each Panel is labeled with the initial metallicity relative to solar, $Z/Z_{\odot}$. At 1/10,000 solar metallicity mass loss does no longer play a role for this non-rotating model. These models, to be published in West and Heger (2018), used Lodders and Palme 2009 solar abundances as their reference

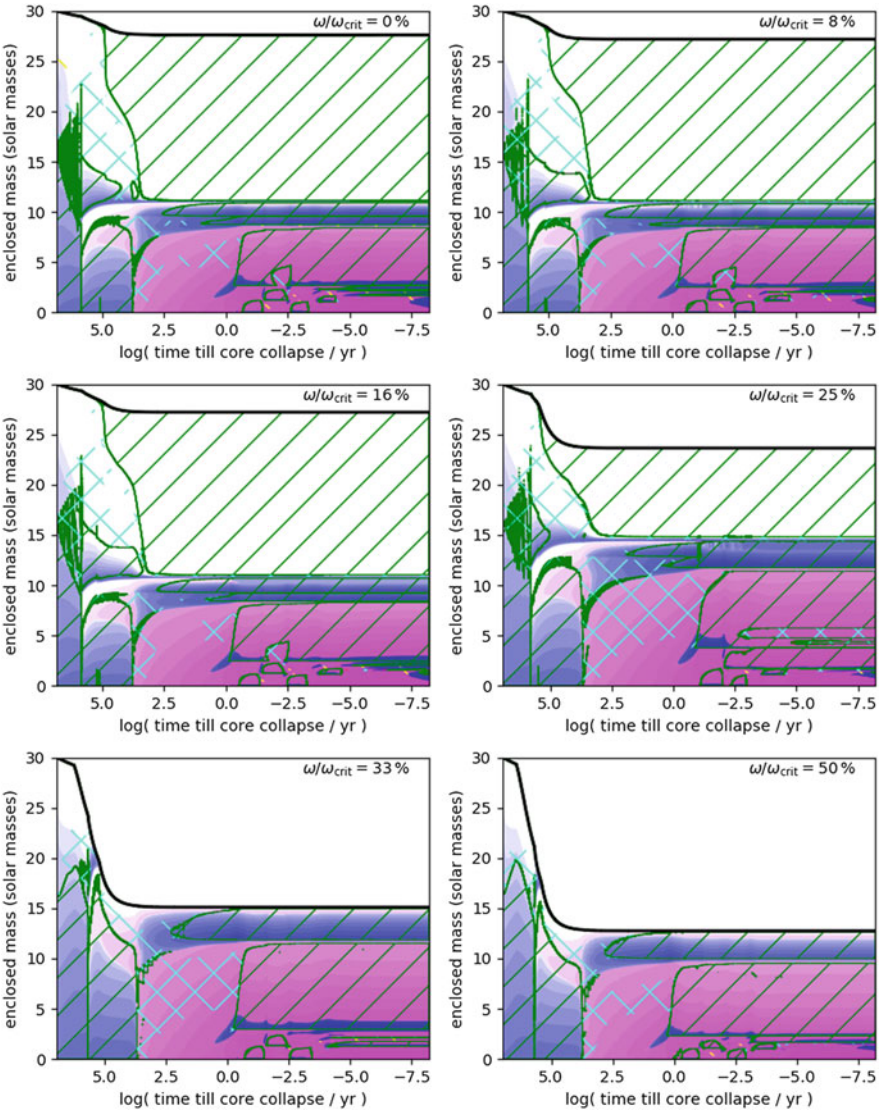

Fig. 4.7 Stellar structure (Kippenhahn) diagrams, which show the for different rotation rates for a $30\,M_{\odot}$ star of 1/10 solar initial metallicity. Each Panel is labeled with the equatorial surface velocity relative to critical velocity, $\omega/\omega_{\rm crit}$, at the zero-age main sequence of the star. Rotation significantly enhances mass loss from the surface of the star, and for $\gtrsim 30\,\%$ of critical rotation the core remains rather well-mixed during core-hydrogen burning, which can be seen as an increase of the convective core rather than a drop. These stars transition to the WNL phase during core hydrogen burning, and later become hydrogen-free WNE/WC/WO stars. This figure is based on unpublished work by Heger (2018)

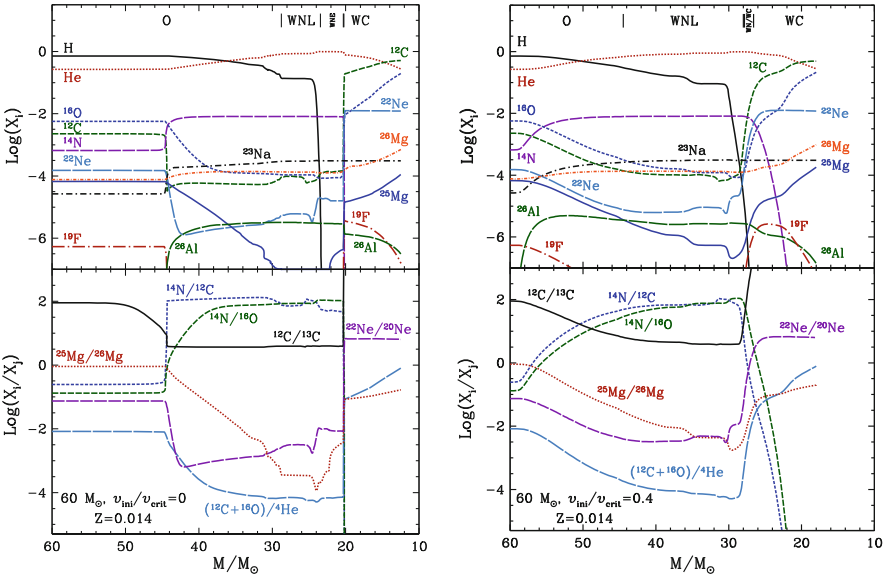

Fig. 4.8 Non-rotation (left) versus rotation-including (right) model comparison of abundance profiles versus mass fractions. Top left: evolution of the surface abundances for a non-rotating 60 $M_\odot$ model. Different evolutionary phases are indicated at the upper axis (the WNC phases occurs in a very narrow region, just before the WC phase, not labelled here). Bottom left: evolution of abundance ratios (in number) as a function of the actual mass of the star. Right panels: Same as left panels, but for the model including stellar rotation (adapted from Georgy et al. 2012)

but it is clearly seen that the outer (H-)burning shell moves further in towards smaller radial mass zones. In addition, the separation of the H- and He-burning shells becomes smaller, which can lead at even lower metallicities to a merging of these shells and a largely increased energy generation and extension of these combined burning zones.

How does rotation change this picture, and how do rotation-induced processes vary with metallicity? At all metallicities, rotation usually increases the core sizes via rotational mixing (compare all panels of Fig. 4.7 with the bottom left panel in Fig. 4.6). The supply of more H-fuel leads to more energy generation and therefore a higher luminosity. The higher luminosity increases the radiation pressure and stellar mass loss. The effect of increased core sizes (and smaller density gradients) can be viewed in all models in Fig. 4.7 with the exception for the highest rotation rate which led to extreme mass loss. Clearly the convective core sizes are increased and the shell burning zones have moved outward. For the metallicity $Z/Z_\odot = 0.1$ shown in this figure, the increased luminosity causes a sufficient increase in radiation pressure so that the mass loss is substantially enhanced (see the decrease of the stellar mass indicated by the top line). Mass loss becomes gradually unimportant for decreasing metallicities. For rotating 20 $M_\odot$ models (not shown here) the stellar fraction lost is more than 50% for solar metallicities, 13% at $Z = 0.001$, less than 3% for $Z = 10^{-5}$, and less than 0.3% for $Z = 10^{-8}$. Figure 4.8 shows the effect of rotation for

a $Z = 0.014$ stellar model with an initial mass of $60\,M_\odot$ on its surface abundances. As a function of time mass loss decreases the total mass which is indicated in the abscissa. The surface abundances are given as a function of this time-dependent mass, the top panels display the actual values and the bottom panels the relative abundance ratios.

This can be different for more massive stars (Meynet et al. 2006). In Fig. 4.9, we show results for a low metallicity 60 $M_\odot$ star with $Z = 0.014$, comparing non-rotating and a fast rotating model. The surface layers of massive stars usually accelerate due to internal transport of angular momentum from the core to the envelope. Since at low Z, stellar winds are weak, this angular momentum dredged up by meridional circulation remains inside the star, and the star reaches critical rotation more easily. At the critical limit, matter can be launched into a Keplerian disk which probably dissipates under the action of the strong radiation pressure of the star. Such an effect can be seen for the $85\,M_\odot$ star, which loses in total more than 75% of its initial mass, and initially about 10% due to critical rotation. The remaining mass loss occurs during the red supergiant phase after rotation and convection have enriched the surface in primary CNO elements. We can also see that this effect becomes vanishingly small for stars with masses $M < 30\,M_\odot$. The two $20\,M_\odot$ models with varying metallicities and degrees of rotation again indicate the influence of metallicity and rotation on the compactness and mass loss of stars. In both cases the mass loss is negligible.

We have not shown here the evolution of extremely low metallicity stars. Below a metallicity of about $Z = 10^{-10}$, the CNO cycle cannot operate when H-burning stars after the star has been formed. The star therefore contracts until He-burning ignites, because the energy generation rate of H burning through the pp-chains cannot balance the effect of the gravitational force. Once enough C and O is produced, the CNO cycle can operate, and the star behaves like stars with $Z > 10^{-10}$ for the rest of the main sequence. Metal-free stellar evolution models are presented in Chieffi and Limongi (2004), Heger and Woosley (2002), Umeda and Nomoto (2005), and Ekström et al. (2008).

Including the effects of both mass loss and rotation, massive star models improve to reproduce many observables of stars with metallicities around solar Z. For example, models with rotation allow chemical surface enrichments already on the main sequence of core hydrogen burning (MS), whereas without the inclusion of rotation, self-enrichment is only possible during advanced burning evolution such as the red supergiant RSG stage (Heger and Langer 2000; Meynet and Maeder 2000). Rotating star models also better reproduce the ratio of star types, for the ones which retain their hydrogen surface layer (O stars), which lose the hydrogen layer completely (WR stars), and which even lose their helium layer. The latter affects also the appearance of later core collapse supernova explosions of massive stars. Indeed, rotation changes the supernova type due to the mass loss of the hydrogen envelope (turning such an event in optical observations from a type II supernova with a strong plateau phase to a type IIb event with a smaller plateau, or even a type Ib event for the case of complete loss of the hydrogen envelope, and a type Ic event with the additional loss of the He-envelope). This is discussed in more detail

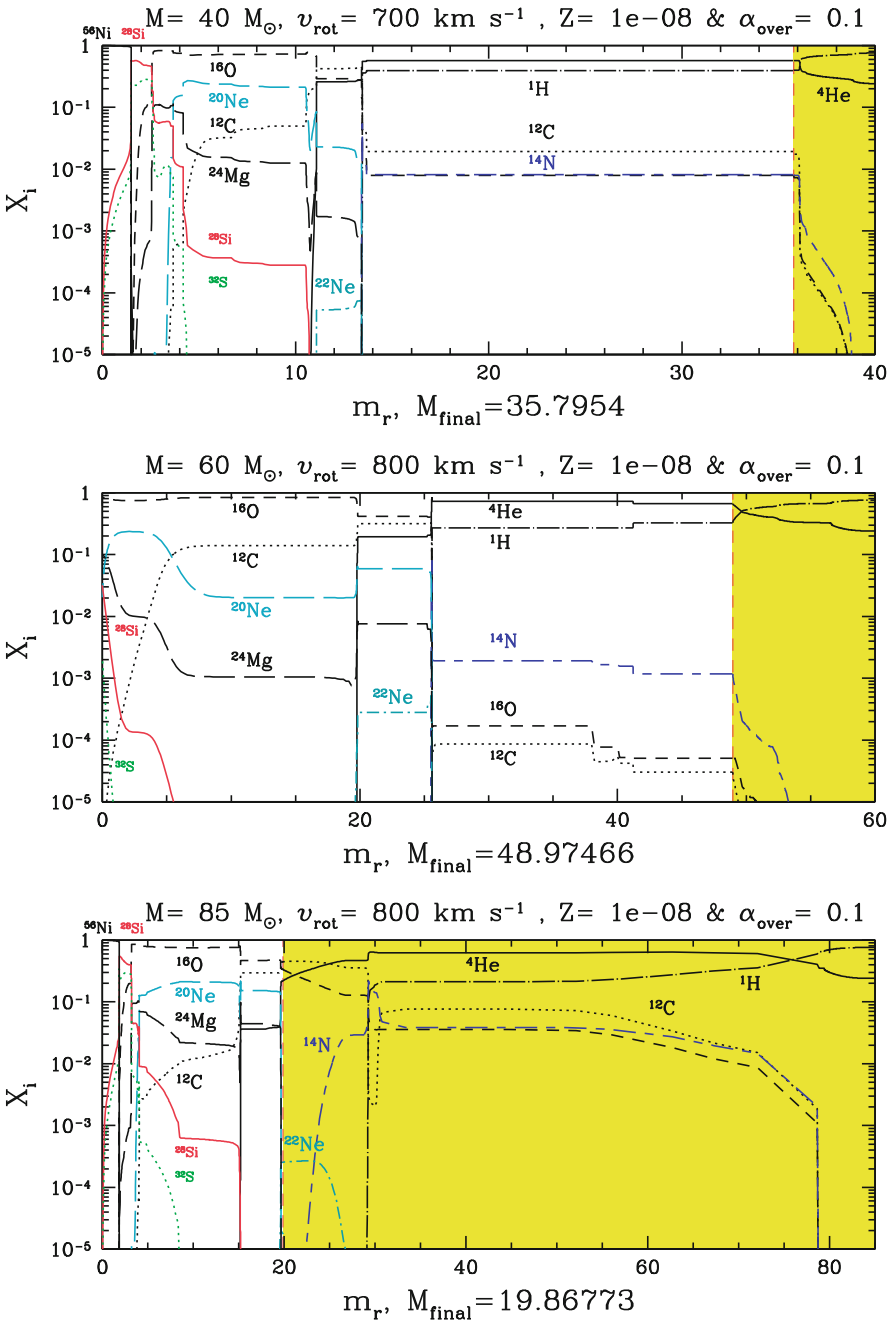

Fig. 4.9 Abundance profiles for 40 (*top*), 60 (*middle*) and 85 (*bottom*) $M_{\odot}$ models (Hirschi 2007). The pre-SN and wind (yellow shaded area) chemical compositions are separated by a red dashed line located at the pre-SN total mass (M_{final}), given below each graph

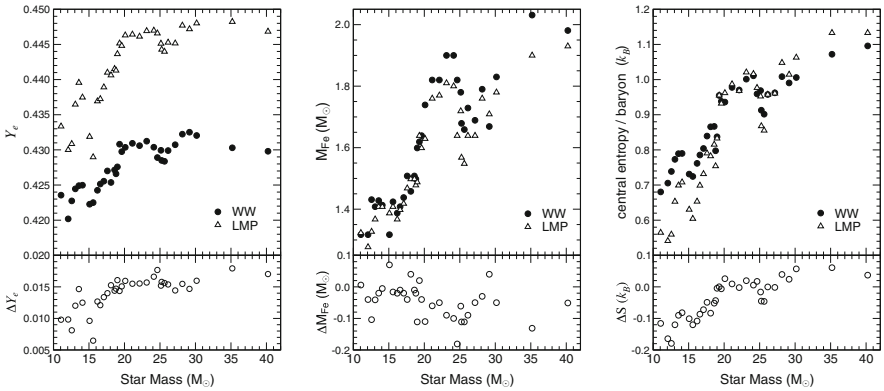

Fig. 4.10 Comparison of the center values of Y_e (left), the iron core sizes (middle) and the central entropy (right) for 11–40 $M_\odot$ stars between the WW models and the ones using the shell model weak interaction rates (LMP) (Heger et al. 2001a). The lower parts define the changes in the three quantities between the LMP and WW models

in Sect. 4.4. Both aspects, the chemical surface enrichment in MS stars as well as the ratio of type Ib+Ic to type II supernovae, as a function of metallicity, are drastically changed compared to models without rotation, which underestimate these ratios (Georgy et al. 2009; Meynet and Maeder 2005). The value of 300 km s^{-1}, used as the initial rotation velocity at solar metallicity, corresponds to an average velocity of about 220 km s^{-1} on the main sequence (MS), which is close to the average value from observations (Fukuda 1982; Meynet et al. 2008). Comparing ratios of stars of different types, as observed in the Magellanic clouds and in our Galaxy, (Maeder et al. 1999; Martayan et al. 2007), points to stars rotating more rapidly at lower metallicities. Fast initial rotation velocities in the range of 600–800 km s^{-1} (Hirschi et al. 2005) are supported by observations of very low-Z stars (Chiappini et al. 2006).

Rotation affects all burning stages and the resulting Fe-core (we will discuss this issue further in the next subsection, see also Fig. 4.10). The size of the Fe-core in turn determines the final fate, whether a supernova explosion with neutron star formation or the collapse to a black hole occurs. The effects of rotation on pre-supernova models are most spectacular for stars between 15 and 25 $M_\odot$. It changes the total size/radius of progenitors (leading to blue instead of red supergiants) and the helium and CO core (bigger by a factor of $\sim$ 1.5 in rotating models). The history of convective zones (in particular the convective zones associated with shell H-burning and core He-burning) is strongly affected by rotation induced mixing (Hirschi et al. 2005). The most important rotation induced mixing takes place while He is burning inside a convective core. Primary C and O are mixed from the convective core into the H-burning shell. Once the enrichment is strong enough, the H-burning shell is boosted (the CNO cycle depends strongly on the C and O mixing at such low initial metallicities). The shell becomes convective

and leads to an important primary ^{14}N production while the convective core mass decreases, leading to a less massive CO-core after He-burning than in non-rotating models. Convective and rotational mixing brings the primary CNO to the surface with interesting consequences for the stellar yields. The yield of ^{16}O, being closely correlated with the mass of the CO-core, is reduced. At the same time the C yield is slightly increased (Hirschi et al. 2005), both due to the slightly lower temperatures in core He-burning. This is one possible explanation for the high [C/O] ratio observed in the most metal-poor halo stars (see Fig. 14 in Spite et al. (2005) and Fabbian et al. (2009)) and in damped Lyman alpha systems DLAs (Pettini et al. 2008).

The fate of rotating stars at very low Z is therefore probably the following: $M < 30$–$40\,M_\odot$: Mass loss is insignificant and matter is only ejected into the ISM during the SN explosion. 30–$40\,M_\odot < M < 60\,M_\odot$: Mass loss (at critical rotation and in the RSG stage) removes 10–20% of the initial mass of the star. The star probably dies as a black hole without a SN explosion and therefore the feedback into the ISM is only due to stellar winds. $M > 60\,M_\odot$: A strong mass loss removes a significant amount of mass and the stars enter the WR phase. These stars therefore end as type Ib/c SNe and possibly as GRBs. This behavior is displayed in Fig. 4.9. At a metallicity $Z = 10^{-8}$, corresponding to an Fe/H ratio $log_{10}[(Fe/H)/(Fe/H)_\odot$ =[Fe/H]~ -6.6, C and O are shown in models to be mixed into the H-burning shell during He-burning. This raises the importance of the shell, and leads to a reduction of the CO-core size. Later in the evolution, the H-shell deepens and produces large amounts of primary nitrogen. For the most massive stars ($M > 60\ M_\odot$), significant mass loss occurs during the red supergiant stage, caused by the surface enrichment in CNO elements from rotational and convective mixing.

The properties of non-rotating low-Z stars are presented in Heger et al. (2003), Hirschi et al. (2008), and several groups have calculated their stellar yields (Heger and Woosley 2002; Chieffi and Limongi 2004; Tominaga et al. 2007). All results for the non-rotating stars (whether at solar metallicity or for low-Z models) are consistent among these calculations, differences are understood from the treatments of convection and the rates used for $^{12}C(\alpha,\gamma)^{16}O$. The combined contributions to stellar yields by the wind and the later supernova explosion (see Sect. 4.4) are assembled separately (see, e.g., Pignatari et al. 2016; Georgy et al. 2012; Ekström et al. 2012). The results for stellar models with metallicities Z close to solar can be described as follows: Rotating stars have larger yields in their stellar winds than the non-rotating ones, because of the extra mass loss and mixing due to rotation, for masses below $\sim 30\,M_\odot$. The ^{12}C and ^{16}O yields are increased by a factor 1.5–2.5 by rotation. At high mass loss rates (above $\sim 30\ M_\odot$), the rotating and non-rotating models show similar yield values. When the wind and explosive contributions are added, the total metal production of rotating stars is larger by a factor 1.5–2.5 (see Sect. 4.4). For very massive stars, the situation varies due to the extreme mass loss, as shown in Fig. 4.9. In order to give a quantitative impression of the influence of initial mass, metallicity and rotation on the evolution of stars, we present in Tables 4.7 and 4.8 results for (a) non-rotating solar metallicity stars (Limongi and Chieffi 2006b) and (b) rotating stars for varying metallicities (Hirschi et al. 2005). Given are the initial and final mass (in order to give an impression of the

Table 4.7 Stellar properties (Limongi and Chieffi 2006a,b)

$M_{ini}/M_\odot$	$M_{fin}/M_\odot$	$M_{He}/M_\odot$	$M_{CO}/M_\odot$
11	10.56	3.47	1.75
15	13.49	5.29	2.72
20	16.31	7.64	4.35
30	12.91	12.68	8.01
40	12.52	16.49	8.98
60	17.08	25.17	12.62
80	22.62	34.71	17.41

Table 4.8 Stellar properties (Hirschi 2007)

$M_{ini}/M_\odot$	Z	v_{rot}	$M_{fin}/M_\odot$	$M_{He}/M_\odot$	$M_{CO}/M_\odot$
9	1×10^{-8}	500	9.00	1.90	1.34
20	2×10^{-2}	300	8.76	8.66	6.59
20	1×10^{-3}	0	19.56	6.58	4.39
20	1×10^{-3}	300	17.19	8.32	6.24
20	1×10^{-5}	300	19.93	7.90	5.68
20	1×10^{-5}	500	19.57	7.85	5.91
20	1×10^{-8}	300	20.00	6.17	5.18
20	1×10^{-8}	600	19.59	4.83	4.36
40	1×10^{-8}	700	35.80	13.50	12.80
60	1×10^{-8}	800	48.97	25.60	24.00
85	1×10^{-8}	800	19.87	19.90	18.80

mass loss), as well as the core size after central H-burning (the He-core) and after central He-burning (the CO-core), and in Table 4.8 also the metallicity Z and initial rotational surface velocity in $\mathrm{km\,s^{-1}}$. As all burning stages after He-burning occur on significantly shorter timescales than the earlier burning phases, the CO-core size is the important quantity in order to determine the final outcome/fate of the star.

4.3.2 Late Burning Stages and the Onset of Core Collapse

Stars more massive than about 8 $M_\odot$ will, after finishing core and shell H- and He-burning, lead to CO-cores which exceed the maximum stable mass of white dwarfs (the Chandrasekhar mass). For later burning stages, when the partial or full degeneracy of the electron gas is important, this critical limit $M_{Ch}(\rho Y_e, T)$ decides upon further contraction and the central ignition of subsequent burning stages, that is C-, Ne-, O- and Si-burning. Dependent on the Fermi energy of the degenerate electron gas, electron capture on the C-burning products ^{20}Ne and ^{24}Mg can initiate a collapse, leading directly via nuclear statistical equilibrium to a central Fe-core. This evolution path occurs for stars in the range 8–10 $M_\odot$ (Nomoto 1987; Kitaura et al. 2006; Wanajo et al. 2009; Jones et al. 2013). More massive stars will

proceed through all burning stages until Si-burning will finally produce an Fe-core. All burning stages after core H- and He-burning proceed on timescales which are shorter my orders of magnitude. The reason is that the energy carried away by freely escaping neutrinos dominates over radiation losses by photons which undergo a cascade of scattering processes before their final escape. While neutrinos are emitted during beta-decay and electron captures, discussed in Sect. 4.1, most of these neutrinos are created as central densities and temperatures increase and new degrees of freedom open up for the state of matter. The following neutrino production reactions are relevant: (1) $e^- + e^+$-pair annihilation (*pair neutrinos*), (2) electron-photon scattering with neutrino-antineutrino pair creation (photo neutrinos), and (3) neutrino-antineutrino pair creation from plasma oscillations (*plasmon neutrinos*), as presented in detail in Clayton (1968). Neutrinos dominate the energy loss in stellar evolution from this point on, and lead to increasingly shorter burning timescales, although the photon radiation luminosity of the star remains roughly constant. The timescales for the individual burning stages are given in Table 4.1 in Sect. 4.2; these values refer to a 20 $M_\odot$ star with solar metallicity and no mass loss. Effects of mass loss, rotation and metallicity can change these timescales somewhat (up to 20%). Due to the large difference in evolution timescales, the dominant mass loss by stellar winds occurs during H- and He-burning, and the final outcome of stellar evolution is determined by the CO-core size after He-burning. Therefore, given all dependencies of stellar evolution via initial metallicities and rotation, the initial main sequence mass of a star is less indicative for the final outcome than the size of its CO-core.

In the late phases of O- and Si-burning (discussed in Sect. 4.2), electrons are moderately to strongly degenerate, dependent on the initial stellar mass, and will be characterized by increasing Fermi energies. This will allow for electron captures on burning products, and will make matter more neutron-rich, i.e decrease Y_e, the electron or proton to nucleon (neutrons plus protons) ratio. In high density O-burning ($\rho > 2 \times 10^7$ g cm^{-3}) two electron capture reactions become important and lead to a decrease in Y_e, $^{33}\mathrm{S}(e^-, \nu)^{33}\mathrm{P}$ and $^{35}\mathrm{Cl}(e^-, \nu)^{35}\mathrm{S}$. Such effects become more extensive at even higher densities in Si-burning and a large range of nuclei has been identified to be of major importance $^{55-68}$Co, $^{56-69}$Ni, $^{53-62}$Fe, $^{53-63}$Mn, $^{64-74}$Cu, $^{49-54}$Sc, $^{50-58}$V, $^{52-59}$Cr, $^{49-54}$Ti, $^{74-80}$Ga, $^{77-80}$Ge, ^{83}Se, $^{80-83}$As, $^{50-58}$V, and ^{75}Zn (Aufderheide et al. 1994). The amount of electron capture and the resulting Y_e has consequences for core sizes. (The core sizes of the late burning stages are shown in Figs. 4.3 and 4.8.) The final size of the inner Fe-core represents the maximum mass which can be supported by the pressure of the degenerate electron gas. It is a function of Y_e, but also reflects temperature effects if the electron gas is not completely degenerate (Bethe 1990), with S_e being the entropy in electrons per baryon

$$M_{Ch}(Y_e, S_e) = 1.44(2Y_e)^2[1 + (\frac{S_e}{\pi Y_e})^2]\mathrm{M}_\odot. \tag{4.3}$$

Stars with masses exceeding roughly 10 $M_\odot$ reach a point in their evolution where their Si-burning core (which will turn eventually into their Fe-core) provides

no further source of nuclear energy. At this point they collapse and bounce, if not too massive, to explode in spectacular core collapse events known as type II or Ib/c supernovae. These explosions create a neutron star or black hole at the end of the life of a star. They play a preeminent role in the nucleosynthesis and chemical evolution of a galaxy.

The collapse is initiated by the capture of degenerate electrons on nuclei, which reduces the dominant contribution of the pressure (i.e. the one from the degenerate electron gas). Alternatively, for lower densities and higher temperatures (in more massive stars), the pressure supporting the core is reduced by endoergic photo-disintegrations of nuclei, reducing the thermal energy. The evolution in the core is determined by the competition of gravity (that causes the collapse of the core) and weak interaction (that determines the rate at which electrons are captured and the rate at which neutrinos are trapped during the collapse).

The early phases of this final stage of stellar evolution are known as *presupernova evolution*. They follow the late-stage stellar evolution, and proceed until core densities of about $10^{10}\,\mathrm{g\,cm^{-3}}$ and temperatures between 5 and $10\times10^{9}\,\mathrm{K}$ are reached. Until this point, modeling stellar evolution requires the consideration of extensive nuclear reaction networks, but is simplified by the fact that neutrinos need only be treated as a sink of energy and lepton number (due to their immediate escape). At later time and towards the collapse, this is no longer valid: As the weak interaction rates increase with the increasing density, the neutrino mean free paths shorten, so that the neutrinos eventually proceed from phases of free streaming, towards diffusion, and trapping. An adequate handling of the transitions between these transport regimes necessitates a detailed time- and space-dependent bookkeeping of the neutrino distributions in the core (see Chap. 8 for neutrino radiation transport and also a recent detailed discussion by Burrows et al. 2018). During collapse, electron capture, accompanied by ν_e neutrino emission, dominates over electron antineutrino emission because the positron abundance is very low under electron-degenerate conditions. Later in the evolution the electron degeneracy is partially lifted, and in addition to the electron flavor neutrinos, also heavy neutrinos, ν_μ and ν_τ and their antiparticles, are usually included in numerical simulations of core collapse and post-bounce evolution.

Advantageously, the temperature during the collapse and explosion are high enough that the matter composition is given by nuclear statistical equilibrium (NSE), i.e. without the need of reaction networks for the strong and electromagnetic interactions. The transition from a rather complex global nuclear reaction network, involving many neutron, proton and alpha fusion reactions and their inverses, to a quasi-statistical equilibrium, in which reactions are fast enough to bring constrained regions of the nuclear chart into equilibrium, to final and global nuclear statistical equilibrium is extensively discussed by Hix and Thielemann (1996, 1999b) and Hix et al. (2007). In the late stages of Si-burning and the early collapse phase, weak interactions are dominated by electron captures on protons and nuclei. These are important equally in controlling the neutronization of matter Y_e and, in a large portion, also the stellar energy loss. Due to their strong energy dependence $\propto E_e^5$, the electron capture rates increase rapidly during the collapse while the density and the temperature increase (the electron Fermi energy E_F scales with $\rho^{2/3}$, see 4.2).

The main weak interaction processes during the final evolution of a massive star are electron capture and β-decays. Their determination requires the calculation of Fermi and Gamow-Teller (GT) transitions. While the treatment of Fermi transitions (important only for β-decays) is straightforward, a correct description of the GT transitions is a difficult problem in nuclear structure physics. In astrophysical environments, nuclei are fully ionized. Therefore, electron capture occurs from the continuum of the degenerate electron plasma, and energies of the electrons are high enough to induce transitions to the Gamow-Teller resonance. Shortly after the discovery of this collective excitation, Bethe et al. (1979) recognized its importance for stellar electron capture. β^--decay converts a neutron inside the nucleus into a proton and emits an electron. In a degenerate electron gas, with fully populated levels up to the Fermi energy E_F, all decays which would produce electrons with smaller energies than E_F are not possible (*blocked*). Then, the decay rate of a given nuclear state is greatly reduced or even completely blocked at high densities. However, there is another pathway, as high temperatures populate a distribution of nuclear states: If an excited and thermally populated state of the decaying nucleus is connected by large GT transition probabilities to low-lying states in the daughter nucleus, producing electrons above the Fermi energy, such transition path can contribute significantly to the stellar β-decay rates. The importance of these states in the parent nucleus for β-decay in astrophysical environments was first recognized by Fuller et al. (1980, 1982, 1985).

Recent experimental data on GT distributions in iron group nuclei, measured in charge exchange reactions, show that the GT strength is strongly *quenched* (reduced), compared to the *independent-particle-model* value, and fragmented over many states in the daughter nucleus. An accurate understanding of these effects is essential for a reliable evaluation of the stellar weak-interaction rates, particularly for the stellar electron-capture rates (Fuller et al. 1980; Langanke and Martínez-Pinedo 2000). The nuclear *shell-model* is the only known tool to reliably describe GT distributions in nuclei. When comparing the shell-model based rates (by Langanke and Martinez-Pinedo) with the those from Fuller et al., one finds that the shell-model based rates are almost always smaller at the relevant temperatures and densities, caused by the above mentioned quenching of the Gamow-Teller strength, and by a systematic misplacement of the energy of the Gamow-Teller resonance. For an extended overview of rates utilized in astrophysical applications see Fuller et al. (1980, 1982), Oda et al. (1994), Langanke and Martínez-Pinedo (2001, 2003), Sampaio et al. (2003), and Juodagalvis et al. (2010).

The influence of these shell-model rates on the late-stage evolution of massive stars has been investigated by Heger et al. (2001a,b), and compared to earlier calculations (Woosley and Weaver 1995). Figure 4.10 illustrates the consequences of the shell model weak interaction rates for presupernova models in terms of the three decisive quantities: the central electron or proton to nucleon ratio Y_e, the entropy, and the iron core mass. The central values of Y_e at the onset of core collapse increased by 0.01–0.015 for the new rates. This is a significant effect. For example, a change from $Y_e = 0.43$ in the Woosley and Weaver model for a $20\,M_\odot$ star to $Y_e = 0.445$ in the new models increases the respective Chandrasekhar mass by about

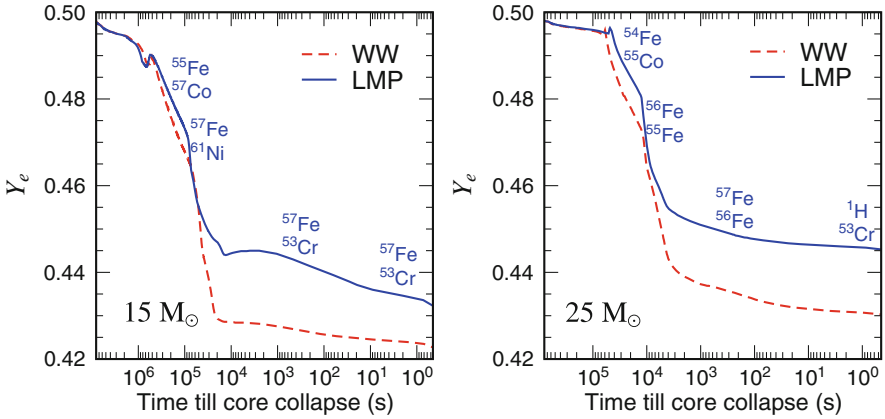

Fig. 4.11 Evolution of the Y_e value in the center of a 15 $M_\odot$ star (left panel) and a 25 $M_\odot$ star (right panel) as a function of time until bounce. The dashed line shows the evolution in the Woosley and Weaver models (WW) (Woosley and Weaver 1995), while the solid line shows the results using the shell-model based weak-interaction rates of Langanke and Martínez-Pinedo (LMP). The two most important nuclei in the determination of the total electron-capture rate, for the calculations adopting the shell model rates, are displayed as a function of stellar evolution time

$0.075\,\mathrm{M}_\odot$ (see Eq.(4.3)). The new models also result in lower core entropies for stars with $M < 20\,\mathrm{M}_\odot$, while for $M > 20\,\mathrm{M}_\odot$, the new models actually have a slightly larger entropy. The Fe-core masses are generally smaller, where the effect is larger for more massive stars ($M > 20\,\mathrm{M}_\odot$), while for the most common supernovae ($M < 20\,\mathrm{M}_\odot$) the reduction is by about $0.05\,\mathrm{M}_\odot$ (the Fe-core is here defined as the mass interior to the point where the composition is dominated by more than 50% of Fe-group elements with $A \geq 48$). This reduction seems opposite to the expected effect due to slower electron capture rates in the new models. It is, however, related to changes in the entropy profile during shell Si-burning which reduces the growth of the iron core just prior to collapse.

The evolution of Y_e during the presupernova phase is plotted in Fig. 4.11. Weak processes become particularly important in reducing Y_e below 0.5 after oxygen depletion ($\approx 10^7$ s and 10^6 s before core collapse for the 15 M and 25 M stars, respectively) and Y_e begins a decline which becomes precipitous during Si-burning. Initially electron captures occur much more rapidly than beta-decays. As the shell model rates are generally smaller the initial reduction of Y_e is smaller in the new models. The temperature in these models is correspondingly larger as less energy is radiated away by neutrino emission. An important feature of the new models is shown in the left panel of Fig. 4.11. For times between 10^4 and 10^3 s before core collapse, Y_e increases due to the fact that β-decay becomes competitive with electron capture after Si-depletion in the core and during shell Si-burning. The presence of an important β-decay contribution has two effects (Aufderheide et al. 1994). Obviously it counteracts the reduction of Y_e in the core, but also acts as an additional neutrino source, causing a stronger cooling of the core and a reduction

in entropy. This cooling can be quite efficient, as often the average neutrino energy from the β-decays involved is larger than for the competing electron captures. As a consequence the new models have significantly lower core temperatures. At later stages of the collapse β-decay becomes unimportant again as an increased electron Fermi energy blocks/reduces its role. The shell model weak interaction rates predict the presupernova evolution to proceed along a temperature-density-Y_e trajectory where the weak processes involve nuclei rather close to stability which will permit to test these effects in the next-generation radioactive ion-beam facilities.

Figure 4.11 identifies the two most important nuclei (the ones with the largest value for the product of abundance times rate) for the electron capture during various stages of the final evolution of $15\,M_\odot$ and $25\,M_\odot$ stars. An exhaustive list of the most important nuclei for both electron capture and beta-decay during the final stages of stellar evolution for stars of different masses is given in Heger et al. (2001b). In total, the weak interaction processes shift the matter composition to smaller Y_e values and hence more neutron-rich nuclei, subsequently affecting the nucleosynthesis. Its importance for the elemental abundance distribution, however, strongly depends on the location of the mass cut in the supernova explosion. It is currently assumed that the remnant will have a larger baryonic mass than the Fe-core, but smaller than the mass enclosed by the O-shell (Woosley et al. 2002). As the reduction of Y_e occurs mainly during Si-burning, it is essential to determine how much of this material will be ejected.

4.4 Core Collapse and Supernova Explosions

4.4.1 Physics of Core Collapse, and Numerical Simulations

Supernova explosions are an application of numerical astrophysical modelling that has a long tradition. Continued improvements of the models are motivated by the following points: (1) open questions regarding the explosion mechanism; (2) availability of observations for individual supernova explosions; (3) interesting input physics that tests matter under conditions that are not accessible on earth; (4) visibility in light and other photon wavelengths, cosmic rays, neutrino emission, decay gamma-rays of radioactive products, perhaps gravitational wave emission; (5) visibility on cosmological distances with improving statistical information on the events and (6) their impact on the interstellar matter (e.g. abundances of metal-poor stars) and Galactic evolution.

As discussed in the previous sections, the death of massive stars $\approx 8 - -40\,M_\odot$ proceeds through several evolutionary and dynamical phases. At first, the modeling of a star must include the evolution through all nuclear burning stages until the resulting inner iron core grows beyond the maximum mass which can be supported by the dominant pressure of the degenerate electron gas. At this point, the inner stellar core enters a dynamical phase of gravitational collapse, during which it

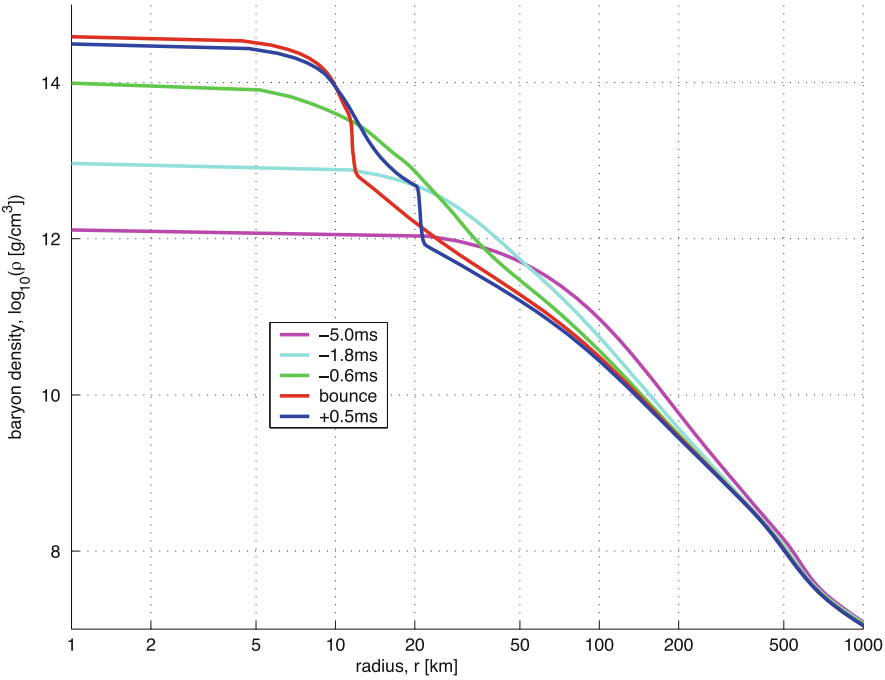

Fig. 4.12 A sequence of density profiles of a 13 $M_\odot$ star before and after core bounce in spherical symmetry. For such a relatively low mass supernova with a small Fe-core the bounce occurs at a maximum density of less than twice nuclear matter density. At the bounce one recognizes the size of the homologous core (with roughly constant density). Thereafter the emergence of an outward moving density (shock) wave can be witnessed, which, however, in spherical symmetry is not leading to an explosion

compactifies by $\sim$ 5 orders of magnitude. The nuclear saturation density (i.e. the density of stable nuclei $\approx 2 \times 10^{14}\,\mathrm{g\,cm^{-3}}$) is exceeded at the center of the collapse and a proto-neutron star (PNS) is formed. The dynamical time scale reduces from a few hundreds of milliseconds at the onset of collapse to a few milliseconds after the core has bounced back at nuclear densities (see Fig. 4.12 from a spherically symmetric simulation by Liebendörfer et al. (2003).

The ensuing accretion phase onto the proto-neutron star with fluid instabilities and radiative transfer phenomena, like the transport of neutrinos, is not, yet, fully understood, but the degree of comprehension is constantly improving. There exists a growing set of 2D and 3D CCSN explosions, see e.g. Hix et al. (2003, 2016), Liebendörfer et al. (2005), Marek et al. (2005), Burrows et al. (2006a, 2018), Sumiyoshi et al. (2007), Langanke et al. (2008), Marek and Janka (2009), Janka (2012), Burrows (2013), Takiwaki et al. (2014), Lentz et al. (2015), Melson et al. (2015), Nakamura et al. (2015), Janka et al. (2016), Bruenn et al. (2016) and the progress of active groups in Garching/Belfast/Monash, Princeton/Caltech/MSU, Oak Ridge/U. of Tennessee/Berkeley, Tokyo/Kyushu, Paris, and

Basel. The accretion may last 0.5–10 seconds and can therefore be interpreted as a second evolutionary stage (much longer than the dynamical or transport time scale). Eventually it will lead to the observed vigorous supernova explosion, a dynamic phase where heavy elements are produced by explosive nucleosynthesis in an outward propagating shock wave. The processed matter is mixed by fluid instabilities and ejected into the interstellar medium, where it contributes to Galactic evolution. The remaining PNS at the center enters another evolutionary phase during which it cools by neutrino emission and contracts or even collapses to a black hole in a last dynamical phase.

While initially such calculations were performed in spherical symmetry and therefore lacked the consistent treatment of turbulent motion, presently performed research is done with multidimensional supernova models (as discussed above). Multi-dimensional effects, including convection, turbulence and shock hydrodynamical instabilities (e.g., SASI), increase the time that a fluid particle spends inside the so-called gain region, in which electron neutrinos (ν_e's) and antineutrinos ($\bar{\nu}_e$) are absorbed and their energy is deposited, heating up matter in this region. This causes a pressure increase and shock revival. Recent multi-dimensional simulations have confirmed that these effects provide more favorable conditions for successful explosions than in spherically symmetric simulations. They rely on radiation (neutrino) transport, (relativistic) hydrodynamics, and the nuclear equation of state at such high densities (Oertel et al. 2017). In addition to non-rotating models without magnetic fields, other efforts explore their role of in multi-dimensional simulations (Winteler et al. 2012; Mösta et al. 2014, 2015, 2017; Nishimura et al. 2015, 2017b; Halevi and Mösta 2018)

Nevertheless, it is still of interest to perform spherically symmetric approaches, although the assumption of spherical symmetry is for many supernovae not compatible with observational constraints, and we now by know that—with the exception of 8–10 $M_\odot$ stars—such simulations do not lead to successful explosions. An important aspect is then to include the knowledge and effects from multi-D simulations into an effective spherically symmetric treatment, which permits to run simulations over a large range of stellar progenitor models. This will be discussed in detail in the next subsection. An important advantage of spherically symmetric models is that sophisticated treatments of the neutrino-matter interactions can be included and that the neutrino spectra and transport are correctly treated in general relativistic space-time. Models of this kind try to address the question of how many neutrinos are emerging from the compactification of an inner stellar core, how is their emission distributed as a function of time and how do these neutrino fluxes generically affect the cooling, heating, or nucleosynthesis in the outer layers of the star without the complication of 3D dynamical fluid instabilities (Liebendörfer et al. 2003, 2004; Fischer et al. 2009, 2010; Martínez-Pinedo et al. 2012). The attempt to combine all these aspects with forefront methods is ongoing in order to achieve the final goal of understanding the multi-D explosion mechanism with up to date microphysics from the equation of state to all neutrino and nuclear interactions.

This includes possible approximate treatments of neutrino transport tested in 1D and then applicable in multi-D approaches (Liebendörfer et al. 2009, 2010) and the test of equation of state effects including a quark-hadron phase transition (Sagert et al. 2009; Fischer et al. 2011; Hempel et al. 2016). A review of the tools to do so is given in Chap. 8.

The phase of stellar core collapse has intensively been studied in spherically symmetric simulations with neutrino transport. The crucial weak processes during the collapse and post-bounce evolution are $\nu + (A, Z) \leftrightarrow \nu + (A, Z)$, $\nu + e^{\pm} \leftrightarrow \nu + e^{\pm}$, $p + e^{-} \leftrightarrow n + \nu_e$, $(A, Z) + e^{-} \leftrightarrow (A, Z-1) + \nu_e$, $\nu + N \leftrightarrow \nu + N$, $n + e^{+} \leftrightarrow p + \bar{\nu_e}$, $(A, Z) + e^{+} \leftrightarrow (A, Z+1) + \bar{\nu_e}$, $\nu + (A, Z) \leftrightarrow \nu + (A, Z)^*$, $(A, Z)^* \leftrightarrow (A, Z) + \nu + \bar{\nu}$, $N + N \leftrightarrow N + N + \nu + \bar{\nu}$, $\nu_e + \bar{\nu_e} \leftrightarrow \nu_{\mu,\tau} + \bar{\nu_{\mu,\tau}}$, $e^{+} + e^{-} \leftrightarrow \nu + \bar{\nu}$. Here, a nucleus is symbolized by its mass number A and charge Z, N denotes either a neutron or a proton and ν represents any neutrino or antineutrino. We note that, according to the generally accepted collapse picture (Bethe 1990; Bethe et al. 1979), elastic scattering of neutrinos on nuclei is mainly responsible for the trapping, as it determines the diffusion time scale of the outwards streaming neutrinos. Shortly after trapping, the neutrinos are thermalized by energy down-scattering, experienced mainly in inelastic scattering off electrons. The relevant cross sections for these processes are discussed in Martínez-Pinedo et al. (2006). The basic neutrino opacity in core collapse is provided by neutrino scattering off nucleons. Depending on the distribution of the nucleons in space and the wavelength of the neutrinos, various important coherence effects can occur: Most important during collapse is the binding of nucleons into nuclei with a density contrast of several orders of magnitude to the surrounding nucleon gas. Coherent scattering off nuclei dominates the scattering opacity of neutrinos (and scales with A^2). Moreover, these neutrino opacities should be corrected by an ion-ion correlation function, this occurs if the neutrino wavelength is comparable to the distances of scattering nuclei and quantum mechanical interference effects appear (Sawyer 2005; Burrows et al. 2006b). Even if current core collapse models include a full ensemble of nuclei in place of the traditional approach with one representative heavy nucleus, it remains non-trivial to adequately determine correlation effects in the ion mixture. Depending on the Q-value of an electron-capturing nucleus, neutrinos are emitted with a high energy of the order of the electron chemical potential/Fermi energy. As the neutrino opacities scale with the squared neutrino energy, the initially trapped neutrinos will down-scatter to lower energies until the diffusion time scale becomes comparable to the thermalization time scale. The thermalization in current collapse models occurs through neutrino-electron scattering because the energy transfer per collision with the light electron is more efficient than with the heavier nucleons. The contribution of inelastic scattering of neutrinos off heavy nuclei depends on the individual nuclei and affects only the high-energy tail of the neutrino spectrum. For latest updates on neutrino opacities and their effect on core-collapse simulations we refer to Burrows et al. (2018).

4.4.2 Early Spherically-Symmetric Modeling

While a number of references in this subsection date back by a decade or more, they give an idea of the evolution of the field still in spherically symmetric approaches but with increasingly sophisticated microphysics included. This will be followed by a short review of present-day multi-D results, before discussing in more detail advanced 1D approximations which take into account the knowledge of the increasing number of multi-D results. Goldreich and Weber (1980) have shown that only the inner $M_{Ch}(Y_e)$ (see the definition in Eq. 4.3) undergo a homologous collapse ($v_{collapse}(r) \propto r$), while at the edge of this core the velocity becomes supersonic and a fraction of the free-fall velocity. The inner core, falling at subsonic velocities where matter can communicate with sound speed, cannot communicate with the free-falling envelope. After the neutrinos are trapped, electron captures and neutrino captures are in equilibrium ($e^- + p \leftrightarrow n + \nu_e$) and the total lepton fraction $Y_L = Y_e + Y_\nu$ stays constant. Y_e stops to decrease and M_{Ch} stops shrinking. Typical values (with the most recent electron capture rates (Langanke et al. 2003) of $Y_L \approx 0.3$ are found in numerical collapse calculations (Hix et al. 2003; Marek et al. 2005) which correspond to $M_{Ch} \approx 0.5\,\mathrm{M}_\odot$. As soon as nuclear densities are reached at the center of the collapsing core, repulsive nuclear forces dominate the pressure in the equation of state. The collapse comes to a halt and matter bounces back to launch an outgoing pressure wave through the core. It travels through the subsonic inner core and steepens to a shock wave as soon as it faces supersonic infall velocities. Hence the matter in the PNS remains at low entropy $\sim 1.4\,\mathrm{k}_B$ per baryon while the supersonically accreting layers become shock-heated and dissociated at entropies larger than $\sim 6\,\mathrm{k}_B$ per baryon. Numerical simulations based on standard input physics and accurate neutrino transport exclude the possibility that the kinetic energy of the hydrodynamical bounce at nuclear densities drives a prompt supernova explosion because of dissociation and neutrino losses.

This can be seen in Fig. 4.12 presenting spherically symmetric calculations of a 13 $\mathrm{M}_\odot$ star. The inner core contains about 0.6 $\mathrm{M}_\odot$ of the initial Fe-core. The transition to free nucleons occurred only in this inner, homologous core and the outward moving shock runs through material consisting of Fe-group nuclei. The dissociation takes 8.7 MeV/nucleon or $8 \times 10^{18}\,\mathrm{erg\,g^{-1}}$. Based on initial shock energies of (4–8) $\times\ 10^{51}$ erg, this is sufficient for passing through 0.25–0.5 $\mathrm{M}_\odot$ and leads in essentially all cases to a stalling of the prompt shock.

While core collapse determines the state of the *cold* nuclear matter inside the PNS, the mass of the hot mantle around the PNS grows by continued accretion. The infalling matter is heated and dissociated by the impact at the accretion front and continues to drift inward. At first, it can still increase its entropy by the absorption of a small fraction of outstreaming neutrinos (heating region). Further in, where the matter settles on the surface of the PNS, neutrino emission dominates absorption and the electron fraction and entropy decrease significantly (cooling region). The tight non-local feedback between the accretion rate and the luminosity is well captured in computer simulations in spherical symmetry that accurately solve the

Boltzmann neutrino transport equation for the three neutrino flavors. All progenitor stars between main sequence masses of 13 and 40 $M_\odot$ showed no explosions in simulations of the post-bounce evolution phase (Liebendörfer et al. 2003). This indicates that the neutrino flux from the PNS does not have the fundamental strength to blow off the surrounding layers for a vigorous explosion. Only recently successful (delayed) explosions could be attained in spherically symmetric models (Sagert et al. 2009; Fischer et al. 2011; Hempel et al. 2016). If a hadron-quark phase transition occurs in the collapsed core at the appropriate time, releasing additional gravitational binding energy in the form of neutrinos from this second collapse, the initially stalled prompt shock can be revived by this QCD effect.

Improved electron capture rates on heavy nuclei overcame the idealized blocking of Gamow-Teller transitions in the traditionally applied single-particle model. In the single-particle picture of nuclei the so-called pf-shell is filled for $Z = 40$ or $N = 40$ for protons or neutrons respectively. Neutron numbers beyond $N = 40$ require a filling of the gd-orbits. If during core collapse nuclei (Y_e) become so neutron-rich that nuclei with $Z < 40$ and $N > 40$ dominate the NSE composition, electron capture would require the conversion of an fp proton to a gd neutron as all pf neutron orbits are filled. This Pauli-blocked transition would lead to the dominance of electron capture on free protons rather than nuclei under such conditions. The recent finding, that configuration mixing and finite temperature effects result in unfilled pf neutron orbits, removes this Pauli-blocking and results in the fact that under these condition electron capture rates on nuclei dominate those on free protons (Langanke et al. 2003). Thus, there are two effects due to the new set of electron capture rates: (1) at low densities for less neutron-rich nuclei the total amount of electron capture is reduced with an improved description of Gamow-Teller transitions (see the discussion of the early collapse phase in Sect. 4.3), (2) at high densities in the late collapse phase the total amount of electron capture is enhanced, leading to smaller Y_e and Y_L values than before. Such changes caused a reduction of homologous core sizes down to $M_{Ch} = 0.5\ M_\odot$ (see discussion above and Hix et al. (2003)). This faster deleptonization in the collapse phase in comparison to captures on free protons alone thus resulted in a 20% smaller inner core at bounce.

When applying all this improved physics in present simulations, a large range of conditions in densities ρ, electron abundance Y_e and entropy s per baryon is encountered where the equation of state or other or other microscopic physics is needed. Figure 4.13 provides this information for a simulation of a 20 $M_\odot$ star (Liebendörfer et al. 2009), i.e. the conditions encountered during the entire simulation in all mass zones involved.

Moreover, a comparison of the effects for a variety of equations of state (see e.g. Oertel et al. 2017) is required. In simulations of massive progenitors that do not explode and exceed the maximum stable mass of the accreting neutron star in the postbounce phase, it was demonstrated that the neutrino signal changes dramatically when the PNS collapses to a black hole (Fischer et al. 2009). Depending on the stiffness of the equation of state or the accretion rate from the external layers of the progenitor star, this can happen at very different time after bounce. Hence, the

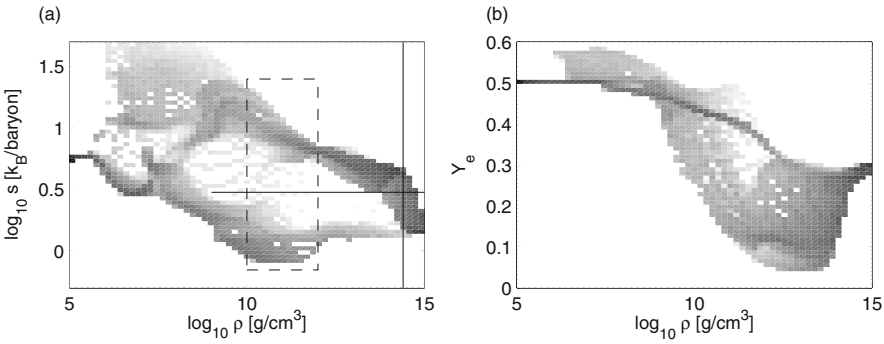

Fig. 4.13 Overview of the conditions attained in a simulation of the collapse, bounce, and explosion (artificially induced) of a 20 $M_\odot$ star. Shown are two histograms of the occurrence of conditions as a function of density ρ, specific entropy s and electron fraction Y_e. The shading of a given bin corresponds to $log_{10}(\int dmdt)$ in arbitrary units, where the integral over mass is performed over the mass dm of matter whose thermodynamic state at a given time falls into the bin. The integral over time extends over the duration of a simulation. Hence, regions of dark shading correspond to states that are experienced by considerable mass for an extended time, while light or absent shading corresponds to conditions that are rarely assumed in the supernova simulation. The vertical black line indicates the nuclear density. The horizontal black line indicates an entropy of 3 k_B/baryon beyond which ions are dissociated. It clearly separates the conditions of cold infalling matter on the lower branch from the conditions of hot shocked matter on the upper branch

neutrino signal carries a clear imprint of the stiffness of the equation of state and the accretion rate to the observer of neutrinos.

The detailed treatment of the neutrino transport and interactions is of great importance for the nucleosynthesis. High electron densities, caused by high Fermi energies of (degenerate) electrons, lead to neutron-rich conditions due to electron captures on free protons. High Y_e material is produced in subsequent ejections, following behind the earlier ejecta, which are strongly affected by neutrino and anti-neutrino captures on protons and neutrons, according to the following reaction sequences

$$\nu_e + n \rightarrow p + e^- \tag{4.4}$$

$$\bar{\nu}_e + p \rightarrow n + e^+. \tag{4.5}$$

These reactions turn matter only neutron-rich if the average anti-neutrino energy $\langle \epsilon_{\bar{\nu}_e} \rangle$ is higher than the average neutrino energy $\langle \epsilon_{\nu_e} \rangle$ by four times the neutron-proton mass difference Δ for similar (electron) neutrino L_{ν_e} and anti-neutrino $L_{\bar{\nu}_e}$ luminosities. This was pointed out initially in Qian and Woosley (1996), leading—when approaching equilibrium conditions for neutrino and antineutrino captures—to

$$Y_e = \left[1 + \frac{L_{\bar{\nu}_e}(\langle \epsilon_{\bar{\nu}_e} \rangle - 2\Delta + 1.2\Delta^2/\langle \epsilon_{\bar{\nu}_e} \rangle)}{L_{\nu_e}(\langle \epsilon_{\nu_e} \rangle + 2\Delta + 1.2\Delta^2/\langle \epsilon_{\nu_e} \rangle)}\right]^{-1}. \tag{4.6}$$

Further details and in-medium corrections for neutrons and protons in comparison to their treatment as free particles are given in Martínez-Pinedo et al. (2012) and Roberts et al. (2012). Thus, in most cases the energetically favorable first reaction (1) wins, changing Y_e from the initial (neutron-rich) conditions towards values beyond $Y_e = 0.5$. A strong νp-process is caused if $Y_e > 0.5$ conditions are attained. In such a case ^{64}Ge is produced in slightly proton-rich conditions of explosive Si-burning. The long beta-decay half-life of ^{64}Ge (which would prevent further processing via proton captures on ^{64}Ga to higher nuclear mass numbers) can be circumvented by an (n, p)-reaction, made possible by neutrons created in antineutrino captures on existing protons in this proton-rich matter. Further proton-captures and fast beta-decays can lead to the production of nuclear masses up to $A = 100$. This has been shown in number of studies (Fröhlich et al. 2006a,b; Pruet et al. 2005, 2006; Wanajo 2006). This also opens an opportunity to investigate neutrino flavor oscillations among electron, muon and tau neutrinos. On the one hand side the long term explosion runs achieve (low) density structures that allow for MSW (Mikheyev-Smirnov-Wolfenstein effect) neutrino flavor oscillations in the outer layers (Wolfenstein 1978; Mikheyev and Smirnov 1985). These may give additional hints on the expansion velocity and density distribution in case that the neutrinos can be observed from a near-by supernova. On the other hand, collective flavor transitions have recently been postulated in regions where the neutrino density exceeds the electron density (Duan et al. 2006, 2007; Fogli et al. 2007). This condition will be achieved in the evacuated zone that surrounds the PNS after the onset of an explosion. The impact of these collective neutrino flavor oscillations on the neutrino heating during the shock expansion, the neutrino wind, and the nucleosynthesis are important points that have recently led to a number of detailed investigation under consideration of accurate neutrino transport and spectra (see e.g. Wu et al. 2014, 2015, 2016b).

4.4.3 Multi-D Simulations: A Short Survey

Initially, spherically symmetric supernova models were the most realistic among all feasible computer representations of the event. With increasing observational evidence for the complexity of the explosions (Hamuy 2003) their primary purpose shifted from a realistic representation to the identification and understanding of the basic principles of the explosion mechanism. This led to the emergence of axisymmetric simulations with sophisticated and computationally intensive spectral neutrino transport (Buras et al. 2003; Walder et al. 2005).

The difficulty to reproduce explosions in spherically symmetric models of core-collapse and post-bounce evolution stimulated the consideration of numerous modifications and alternatives to this basic scenario, mostly relying on multi-dimensional effects that could not be treated in spherical symmetry. It was discussed whether convection inside the PNS could accelerate the deleptonization and increase the neutrino luminosity (Wilson and Mayle 1993). The convective overturn between

the PNS and shock front was shown to increase the efficiency of neutrino energy deposition (Herant et al. 1994). Asymmetric instabilities of the standing accretion shock (Blondin et al. 2003; Foglizzo 2009) may help to push the shock to larger radii and g-mode oscillations of the PNS may contribute to neutrino heating by the dissipation of sound waves between the PNS and the shock (Burrows et al. 2006a). Moreover, it has been suggested that magnetic fields have an impact on the explosion mechanism (Kotake et al. 2006). Most of the above-mentioned modifications of the explosion mechanism are essentially of a three-dimensional nature. In order to illustrate the complexity of the crucial accretion phase we show in Fig. 4.14 a slice through a three-dimensional simulation of core-collapse and post-bounce evolution of a recent run (Liebendörfer et al. 2008). Its input physics uses the Lattimer-Swesty equation of state (Lattimer and Douglas Swesty 1991) and a parameterization of the neutrino physics for the collapse phase (Liebendörfer et al. 2005). The treatment of neutrino cooling and heating in the post-bounce phase is based on multi-group diffusion (the isotropic diffusion source approximation, IDSA, of Liebendörfer et al. 2009).

One goal of core-collapse supernova theory is to explain the mechanism of the explosion in terms of physics. We have learned that in such studies it is necessary to establish numerical simulations which include complicated multi-dimensional radiation hydrodynamics, that is, codes which incorporate the inter-related neutrino, nuclear, and gravitational physics. Then we demand that such codes reproduce explosions in a robust way. So, simulations should predict asymptotic explosion energies which are consistent with observations, the resulting neutron star masses, and last but not least the accompanying nucleosynthesis.

Many references reflect progress in this field (see Hix et al. 2003, 2016; Liebendörfer et al. 2005; Marek et al. 2005; Burrows et al. 2006a; Sumiyoshi et al. 2007; Langanke et al. 2008; Marek and Janka 2009; Janka 2012; Burrows 2013; Takiwaki et al. 2014; Lentz et al. 2015; Melson et al. 2015; Nakamura et al. 2015; Janka et al. 2016; Bruenn et al. 2016). An excellent and extended discussion has been given by Burrows et al. (2018) on successes, convergence, on similar and contradictory results. Rather than repeating such here, we draw and state as the main results that (1) 2D simulations seem to lead more easily to explosions than those in 3D (but not necessarily giving larger explosion energies), and (2) a key issue for successful explosions is the compactness of the central part of the progenitor star, or, related, the binding energy of the envelope. Explosions can be obtained for a large range of progenitor masses, even up to and beyond $40\,M_\odot$, while black hole formation can occur also for lighter object (e.g. in the range 20–$30\,M_\odot$) and for the more massive ones.

An example for the complexity of such multi-D simulations is given in Fig. 4.14, indicating entropy, magnetic field strength, and matter velocities from a 3D simulation with the Basel code ELEPHANT. A detailed comparison of a set of codes (SPH, FLASH, ELEPHANT, and fully relativistic M1) actually leads to very similar results for the same input physics, which is a positive indication for convergence on numerical aspects.

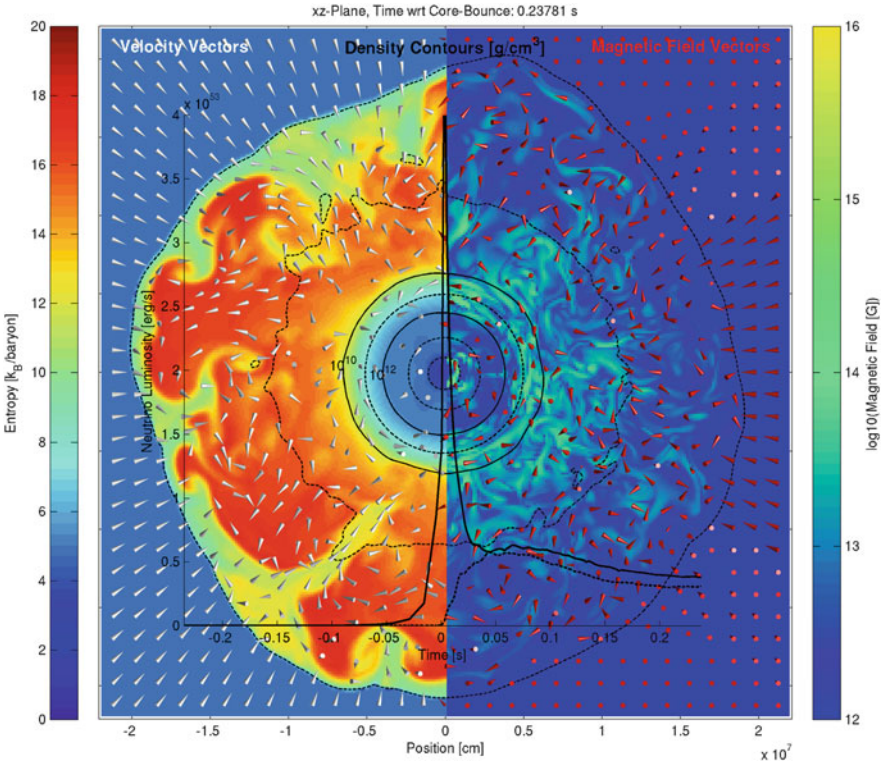

Fig. 4.14 Illustration of the early accretion phase in a three-dimensional simulation with a resolution of 600^3 zones and the isotropic diffusion source approximation for 3D neutrino transport (Liebendörfer et al. 2009). Shown are density contours as black lines for a 15 $M_\odot$ star from Woosley and Weaver (1995). *Left:* The color indicates the specific entropy and the cones the direction of the velocity. *Right:* The color refers to the magnetic field strength and the cones to its direction. The cool high-density interior of the PNS and the hot low-density accreted matter behind the standing accretion front are clearly distinguishable. Also shown is the luminosity of electron neutrinos (solid line) and electron antineutrinos (dashed line) as a function of time

Few and preliminary nucleosynthesis results exist from multi-dimensional simulations, e.g. Wanajo et al. (2011), Harris et al. (2017), Eichler et al. (2018), Wongwathanarat et al. (2017), and Yoshida et al. (2017). We show here the results of a detailed nucleosynthesis study by Eichler et al. (2018), based on long-term, two-dimensional core-collapse supernova simulations of an 11.2 $M_\odot$ star (Nakamura et al. 2015). This CCSN model shows an axisymmetric neutrino-driven explosions of a non-rotating, solar metallicity model. The numerical treatment was described in Nakamura et al. (2015), including spectral transport of electron and anti-electron neutrinos, using the isotropic diffusion source approximation (IDSA Liebendörfer et al. 2009) and a Lattimer and Swesty equation of state (Lattimer and Douglas Swesty 1991) with compressibility $K = 220$ MeV. After a successful shock revival,

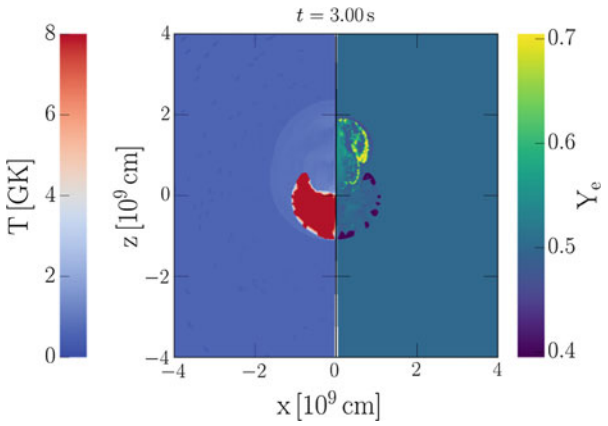

Fig. 4.15 Distribution of temperature and Y_e during the SN explosion of a 12.7 $M_\odot$ star at t = 3s, based on a 2D simulation (Nakamura et al. 2015). It can be seen that Y_e values >0.5 and <0.5 exist, dependent on the initial core-collapse phase with high electron capture effects and electron neutrino and antineutrino absorption on neutrons and protons during the explosion, see Eichler et al. (2018)

the axis-symmetric nature of the simulation causes a preference of the outflow towards polar directions (see Fig. 4.15).

This behavior is usually not observed in 3D simulations of regular CCSNe, since they do not have an imposed symmetry. Explosion times and energies are also different between 2D and 3D simulations, with 2D simulations being usually "more optimistic" to obtain successful explosions, as is shown e.g., in Takiwaki et al. (2014), Lentz et al. (2015), Melson et al. (2015), Janka et al. (2016), and Hix et al. (2016). In these simulations it is found that nuclei well beyond the iron group (up to $Z \approx 44$) can be produced, including the p-nuclei ^{92,94}Mo and ^{96,98}Ru (see Fig. 4.16). While ^{92}Mo and ^{94}Mo can be produced in slightly neutron-rich conditions, ^{96,98}Ru can only be produced efficiently via the νp-process, which depends heavily on the presence of very proton-rich material in the ejecta, obtained in polar outflows. Figure 4.15 shows the Y_e distribution of ejecta 3s after bounce. One realizes low Y_e material (<0.5) in early outflows (typically at the outer edges of ejecta) which still have values close to the ones inherited from core collapse. The effect of neutrinos on Y_e and the working of the νp-process was discussed in the previous subsection.

4.4.4 *Spherically-Symmetric Simulations, New Generation*

3D simulations show many effects that result from implementation details of the physics involved, and will at the end be used as a method to also describe the nucleosynthesis of the ejecta. But for a large set of supernova progenitor models they

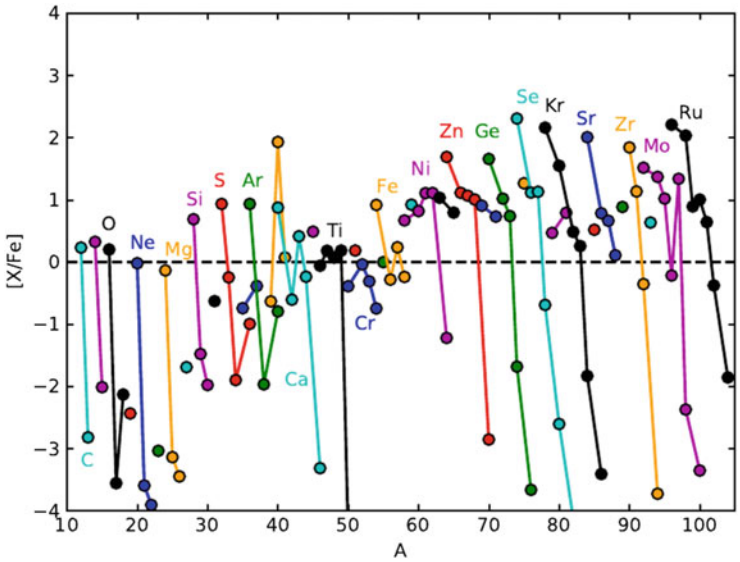

Fig. 4.16 Nucleosynthesis features of a 12.7 $M_\odot$ SN explosion from a 2D simulation (Nakamura et al. 2015), featuring a strong νp-process with the production of nuclei up to A = 100 (see also Eichler et al. 2018)

are still computationally extremely expensive. Therefore, spherically symmetric models still have several assets in supernova modeling. Taking the lessons from 3D on the explosion mechanism, explosions can be artificially launched by introducing a specific additional energy input. Early investigations with the main aim of finding the nucleosynthesis effects were just phenomenological: Artificially, explosions were induced via a "piston", or energy deposition in terms of a "thermal bomb". More realistic approaches add the energy which leads to explosions based on insight from multi-D simulation studies and their inferred behavior. This is an important step towards "self-consistent" treatment including neutrino transport, which is necessary to analyse the effect of neutrinos on the nucleosynthesis of the innermost ejecta.

The past simplified approaches artificially induced explosions with estimates for typical explosion energies. First attempts to predict supernova nucleosynthesis in this way induced the explosion energy through pistons (e.g. Woosley and Weaver 1995), or through thermal energy bomb models (e.g. Thielemann et al. 1996; Umeda and Nomoto 2008), or kinetic energy bomb models (e.g. Limongi and Chieffi 2006b, 2012; Chieffi and Limongi 2013, 2017). In the first case, the motion of a mass shell is imposed along a ballistic trajectory with a typical explosion energy of $E = 1.2\text{B} = 1.2 \times 10^{51}$ erg at a radial position related to a value of the entropy that was expected to result in the most realistic mass cut (i.e., the bifurcation between the PNS and the ejecta). In the latter cases, explosions are triggered by adding typical kinetic or thermal energies to a specific mass zone (usually in deeper zones). The

mass cut was then determined by integrating the nucleosynthesis yields from the outside inwards, up to the point where the observationally indicated amount of ^{56}Ni was reached. In all cases the explosion energy is not determined self-consistently, and the physics of the explosion is not included. The mass cut and the explosion energy are free parameters of the model and have to be constrained from the yields of the innermost ejecta, separately for each progenitor. These approaches are suitable for the outer layers, where the nucleosynthesis mostly depends on the strength of the shock wave.

Interim approaches beyond piston or thermal bomb models of Woosley and Heger (2007), Heger and Woosley (2010), Limongi and Chieffi (2006b, 2012), Nomoto et al. (2006, 2013), Nomoto (2017), and Chieffi and Limongi (2017) exist by now, trying to mimic multi-D neutrino heating in a spherical approach, in order to obtain more appropriate predictions of the explosion energy, mass cut between neutron star and ejecta, as well as nucleosynthesis (including the effects of neutrinos on Y_e, the proton/nucleon ratio). This includes the "neutrino light-bulb" method, where the PNS is excised and replaced with an inner boundary condition which contains an analytical prescription for the neutrino luminosities. Suitable choices of the neutrino luminosities and energies can trigger neutrino-driven explosions (e.g. Yamasaki and Yamada 2005; Iwakami et al. 2008; Yamamoto et al. 2013). In "absorption methods" (Fröhlich et al. 2006a,b; Fischer et al. 2010) the increase in the neutrino energy deposition is obtained by modifying the neutrino opacities in spherically symmetric models with detailed Boltzmann neutrino transport, i.e. this means that neutrino-capture rates are multiplied by a factor, causing additional ν-heating, in order to trigger explosions. This led to the prediction of Y_e-values affected by the central neutrino flux (see Fig. 4.17), improving strongly the Fe-group composition due to the discovery that proton-rich conditions are attained in the innermost ejecta (see the discussion on the effect of neutrino and antineutrino capture in Sect. 4.4.2).

One of the lessons from these investigations was the discovery of the νp-process, also discussed in Sect. 4.4.2. Both aspects led to an improvement of nucleosynthesis predictions for Fe-group nuclei and opened an explanation for understanding light p-nuclei, which cannot be produced in the typical p/γ-process in explosive burning of outer stellar shells, i.e. the Ne-shell. The major drawback of these methods is, however, either the explicit modification of the electron neutrino and antineutrino luminosities or the modification of neutrino opacities, which (while apparently improving nucleosynthesis results) could directly impact the composition of the innermost ejecta in a non-consistent way.

Recent (spherically symmetric) approaches try to mimic the effect of multi-D neutrino transport in a way adapted more consistently to core-collapse and proto-neutron star accretion. They need, however, calibrations which can be provided by comparison with a variety of observations of explosion energies, deduced ejected ^{56}Ni-masses, and progenitor properties. Ugliano et al. (2012) presented a more sophisticated light-bulb method to explode spherically symmetric models, using neutrino energy deposition in post-shock layers. They used an approximate, grey neutrino transport and replaced the innermost 1.1 $M_\odot$ of the PNS by an inner

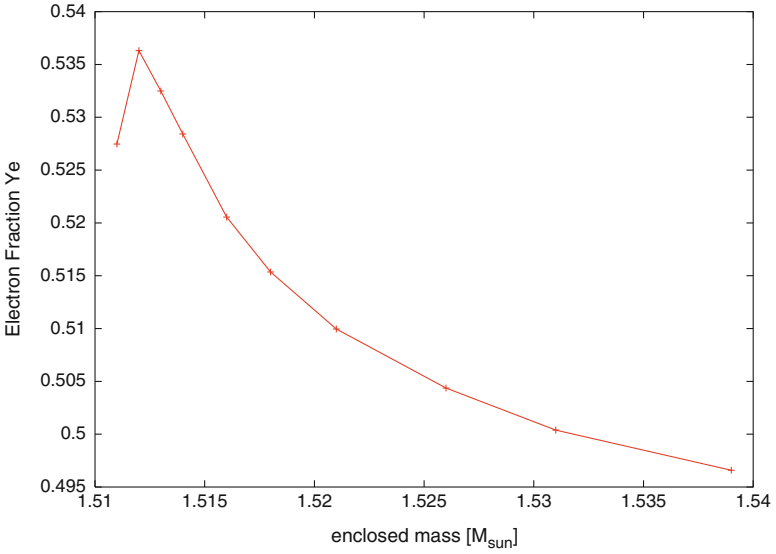

Fig. 4.17 Y_e of the innermost ejecta due to neutrino interactions with matter. At high temperatures electrons are not degenerate, thus the reduction of Y_e due to electron captures is ineffective. For similar neutrino and antineutrino spectra the neutron-proton mass difference favors $\nu_e + n \leftrightarrow p + e^-$ over $\bar{\nu}_e + p \leftrightarrow n + e^+$ (from Fröhlich et al. 2006a)

boundary. The evolution of the neutrino boundary luminosity was based on an analytic cooling model of the PNS, which depends on a set of free parameters. These parameters (within the so-called PHOTB approach) are set by fitting observational properties of SN 1987A for progenitor masses around 20 $M_\odot$ (see also Ertl et al. 2016; Sukhbold et al. 2016). Perego et al. (2015) utilize the energy in muon and tau neutrinos as an additional energy source that approximately captures the essential effects of (3D) neutrino transport (the PUSH method which is discussed in more detail below). Both approaches make it possible to predict the variation of explosion energies (and other parameters like neutron star mass cuts) as a function of stellar mass and thus can provide improved nucleosynthesis yields for chemical evolution modeling. There exist detailed results by now from PHOTB, but only PUSH includes the Y_e-effects due to neutrino interactions with nuclei, which is highly important for the Fe-group composition.

A major open question is whether core collapse leads finally to a supernova explosion with a neutron star remnant or whether the final outcome is a central black hole. Expectations from observations and their interpretation (e.g. Nomoto et al. 2006, 2013) would argue for a gradual transition between these two regimes as a function of initial stellar mass. PHOTB (Sukhbold et al. 2016) shows that both possible outcomes can occur within the same mass interval, mainly dependent on the pre-collapse stellar model and its compactness parameter. This needs further investigations and might pose questions about the stellar models. Could such scatter

of the pre-core-collapse models in a narrow mass range, which is due to the properties of the last Si-shell burning stages, be avoided in general by the inclusion of rotation, leading possibly to a smearing out of radial gradients? The transition from central neutron star to black hole remnants can involve the effect of fallback of material from the innermost regions as a result of the outgoing shock wave being reflected by density gradients, causing a reverse shock. A pragmatic solution, utilizing a combination of mixing and fallback, can on the one hand minimize the effect of inconsistent Y_e-values in the innermost regions for approximated spherical models which do not include neutrino interactions (i.e. of the piston or bomb type). This mixes some Fe-group nuclei to larger radii, while the fallback reduces in total the ejected amount of Fe-group elements and can this way create overall C-rich ejecta, as observed in some extremely low metallicity stars. Such behavior is suggested to stem from some very massive stars, possible being more frequent in the early Galaxy (Nomoto et al. 2006, 2013). However, in the following we want to concentrate on the recent advances within the PUSH method.

The PUSH method provides a computationally efficient and physically motivated framework to explode massive stars in spherical symmetry. It allows to study multiple aspects related to core-collapse supernovae that require modeling of the explosion for a duration of several seconds after its onset, and also for extended sets of progenitor models. The PUSH method was primarily designed to study explosive nucleosynthesis, but it is also well suited to explore other relevant aspects, including the effects of the shock passage through the star, the neutron star mass distribution, and the distribution of the explosion energies. PUSH relies on the so-called delayed neutrino-driven mechanism as a central engine of core-collapse supernovae. In particular, it provides an artificially enhanced neutrino energy deposition inside the gain region, inspired by the increase of the net neutrino heating that a fluid element experiences due to the presence of multi-dimensional effects. Unlike other methods (that employ external energy sources or that use modified electron flavor neutrino luminosities), a fraction of the energy carried away by heavy flavor neutrinos ($\nu_x = \nu_\mu, \bar{\nu}_\mu, \nu_\tau, \bar{\nu}_\tau$) is deposited behind the shock, in order to ultimately provide successful explosion conditions. In self-consistent core-collapse models, the ν_x's present a marginal dependence on the temporal evolution of the accretion rate (e.g. Liebendörfer et al. 2004), and their contribution to the energy deposition inside the gain region is negligible. Including them in PUSH nevertheless presents a number of advantages towards a more realistic nucleosynthesis: As one of these, the properties of the ν_x emission, which includes dynamical feedback from accretion history, as well as cooling properties of the forming compact object, correlate significantly with the main features of the ν_e and $\bar{\nu}_e$ emission (O'Connor and Ott 2013). As another, the accretion luminosity depends not only on the accretion rate but also on the evolution of the mass and radius of the PNS, which is treated accurately and self-consistently in this method. This achieves an explosion trigger in 1D simulations without modifying ν_e and $\bar{\nu}_e$ luminosities nor changing charged current reactions. It increases the accuracy of electron fraction treatment for the innermost ejecta, which is a crucial ingredient for nucleosynthesis. In addition, unlike the electron (anti-) neutrino luminosities, which decrease suddenly once the shock has been revived

in spherically symmetric models, ν_x luminosities are only marginally affected by the development of an explosion. This allows PUSH to continue injecting energy inside the expanding shock for a few hundreds of milliseconds after the explosion has set in. A first implementation of the PUSH method was presented in Perego et al. (2015). The hydrodynamical evolution in spherical symmetry uses the general relativistic hydrodynamics code AGILE (Liebendörfer et al. 2001). For the stellar collapse, the deleptonization scheme of Liebendörfer (2005) was applied. The Isotropic Diffusion Source Approximation (IDSA) was employed for the electron neutrino and anti-neutrino transport (Liebendörfer et al. 2009), while the heavy-lepton flavor neutrinos were modelled by an Advanced Spectral Leakage scheme (ASL, Perego et al. 2016). An extended Equation of State (EOS), comprising both nuclear statistical equilibrium (NSE) and non-NSE conditions, was included in the model. For the former, the tabulated microphysical EOS HS(DD2) was employed (Hempel and Schaffner-Bielich 2010), while for the latter an ideal gas of electrons, positrons, photons and 25 representative nuclei from neutrons and protons to iron-group nuclei was used. For conditions not permitting to use NSE, the changes in nuclear composition were followed by an approximate α-network.

PUSH is not a fully self-consistent method, it requires a calibration of the free parameters $k_{\rm push}$ and $t_{\rm rise}$. This has been done comparing explosion and nucleosynthetic properties with those observed for SN 1987A (Woosley et al. 2002). Such calibration ensures that the artificially increased heating efficiency has an empirical foundation and the model has a predictive power in the sense of an effective model.

The analysis of explosion models with a broad parameter exploration revealed a clear dependence on the compactness of the progenitors. This is defined as ξ_M (O'Connor and Ott 2011), with $\xi_M \equiv (M/M_\odot) \,/\, (R(M)/1000{\rm km})$, where $R(M)$ is the radius of the enclosed mass M, computed for $M = 1.75\,{\rm M}_\odot$ at the onset of the collapse. The requirement of an explosion energy around 1 Bethe was achieved only by progenitors with a moderately high compactness parameter. Explosions tend to set in earlier, with lower explosion energies and lower remnant masses in the case of progenitors with low compactness. For high-compactness progenitors, explosions are more difficult to achieve and require more time to develop. However, when they occur, they are more energetic and produce more massive proto-neutron stars. These differences plausibly relate to different accretion histories: For high compactness, neutrino luminosities are larger and neutrino spectra are harder, due to the larger accretion rates. In order to overcome the stronger ram pressure at the shock front, a more intense neutrino energy deposition is required.

All the simulations start from a progenitor star including all mass up to the helium shell, corresponding to a radius of $R \approx (1.3\text{–}1.5) \times 10^{10}\,{\rm cm}$. Simulations were run for a total time of 5 s, corresponding to $\gtrsim 4.6\,{\rm s}$ after core bounce. During this time, the shock was always contained inside the computational domain. Tracer mass elements (shells) were extracted from the simulation and post-processed with the `WINNET` (Winteler et al. 2012) nuclear network.

Initial calibration attempts found a systematic overproduction of ^{56}Ni for runs with an explosion energy around and above 1 Bethe. This discrepancy was cured

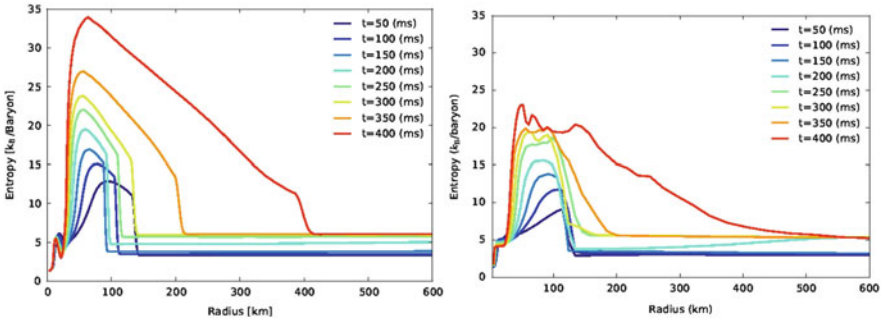

Fig. 4.18 Radial profiles of the spherically averaged entropy per baryon obtained from a spherically symmetric simulation with PUSH (left panel) and from a axisymmetric Flash simulation (right panel) of a 20 $M_\odot$ progenitor

by invoking a relatively large amount of fallback (0.1 $M_\odot$). The more recent implementations achieve a satisfactory agreement with SN 1987A observables without invoking any fallback (Ebinger et al. 2017, 2018), when using dedicated blue supergiant progenitors and slightly different parameters than those in Perego et al. (2015). As a result, the SN 1987A remnant should host a neutron star with a baryonic mass of $\sim$1.66 $M_\odot$, corresponding to a gravitational mass of $\sim$1.50 $M_\odot$ for a cold neutron star with the HS(DD2) EOS. The formation of a black hole seems unlikely, as a very large fallback ($\gtrsim$ 0.5 $M_\odot$) would be required to reach the observed neutron star maximum mass limit, and an even larger fallback ($\sim$1.3 $M_\odot$) to reach the maximum neutron star baryonic mass as predicted by the HS(DD2) EOS.

In Fig. 4.18 the spherically averaged entropy per baryon as a function of radius is shown, obtained (a) from a 2D Flash simulation (Pan et al. 2016), see right panel, and (b) from a 1D simulation performed with PUSH for the same progenitor (see left panel). The PUSH method presents a behavior more consistent with multi-dimensional models than older methods (e.g. pistons and thermal bombs) (Ebinger et al. 2017, 2018).

This method also allows to explore other important stellar collapse features, such as their explodability versus the formation of a stellar black hole (BH) from a failed supernova, over a large set of progenitors. Figure 4.19 shows the explosion energy obtained with PUSH for a set of progenitor models that encompasses a large portion of the mass range for core collapse progenitors (IMF). We see a rise in explosion energies up to about 18–20 $M_\odot$ (accompanied by an increasing compactness of the stellar models). Similar to Sukhbold et al. (2016) one can see that there is a transition to BH formation beyond 20 $M_\odot$, but that still individual models above that mass range can experience explosions, while BHs can also form for some lower mass progenitors. The window above 20 $M_\odot$, where BHs are formed, is followed by a range where explosions are possible again, continuing to a general tendency to black hole formation above 35 $M_\odot$. This procedure has been carried through for a number of stellar model samples, also from Heger and Woosley (and for different metallicities). The results differ in detail; dependent on the compactness of stellar

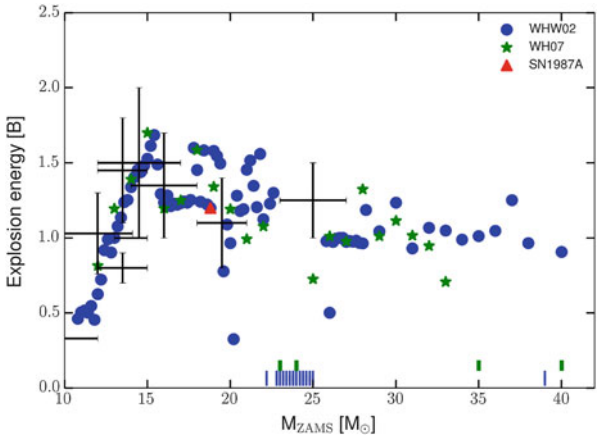

Fig. 4.19 Explosion energies as a function of progenitor mass deduced from observations (Nomoto et al. 2013) (black crosses) and predicted from PUSH simulations (Ebinger et al. 2017, 2018) for two sets of progenitor models (blue dots Woosley et al. 2002) and (green stars Woosley and Heger 2007). Dashed vertical lines close to the abscissa indicate no explosions (in blue and green for the two sets, mentioned above), i.e. black hole formation in PUSH simulations in the range 22–25 $M_\odot$ and beyond 33 $M_\odot$

models, black hole formation can also occur in some cases for lower initial masses, but the general tendency remains (Ebinger et al. 2017, 2018). Clearly, there is strong dependence of the core-collapse outcome on the detailed structure of progenitor models, hence on accurate modeling of the entire stellar evolution.

We conclude to state that improved spherically-symmetric modeling approaches such as PHOTB and PUSH provide for the first time results with self-consistent values for supernova explosion energies and resulting neutron star masses, as well as the transition to black hole formation. Thus, this modeling also permits to predict the transition from regular CCSNe to faint or failed supernovae. But, as the present models do not include stellar rotation nor magnetic fields, predictions of the hypernova branch, leading to long-duration gamma-ray bursts, cannot be made within this approach. On the other hand, the correct inclusion of electron neutrino and antineutrino interactions with matter permit also to predict reliable values of the electron fraction Y_e and therefore also a reliable prediction for nucleosynthesis with the detailed isotopic composition of the Fe-group.

4.5 Exotic Explosions: Hypernovae, Gamma-Ray Bursts, Neutron Star Mergers

Massive stars in the range of 8–$\sim$ 130 $M_\odot$ undergo core-collapse at the end of their evolution and become Type II and Ib/c supernovae, unless the entire star collapses into a black hole with no mass ejection (Heger et al. 2003). Such Type

II and Ib/c supernovae (as well as Type Ia supernovae, see Chap. 5) release large explosion energies and eject matter which experienced explosive nucleosynthesis. So, they have a strong dynamical, thermal, and chemical influence on the evolution of interstellar matter and of galaxies as a whole.

The explosion energies of core-collapse supernovae are fundamentally important quantities, and an estimate of $E \sim 1 \times 10^{51}$ erg has often been used in calculating nucleosynthesis and the impact on the interstellar medium. (Here we use the explosion energy E for the final kinetic energy of the explosion.) A close-by example is SN1987A in the Large Magellanic Cloud, whose energy is estimated to be $E = (1.0 - 1.5) \times 10^{51}$ ergs from its early light curve.

But without rotation and magnetic fields, simulations show that more massive objects will end up as black holes, even in multi-D simulations. In that case a major question is, at which progenitor mass the turnover takes place from successful explosions with neutron star formation to black holes as the final outcome (if there exits such a clear limit!). The previous section addressed this transition to faint or failed supernovae by advanced recent spherically symmetric approaches (i.e., emulating 3D effects). Here we show a case of a 2D simulation which leads to black hole formation after core-collapse of a non-rotating 40 $M_\odot$ progenitor star (Pan et al. 2017). This study also makes use of the isotropic diffusion source approximation (IDSA) for the transport of electron flavor neutrinos and a modified gravitational potential for general relativistic effects. It was performed for four different neutron star equations of state (EoS), including LS220, SFHo, BHB$\Lambda\Phi$ and DD2, examining the impact of the equation of state on black hole formation dynamics and gravitational wave emissions. The simulations utile the FLASH code (Fryxell et al. 2000).

It is found that the black hole formation time is sensitive to the equation of state and is delayed in multiple dimensions due to finite entropy effects that enlarge the maximum proto-neutron star (PNS) mass and via proto-neutron star convection. Depending on the equation of state, these simulations also show the possibility that the shock is revived together with the formation of a black hole. Figure 4.20 displays the behavior of the average shock radius as a function of time. In Fig. 4.21 the multi-D behavior is indicated, utilizing the EoS SFHo (Oertel et al. 2017). Convective regions, where neutrino heating takes place, are characterized by negative Brunt-Väisälä frequencies. Here not only the average but also the maximum shock radius is given as a function of time. We see that the radius of the PNS recedes, finally forming a black hole.

There exist similar results with the aid of fully relativistic 3D simulations (Kuroda et al. 2018), which indicate stellar mass black hole formation in failed supernovae for models without rotation, being responsible for the faint branch of the so-called Nomoto plot (Nomoto et al. 2013).

The key questions that remain are:

- do 8–10 $M_\odot$ stars which produce an Fe-core in a collapse initiated via electron capture after core He-burning (electron capture supernovae) have a different explosion mechanism than more massive stars? Is here only a small amount of material involved outside the collapsing C-core and little Ni-ejection occurring?

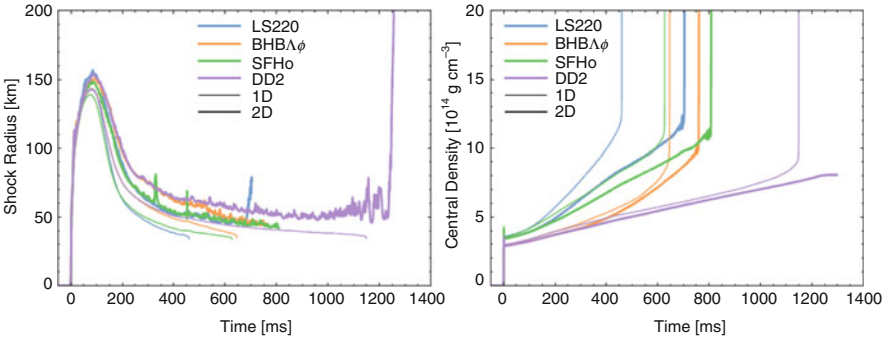

Fig. 4.20 Time evolution of averaged shock radius (left) and central density (right). Different colors represent simulations with different nuclear EoS. Thick and thin lines indicate simulations in 2D and 1D respectively. Except for EoS DD2, all utilized EoSs lead to black hole formation (Pan et al. 2017)

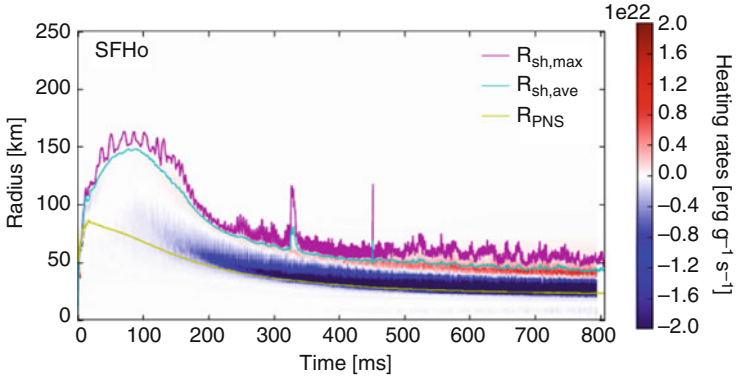

Fig. 4.21 Color maps of the Brunt-Väisälä frequency as a function of time and radius. Negative values, indicated by the red color represent unstable regions based on the Ledoux criterion for convection. These are the regions where convective overturn takes place and neutrino heating is active. The magenta and light blue lines show the maximum and averaged shock radius. The yellow line indicates the radius of the PNS (Pan et al. 2017)

- for which stellar progenitor masses do we have a transition from the formation of neutron stars to the formation of black holes after collapse?
- to which extent is this transition region influenced by the nuclear equation of state?
- for which transition region are initially neutron stars formed, causing a regular supernova explosion, but followed by fall back from the reverse shock that swallows inner matter, leading to a small final Ni-ejection and faint light curves?
- for which progenitor masses are black holes formed directly during collapse and how can this be observed?

- what is the role of rotation and magnetic fields with respect gamma-ray bursts/hypernovae?
- can we give reliable nucleosynthesis yields for such events?

So far we have covered most of these items, except for the last two. Thus, how can the hypernova branch of existing observations with high to very explosion energies, even for massive stars, be explained?

4.5.1 Hypernovae/Long Duration Gamma-Ray Bursts/Collapsars

One of the most interesting developments in the study of supernovae (SNe) is the discovery of some very energetic supernovae (see e.g. Nomoto et al. 2006), whose kinetic energy (KE) (in spherically symmetric analysis, see also Piran 2004) exceeds 10^{52} erg, about 10 times the KE of normal core-collapse SNe (hereafter $E_{51} = E/10^{51}$ erg). The most luminous and powerful of these objects, the Type Ic supernova (SN Ic) 1998bw, was probably linked to the gamma-ray burst GRB 980425, thus establishing for the first time a connection between (long-duration) gamma-ray bursts (GRBs) and the well-studied phenomenon of core-collapse SNe. However, SN 1998bw was exceptional for a SN Ic: it was as luminous at peak as a SN Ia, indicating that it synthesized $\sim 0.5\,M_\odot$ of ^{56}Ni, and its KE was estimated at $E \sim 3 \times 10^{52}$ erg.

Before going into a too involved discussion of the causes of these events, let us first consider the possible effect which higher energy explosions have on the ejecta, i.e. nucleosynthesis products. Here we use the term 'hypernova' to describe an extremely energetic supernova with $E \geq 10^{52}$ erg without specifying the explosion mechanism (Nomoto et al. 2001). Following SN 1998bw, other *hypernovae* of Type Ic have been discovered or recognised. Nucleosynthesis features in such hyper-energetic supernovae must show some important differences in comparison to normal supernova explosions. The higher explosion energies could lead to larger ejected ^{56}Ni masses, as observed in such explosions. They also cause higher entropies in the innermost ejecta, which result in a more extreme alpha-rich freeze-out from explosive Si-burning. Such conditions permit the sizable production of Fe-group nuclei beyond ^{56}Ni, up to ^{64}Ge which decays to ^{64}Zn (Nakamura et al. 2001). This feature could have an influence on abundance patterns observed in extremely metal-poor halo stars. In fact, the observational finding that Zn behaves like an Fe-group element in galactic evolution - and was underproduced in existing supernova models (which were not including the νp-process)—was used as a strong argument that a large fraction of massive stars explode as hypernovae (Nomoto et al. 2006, 2013; Kobayashi et al. 2006; Nomoto 2017).

We know that for non-rotating cases only the supernova branch (with neutron stars as final outcome) can be attained, and the faint or failed supernova branch (leading eventually to black holes, but not to gamma-ray bursts and high ejecta

masses). Thus, massive stars, which fail to explode as CCSNe via neutrino-powered explosions, will eventually experience the formation of central black hole (BH) remnants. However, rotating BHs and the formation of accretion disks with accretion rates of about $\approx 0.1\,M_\odot$/s can lead—for certain conditions (strong magnetic fields)—to long duration gamma-ray bursts (lGRBs) or hypernovae (Nomoto's hypernova branch), also dubbed collapsars as they result from a core-collapse to the formation of a black hole. Many authors have contributed to the discovery and shaping of first ideas for theoretical explanations (e.g. Klebesadel, Bloom, Paczynski, Mezaros, Rees, Piran, see the review by Piran (2004)). The collapsar model was proposed by Woosley, MacFadyen and others (see also MacFadyen and Woosley 1999; MacFadyen et al. 2001; Nagataki et al. 2007; Sekiguchi and Shibata 2011; Nagataki 2011), based on neutrino heating from the accretion disk and/or the winding of strong magnetic fields and MHD jets (McKinney et al. 2013; Ono et al. 2012). Hydrodynamic simulations (injecting explosion energies artificially) were performed by Umeda, Nomoto, Maeda, Iwamoto, Nagataki, either by introducing high explosion energies (up to 10^{52} erg) in a spherically symmetric way or aspherically in order to understand jet-like explosions (Nakamura et al. 2001; Nomoto et al. 2006, 2013; Nomoto 2017). The role of weak interactions and resulting nucleosynthesis was the focus of contributions by Pruet, Surman, McLaughlin, Hoffman, Hix, Janka, Ruffert, Fuller, Lemoine, Inoue, Fujimoto, Beloborodov, Janiuk (for specific nucleosynthesis results see e.g. Surman et al. 2006; Janiuk 2014). The basic (consensus) picture is the following: explosion energies can be found up to 5×10^{52} erg, ^{56}Ni ejecta up to $0.5\,M_\odot$, and the ejecta are beamed with relativistic jets. Many attempts have been undertaken to model such events. There exists uncertainty in predicting Y_e, due to weak interactions and especially neutrino transport in disks and jets, but there exists also the constraint of high ^{56}Ni ejecta. Therefore, the dominant Y_e in matter has to be of the order of 0.5. High explosion energies lead to high entropies and a strong alpha-rich freeze-out, including interesting amounts of ^{45}Sc, ^{64}Zn (from ^{64}Ge-decay) and other Fe-group elements. For general and more detailed considerations see Nomoto (2017), concluding that larger abundance ratios for (Zn,Co,V,Ti)/Fe and smaller (Mn,Cr)/Fe ratios are expected than for normal SNe, which seems to be consistent with observations in extremely metal-poor (EMP) stars, as will be discussed later.

4.5.2 MHD-Driven Supernovae/Magnetars

Recent observations (and their interpretation) (Greiner et al. 2015; Bernardini 2015) underline that there exist core-collapse supernova explosions whose light curves are not determined by (large) amounts of ^{56}Ni ejecta, but rather by the energy release of a fast rotating neutron star (pulsar) with extremely strong magnetic fields of the order 10^{15} G (magnetars). The question is how can neutron stars of such extremely high magnetic fields (in comparison to the typical 10^{12} G) emerge from a supernova explosion? A reasonable assumption is that such objects originate from massive

stars which are fast rotators with initially also rather strong magnetic fields. Such objects, with assumptions made for the initial rotation rate and magnetic fields, have been modeled extensively (Fujimoto et al. 2007, 2008; Winteler et al. 2012; Mösta et al. 2014, 2015, 2017; Nishimura et al. 2015, 2017b; Halevi and Mösta 2018) and will be called here magneto-rotational or MHD-jet supernovae. The result is typically (when starting with very large initial fields of the order 10^{12} G) that the winding up of magnetic fields results in strong magnetic pressure along the polar rotation axis and jet-like ejection of matter. This matter has experienced high densities (and thus degenerate electrons with high Fermi energies), leading via electron captures on protons and nuclei to strongly neutron-rich matter with a Y_e of the order 0.1–0.15. The fast ejection along the poles avoids that the interaction with neutrinos and anti-neutrinos causes a major rise of Y_e (see Eqs. (4.5)–(4.6)). Such conditions permit a strong r-process, dependent on the initial magnetic field strength and rotation rate (Winteler et al. 2012; Nishimura et al. 2015, 2017b; Mösta et al. 2017; Halevi and Mösta 2018). In this process, due to a high fraction of neutrons per nucleus after the freeze-out of charged-particle reactions during the expansion at $\approx 3 \times 10^9$ K, rapid neutron capture can occur, leading to nuclei far from stability with extremely short beta-decay half-lives and the production of heavy nuclei up to the actinides. In Fig. 4.22 we show the nucleosynthesis results of the 3D collapse of a fast rotator with a strong initial magnetic field of 5×10^{12} G in z-direction before core collapse. A 15 $M_\odot$ progenitor with an initial shellular rotation with period of 2 s at a 1000 km radius results in a rare class of supernovae with a central magnetar and negligible amounts of Fe-group ejecta. Initial results (Winteler

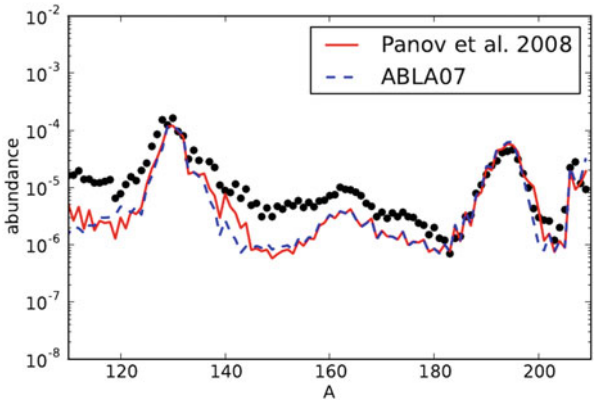

Fig. 4.22 Nucleosynthesis features of an MHD-jet supernova, originating from a 15 $M_\odot$ progenitor with a 5×10^{12} G magnetic field of the collapsing Fe-core. The original simulation (Winteler et al. 2012) showed that the second and third t-process peak could be reproduced very well with a $Y_e = 0.1 - 0.15$ of the ejecta, but big troughs occurred below and above the second r-process peak at A = 130. Utilizing more modern fission fragment distributions (here ABLA07 and Panov08, Kelic et al. 2008; Panov et al. 2008) improved these features strongly for not extremely neutron-rich environments with only weak fission-cycling

et al. 2012) made use of older fission fragment distributions. Figure 4.22 shows the effect of more modern fission yields which avoid the abundance troughs below and above the A = 130 peak. This result should be compared to other investigations (Shibagaki et al. 2016), which rely on quite different abundance features for MHD-jet supernovae and neutron star mergers, based on fission barriers which introduce fission in the r-process only above A = 300.

A fully self-consistent treatment would require high resolution simulations which can resolve magneto-rotational instabilities (MRI) in order to predict reliably the possible amplification of magnetic fields during the explosion. While the latter is actually possible by now (Nishimura et al. 2017b), present calculations depend on the uncertain and therefore assumed initial conditions, that either cause strong jet ejection or can develop kink instabilities of the jets (Mösta et al. 2015, 2017). Based on initial conditions, either neutrino heating or magnetic pressure is causing the supernova explosion, for which the production of heavy neutron capture elements varies strongly. This is shown in Fig. 4.23, which underlines that results can range from a weak r-process, barely proceeding up to the second peak at A = 130, to a full r-process with a strong contribution to the actinides.

In terms of applications to galactic chemical evolution it should be noticed that the MHD-jet supernovae discussed here are expected to occur as a fraction of 0.1–1% of all CCSNe, probably being somewhat metallicity dependent. Higher metallicities lead to stronger stellar wind loss which will be accompanied by a loss of angular momentum, thus reducing the fast rotation necessary for this type of SN explosions. Another feature is that these events can lead to small amounts of Fe-group ejecta for the cases of strong r-processing (Nishimura et al. 2015, 2017b). Plotting the results of Fig. 4.24 with respect to the relative influence of neutrino heating vs. magnetic field effects, one can see that the Ni/Eu-ratio (and similarly the Fe/Eu-ratio) varies strongly (see Fig. 4.24).Thus, if these types of supernovae would contribute already at low metallicities, they alone would be able to provide a large spread in Eu/Fe and might even explain the variations in actinides vs. Eu, seen in a number of cases at low metallicities (see e.g. Wehmeyer et al. 2015; Thielemann et al. 2017a).

4.5.3 Pair-Instability Supernovae (PISNe)

We limit our discussion of massive-star fates in this Chapter to stars below 130 $M_{\odot}$ which still undergo core collapse and do not explode via explosive O-burning like the so-called pair-creation supernovae (Heger et al. 2003). Such explosions seem theoretically possible, provided that these massive cores can result from stellar evolution. The apparent absence of predicted abundance patterns in low metallicity stars, as well as our current understanding of massive stars with the effects of stellar rotation (Maeder and Meynet 2012) cast some doubts, and the existence of PISNe remains an exciting possibility to be proven.

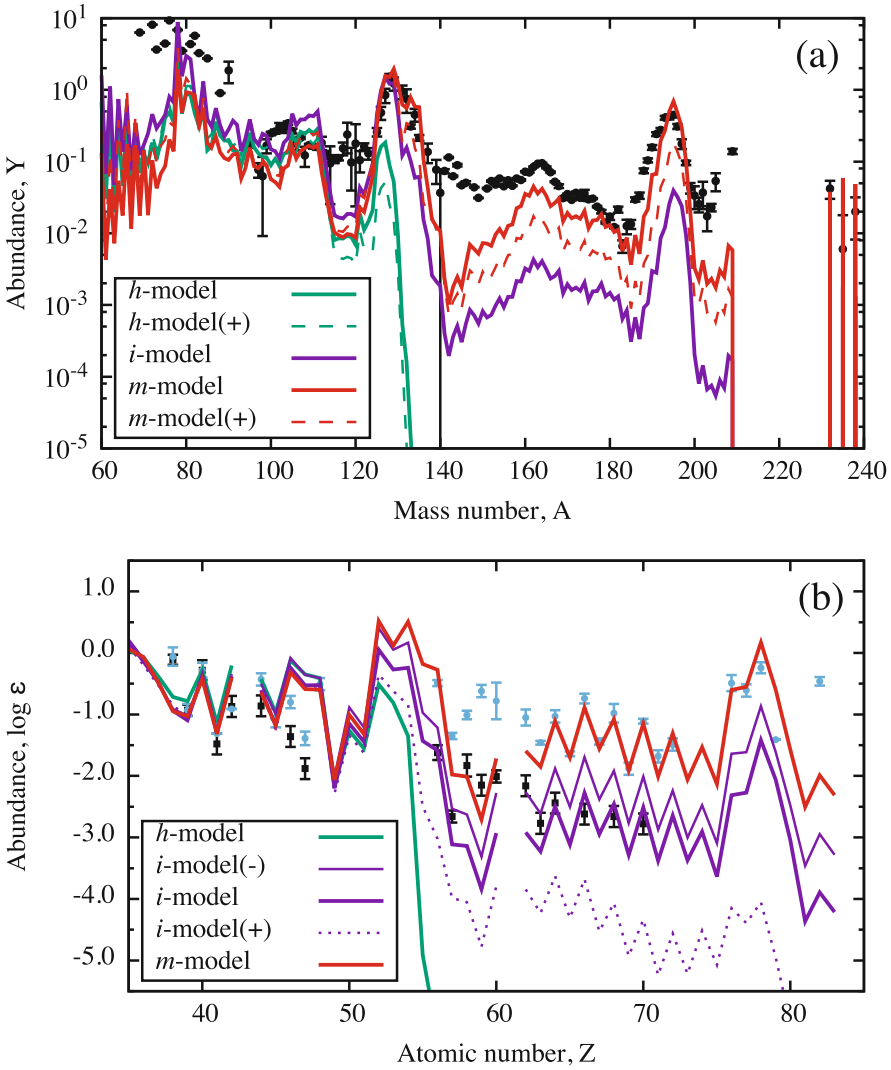

Fig. 4.23 Abundances from nucleosynthesis calculations with varying ratios of magnetic field strength with respect to the neutrino heating mechanism of regular CCSNe, increasing for the models h, i−, i, i+, and m (for details see Nishimura et al. 2017b). For comparison also (**a**) solar r-process abundances are shown (black dots Arlandini et al. 1999), as well as (**b**) abundances from metal-poor stars with a weak r-process, i.e. HD122563 (black dots Honda et al. 2006), and solar-type r-process observations from CS22892-052 (blue dots Sneden et al. 1996). Abundances are normalized for Z = 40 of HD122563. Observations of low metallicity stars with strong r-process contributions vary for abundances below Z = 50 (Sneden et al. 2008)

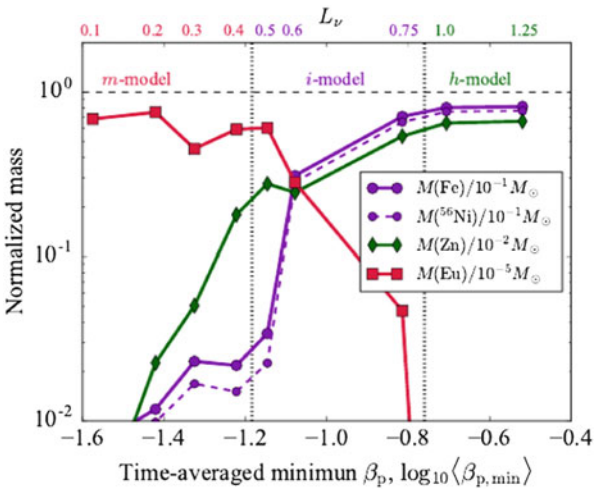

Fig. 4.24 Nucleosynthesis features of rotating CCSN models (h, i−, i, i+, m) with varying ratios of neutrino luminosity and magnetic field strengths as in Fig. 4.23. Model m represents a strong MHD-jet supernova. One can see the transition from a regular CCSN pattern, dominated by ^{56}Ni, total Fe (after decay), and Zn to a strong r-process pattern with a high Eu abundance (for details see Nishimura et al. 2017b)

4.5.4 Neutron Star Mergers

Short-duration GRBs (sGRBs, with a light curve decline of less than about 2 s) are due to relativistic jets created by the merger of two compact stellar objects (specifically two neutron stars or a neutron star and a black hole). Mergers of this kind are also expected to produce significant quantities of neutron-rich radioactive species, whose decay should result in a faint transient, known as kilonova,[9] in the days following the burst. Recent calculations suggest that much of the kilonova energy should appear in the near-infrared, because of the high optical opacity created by these heavy r-process elements. Optical and near-infrared observations of such an event, accompanying the short-duration GRB130603B have been reported in recent years by Tanvir et al. (2013), (see also Barnes et al. 2016). The first gravitational wave detection of such an event (GW170817), combined with a short GRB (GRB170817A) and the optical and infrared afterglow (see e.g. Abbott et al. 2017) has clearly underlined this r-process production site (Metzger 2017a). After the first detailed nucleosynthesis predictions (following ideas of Lattimer and Schramm (1974) and Eichler et al. (1989) of such an event) by Freiburghaus et al. (1999b), many more and more sophisticated investigations have been undertaken (for a review see Thielemann et al. 2017b). Because this book chapter is dedicated to nucleosynthesis in supernovae, we do not want to treat such neutron star merger events in great detail, just to mention them here as a valid (and possibly dominant) site of the astrophysical r-process.

[9]The term 'kilonova' appears to imply luminosities of 10^3 times those of novae; therefore, many scientists prefer the term 'macronova' for these transients, with their luminosities in between novae ad supernovae.

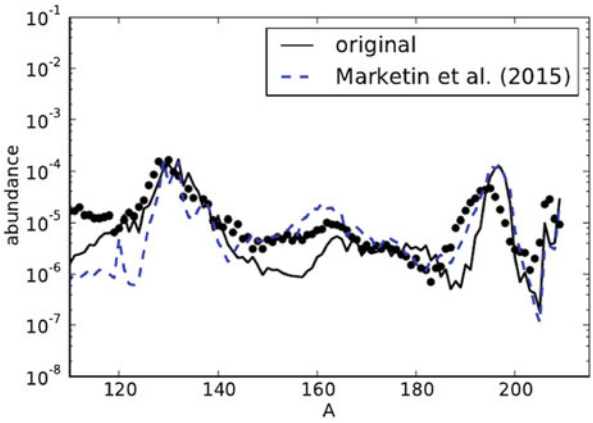

Fig. 4.25 r-process abundance distribution in dynamical ejecta of neutron star mergers, utilizing different mass models, fission fragment distributions, and half-lives (Eichler et al. 2015). Here the effect of improved half-life calculations (Marketin et al. 2016) in comparison to the original FRDM half-lives (Möller et al. 2003) is shown (from Eichler et al. 2015)

Figure 4.25 displays the early dynamical ejecta and their dependence on nuclear properties. Non-relativistic simulations (e.g. Korobkin et al. 2012; Rosswog et al. 2014) lead to large amounts of ejecta of the order $10^{-2}\,M_\odot$ with very small Y_e-values of 0.04 and less. This causes a very strong r-process with fission cycling. The utilized mass model, beta-decay half-lives, fission barriers, and fission yield prescriptions have a strong effect on the final abundance distribution. While during the r-process (when reactions are still in $n, \gamma - \gamma, n$ equilibrium) the second and third r-process peak are exactly at the right position, the neutron capture of large amounts of fission neutrons (after freeze-out from this equilibrium) has some effect on abundances below $A = 165$, and the third peak seems always shifted to heavier nuclei. Deviations (troughs) in the mass range $A = 130 - 165$ can be improved with modern fission fragment distribution (Kelic et al. 2008, ABLA07,), but not the shift of the third peak. One option to remedy this effect are variations in beta-decay rates. Shorter half-lives (Marketin et al. 2016) of heavies release neutrons from fission earlier, when $n, \gamma - \gamma, n$ equilibrium is still in place and can avoid or strongly reduce the late shift of the 3rd peak (Eichler et al. 2015). This effect is also seen with the HFB mass model (see also Goriely 2015; Goriely et al. 2015), while Mendoza-Temis et al. (2015) analyzed additional nuclear uncertainties and showed especially an improvement with the Duflo-Zuker mass model (Duflo and Zuker 1995). Alternative ways to cure the problems of the third r-process peak discussed above, come from full general relativistic modeling of the merger event. This leads to deeper gravitational potentials, higher temperatures (including neutrino energies), electron-positron pairs, which—via positron captures and neutrino interaction with nuclei/nucleons—increase Y_e to values of the order 0.15 in equatorial dynamic ejecta, comparable to those mentioned above in MHD-supernova (magnetar) jets (Wanajo et al. 2014; Goriely et al. 2015; Martin et al. 2017), where the third peak shift did not occur (Fig. 4.26).

After ballistic/hydrodynamic ejection of matter (i.e. the dynamic ejecta), dependent on the equation of state, a hot and massive combined neutron star forms and, before collapsing to a black hole, evaporates a neutrino wind (Rosswog et al. 2014;

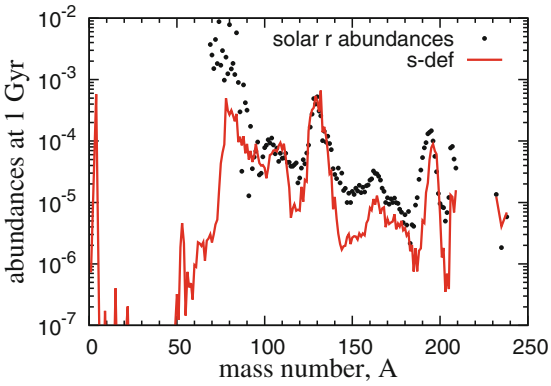

Fig. 4.26 Resulting r-process abundances (in comparison to solar values—black dots) from black hole accretion disk simulations (Wu et al. 2016a), making use of a black hole mass of 3 $M_\odot$, a disk mass of 0.03 $M_\odot$, an initial Y_e of 0.1, entropy per baryon of $8k_b$, an alpha parameter of the viscous disk of 0.03, and a vanishing black hole spin

Perego et al. 2014; Martin et al. 2015) which contributes matter in more polar directions with Y_e's up to 0.4. These winds contain also the lighter r-process nuclei. Outflow from the black hole accretion disk, also powered by neutrinos (and viscous disk heating), can provide the abundance component of light r-process nuclei, in addition to heavy r-process nuclei (Wanajo et al. 2014; Just et al. 2015; Goriely et al. 2015; Wu et al. 2016a).

4.6 Nucleosynthesis in Explosions from Massive Stars

4.6.1 Nuclear Burning During Explosions

Despite considerable improvements of stellar models and numerical simulations in recent years, some fundamental problems remain in nucleosynthesis predictions. It has become evident that certain evolution aspects can only be followed in models going beyond one-dimensional simulations, such as convection, rotation, and the explosion mechanism. There exist also a few multi-D nucleosynthesis studies by now (e.g. Harris et al. 2017; Eichler et al. 2018), and we gave also a few examples of these in Sect. 4.5. However, it is still not feasible to directly couple full reaction networks, containing several thousand nuclei, to multi-dimensional hydrodynamic calculations due to the lack of required computing power, even in modern computers. Thus, post-processing after explosion models with parameterized networks still remains an important approach. One-dimensional models can directly accommodate increasingly larger networks but they cannot capture all of the necessary physics. On the other hand, It has been shown that the delayed neutrino mechanism works combined with a multi-D convection treatment for unstable layers (possibly with the aid of rotation, magnetic fields and/or still existent uncertainties in neutrino opacities). As outlined in the previous sections, a truly self-consistent treatment of core collapse supernovae in 1D does not lead to successful explosions, when using presently known input physics while 2D models show some promise. Therefore,

hybrid approaches using certain parameterizations or approximations have been and are still necessary when predicting the nucleosynthetic yields required for the application described above. Intelligently added energy via neutrino absorption, guided by existing multi-D results of e.g. PHOTB and PUSH, can recover many shortcomings of the early spherically symmetric results. We will discuss explosive nucleosynthesis still in this framework, but present the improvements since the early "piston" and "thermal bomb" approaches.

Supernova nucleosynthesis predictions have a long tradition. All of these predictions relied on an artificially introduced explosion, either via a piston or a thermal bomb introduced into the progenitor star model. The mass cut between the ejecta and the remnant does not emerge from this kind of simulations but has to be determined from additional conditions. While the usage of artificially introduced explosions is justifiable for the outer stellar layers, provided we know the correct explosion energy to be dumped into the shock front (on the order of 10^{51} erg seen in observations), it clearly is incorrect for the innermost ejected layers which should be directly related to the physical processes causing the explosion. This affects the Fe-group composition, which has been recognized as a clear problem by many groups (Woosley and Weaver 1995; Thielemann et al. 1990, 1996; Nakamura et al. 1999, 2001; Nomoto et al. 2006, 2013; Fröhlich et al. 2006a,b; Pruet et al. 2005, 2006). The problem is also linked to the so-called neutrino wind, emitted seconds after the supernova explosion, which was considered as a possible source of the r-process to produce the heaviest elements via neutron captures (Woosley et al. 1994; Woosley and Weaver 1994; Takahashi et al. 1994; Qian and Woosley 1996; Hoffman et al. 1997; Arcones and Thielemann 2013; Farouqi et al. 2010).

Given the above detailed discussion of the physics, problems and options regarding core collapse supernovae, we will adopt the following approach in order to predict the most reliable nucleosynthesis predictions for the ejecta in a 1D spherically symmetric treatment, based on the PUSH approach discussed in Sect. 4.5, which can mimic the enhanced energy deposition which multi-D models show. The free parameters are tuned to give correct explosion energies and ^{56}Ni yields for a number of well known supernovae. This approach provides clear predictions for the mass cut between the remaining neutron star and the ejecta. It also includes the effect neutrinos can have on the correct Y_e in the ejecta and the related nucleosynthesis. In the outer explosively burning layers, essentially only the energy in the shock front matters, but opposite to earlier piston or thermal bomb approaches "self-consistent" explosion energies as a function of progenitor mass can be determined. The behavior of these zones can be easily understood from the maximum temperatures attained in the radiation bubble and for a first discussion we will just focus on these features, which can also be obtained with an artificially induced thermal bomb treatment.

For a given/known Y_e and density ρ, the most significant parameter in explosive nucleosynthesis is the temperature, and a good prediction for the composition can already be made by only knowing T_{max}, without having to perform complex nucleosynthesis calculations. Weaver and Woosley (1980) already recognized, that matter behind the shock front is strongly radiation dominated. Assuming an almost

homogeneous density and temperature distribution behind the shock (which is approximately correct), one can equate the supernova energy with the radiation energy inside the radius r of the shock front

$$E_{SN} = \frac{4\pi}{3} r^3 a T^4(r). \tag{4.7}$$

This equation can be solved for r. With $T = 5 \times 10^9$ K, the lower bound for explosive Si-burning with complete Si-exhaustion, and an induced thermal bomb energy of $E_{SN} = 10^{51}$ erg, the result is $r \approx 3700$ km. For the evolutionary model by Nomoto and Hashimoto (1988) of a 20 $M_\odot$ star this radius corresponds to 1.7 $M_\odot$, in excellent agreement with the exact hydrodynamic calculation. Temperatures which characterize the edge of the other explosive burning zones correspond to the following radii: incomplete Si-burning (T_9=4, r=4980 km), explosive O-burning (3.3, 6430), and explosive Ne/C-burning (2.1, 11750). This relates to masses of 1.75, 1.81, and 2.05 $M_\odot$ in case of the 20 $M_\odot$ star. The radii mentioned are model independent and vary only with the supernova energy. In the following we present a number of plots which show the different mass fractions $X_i = A_i Y_i$ as a function of radial mass $M(r)/M_\odot$, passing outwards through a 20 $M_\odot$ star through all explosive burning regions.

Matter between the mass cut $M(r)$=M_{cut} and the mass enclosed in the radius corresponding to explosive Si-burning with complete Si-exhaustion is indicated with M(ex Si-c). Then follows the zone of incomplete Si-burning until M(ex Si-i), explosive O-burning until M(ex O), explosive Ne/C-burning until M(ex Ne), and unprocessed matter from the C/Ne-core is ejected until M(C-core). In these early calculations the mass cut was artificially determined by integrating the ^{56}Ni-yields inwards down to a radius when the observed 0.07 $M_\odot$ were obtained. We will discuss improvements, resulting from the PUSH approach below. The zones beyond explosive Ne/C-burning ($T_{max} < 2.1 \times 10^9$ K) are essentially unaltered and the composition is almost identical to the pre-explosive one. When performing such calculations for a variety of progenitors over a range of initial stellar masses, one can analyze the dependence of the mass involved in these different burning regimes as a function initial stellar mass (see Sect. 4.5).

For pedagogical reasons, here early results for a 20 $M_\odot$ star (Nomoto and Hashimoto 1988) are still given as examples for the abundance behavior in a series of Figs. 4.27, 4.28, 4.29 and 4.30. It should be mentioned here that these still resulted a simplified thermal bomb treatment for the pre-collapse model rather than from a 1D spherically symmetric simulation with modified neutrino energy absorption, i.e. the PUSH approach which ensures more realistic explosion conditions. The explosion energy used corresponds to a supernova energy of 10^{51} erg. As mentioned before, this treatment could not predict a self-consistent explosion and the position of the mass cut between neutron star and ejecta. Only the observation of 0.07 ± 0.01 $M_\odot$ of ^{56}Ni in SN1987A (a 20 $M_\odot$ star) gives an important constraint, because ^{56}Ni is produced in the innermost ejected zones. The explosive nucleosynthesis due to burning in the shock front is shown in Fig. 4.27 for a few major nuclei. Inside

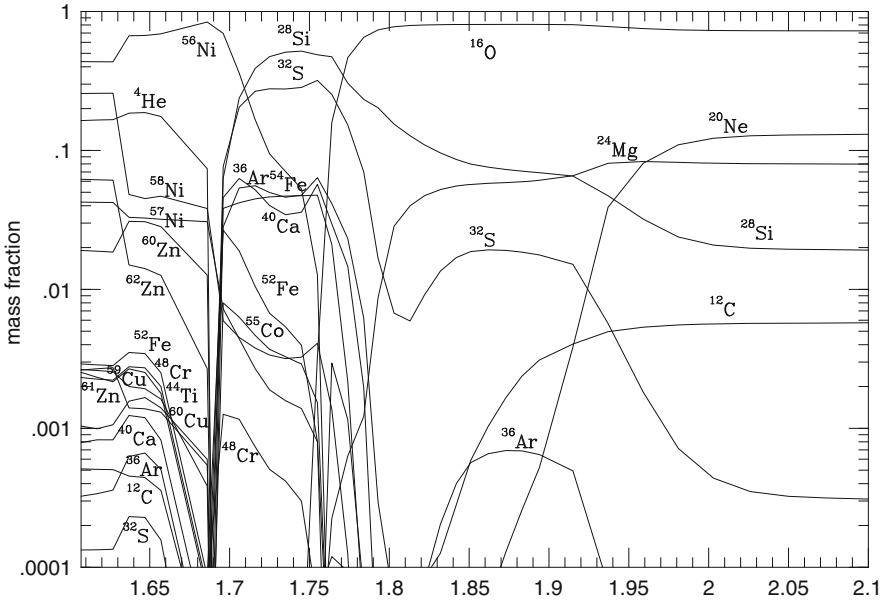

Fig. 4.27 Mass fractions of a few major nuclei after passage of the supernova shockfront through a star with an intimal mass of 20 $M_\odot$ obtained with a thermal bomb approach. Matter outside 2 $M_\odot$ is essentially unaltered. Mass zones further in experience explosive Si, O, Ne, and C-burning. The strange variation of yields in the innermost zones result from utilizing the initial Y_e existing in the progenitor star before the explosion, which would be affected by the and during the explosion. For ejecting 0.07 $M_\odot$ of ^{56}Ni the mass cut between neutron star and ejecta is required to be located at 1.6 $M_\odot$

1.7 $M_\odot$ all Fe-group nuclei are produced in *explosive* Si-burning during the SN II event. At 1.63 $M_\odot$ Y_e changes from 0.494 to 0.499 and leads to a smaller ^{56}Ni abundance further inside, where more neutron-rich Ni-isotopes share the abundance with ^{56}Ni. This is an artefact of the Y_e gradient in the pre-collapse model which can be changed in a consistent explosion treatment via neutrino interactions with this matter (Fig. 4.31).

For comparison we show also recent PUSH results (Sinha et al. 2017; Curtis et al. 2018) for a 16 $M_\odot$ model which leads to an explosion energy of 1.5×10^{51} erg (see Fig. 4.19) avoids the Y_e-problem of the innermost ejecta in the early piston or thermal bomb approaches.

In explosive Si-burning only alpha-rich freeze-out and incomplete Si-burning are encountered. Contrary to SNe Ia, densities in excess of 10^8 g cm^{-3}, which would result in a normal freeze-out, are not attained in the ejecta (see also Fig. 4.2). The most abundant nucleus in the alpha-rich freeze-out is ^{56}Ni. For the less abundant nuclei the final alpha-capture plays a dominant role transforming nuclei like ^{56}Ni, ^{57}Ni, and ^{58}Ni into ^{60}Zn, ^{61}Zn, and ^{62}Zn (see Fig. 4.28).

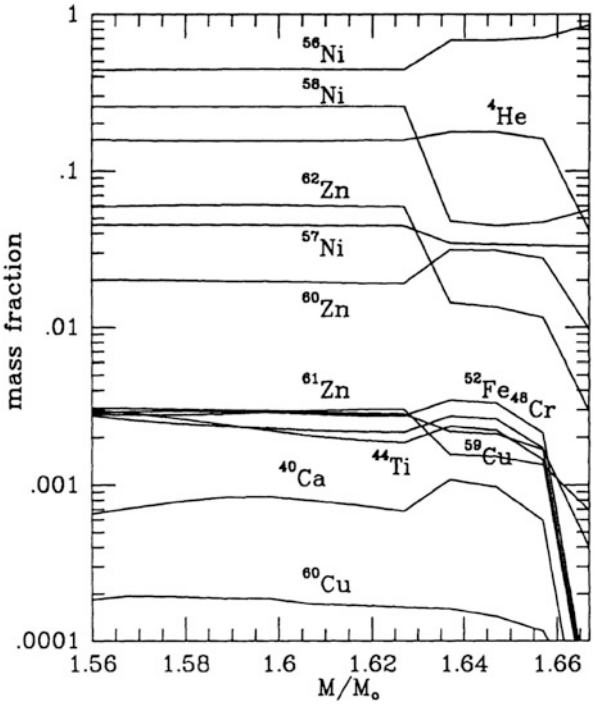

Fig. 4.28 Mass fractions of the dominant nuclei in zones which experience alpha-rich freeze-out. Notice the relatively large amounts of Zn and Cu nuclei, which originate from alpha-captures on Ni and Co. One can recognize their strong decrease beyond 1.66 $M_\odot$, which goes parallel with the decrease of the ^{4}He-abundance and other alpha-nuclei like ^{40}Ca, ^{44}Ti, ^{48}Cr, and ^{52}Fe. Nuclei which would dominate in a nuclear statistical equilibrium like ^{56,57,58}Ni stay constant or increase even slightly. The increase of all nuclei with $N = Z$ at 1.63 $M_\odot$ and the decrease of nuclei with N>Z is due to the change in Y_e in the original stellar model before collapse, neglecting changes which would have taken place during a realistic explosion simulation (see also Fig. 4.27)

The region of the previously discussed 20 $M_\odot$ star which experiences incomplete Si-burning starts at 1.69 $M_\odot$ and extends out to 1.74 $M_\odot$. In the innermost zones with temperatures close to 4×10^9 K there exists still a contamination by the Fe-group nuclei ^{54}Fe, ^{56}Ni, ^{52}Fe, ^{58}Ni, ^{55}Co, and ^{57}Ni. Explosive O-burning occurs in the mass zones up to 1.8 $M_\odot$ (see Fig. 4.29). The main burning products are ^{28}Si, ^{32}S, ^{36}Ar, ^{40}Ca, ^{38}Ar, and ^{34}S. With mass fractions less than 10^{-2} also ^{33}S, ^{39}K, ^{35}Cl, ^{42}Ca, and ^{37}Ar are produced. Explosive Ne-burning leads to an ^{16}O-enhancement over its hydrostatic value in the mass zones up to 2 $M_\odot$ (see Fig. 4.30).

Complete explosive nucleosynthesis predictions for a range of progenitor stars with induced explosions have been given by a number of authors in recent years (Rauscher et al. 2002; Woosley et al. 2002; Chieffi and Limongi 2004, 2017; Nomoto et al. 2006, 2013; Limongi and Chieffi 2006b, 2012; Woosley and Heger 2007; Umeda and Nomoto 2008; Nomoto 2017), updating some of the discussions

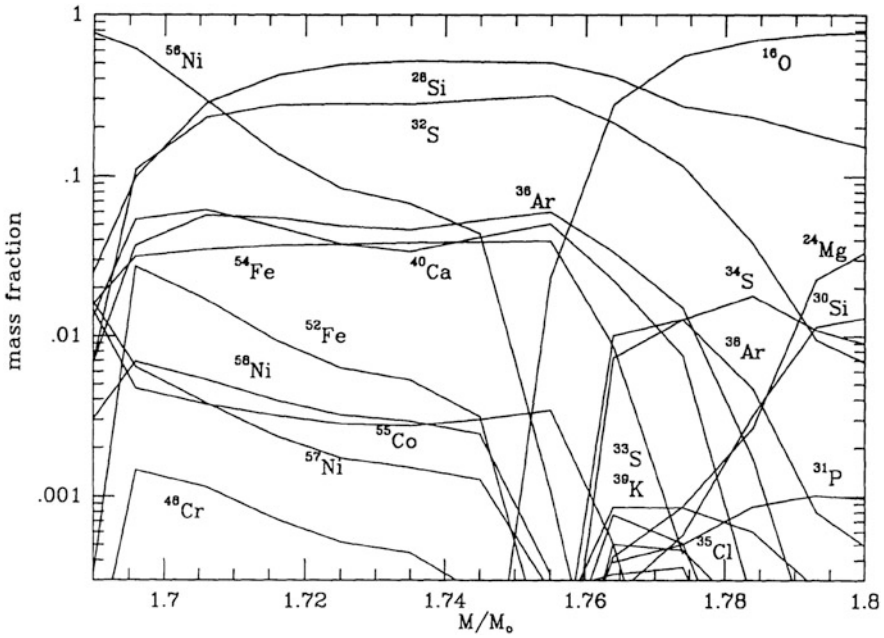

Fig. 4.29 Mass fractions of nuclei in the zones of incomplete Si-burning $M<1.74\,M_\odot$ and explosive O-burning $M<1.8\,M_\odot$. The Si-burning zones are characterized by important quantities of Fe-group nuclei besides ^{28}Si, ^{32}S, ^{36}Ar, and ^{40}Ca. Explosive O-burning produces mostly the latter, together with more neutron-rich nuclei like ^{30}Si, ^{34}S, ^{38}Ar etc

made above, based on earlier models (Woosley and Weaver 1995; Thielemann et al. 1996). Also specific investigations were undertaken for Pop III low metallicity stars (Umeda and Nomoto 2005; Chieffi and Limongi 2004; Tominaga et al. 2007; Ohkubo et al. 2008).

New spherically symmetric nucleosynthesis predictions have recently become available (Ertl et al. 2016; Sukhbold et al. 2016; Sinha et al. 2017; Curtis et al. 2018), which also provide complete isotopic yields. They are based on PHOTB and PUSH approaches discussed above. Especially with PUSH the Y_e of the innermost zones is treated more consistently, and is expected to result in a more realistic Fe-group composition. One of the possible tests is to compare the composition of explosive ejecta with abundances found in low metallicity stars. Their abundances are determined by the explosive yields of massive stars before type Ia supernovae can set in during the evolution of the Galaxy (being delayed due their origin in lower/intermediate mass stars producing white dwarfs and the effects of binary evolution). Figure 4.32 presents the observed abundance ratios of Fe-group elements (Sneden et al. 2016) for the very metal-poor main sequence turnoff star HD 84937. PUSH yields (Sinha et al. 2017; Curtis et al. 2018) are shown along with piston yields (Woosley and Weaver 1995) and thermal bomb yields (Thielemann et al. 1996) for a $20\,M_\odot$ model from Woosley and Heger (2007) progenitor set.

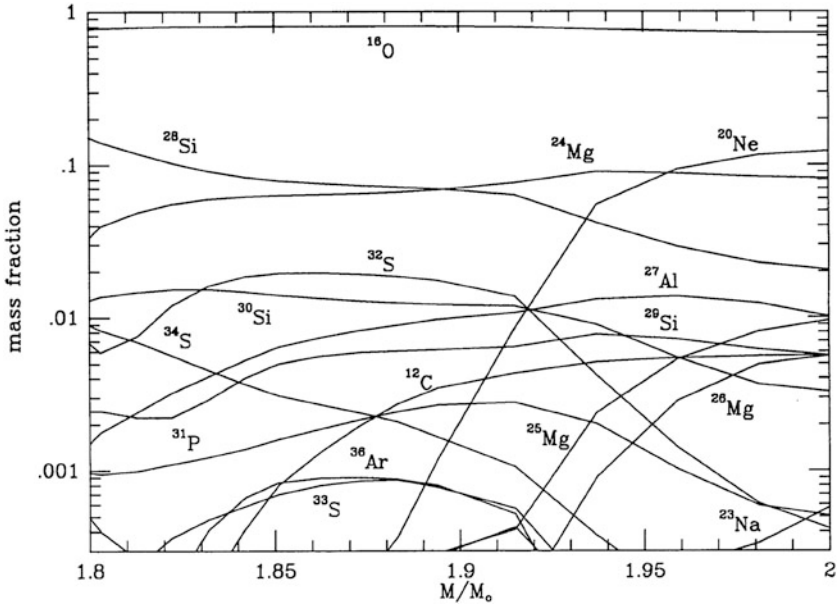

Fig. 4.30 Composition in mass zones of explosive Ne and C-burning. The dominant products are ^{16}O, ^{24}Mg, and ^{28}Si. Besides the major abundances, mentioned above, explosive Ne-burning supplies also substantial amounts of ^{27}Al, ^{29}Si, ^{32}S, ^{30}Si, and ^{31}P. Explosive C-burning contributes in addition the nuclei ^{20}Ne, ^{23}Na, ^{24}Mg, ^{25}Mg, and ^{26}Mg

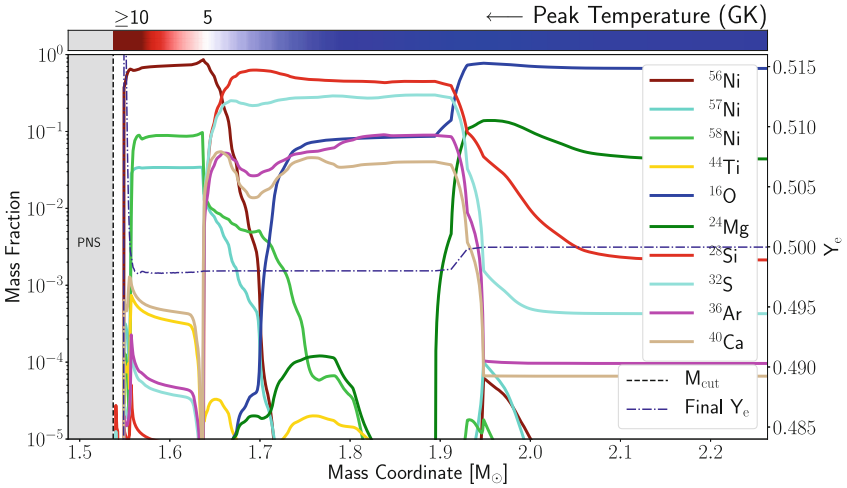

Fig. 4.31 Composition in ejected mass zones after passage of the supernova explosion front for a 16 $M_\odot$ star, utilizing the PUSH approach (Sinha et al. 2017; Curtis et al. 2018). In contrast to what is shown in Fig. 4.27, the unrealistic Y_e-caused features disappear here in the innermost ejected zones

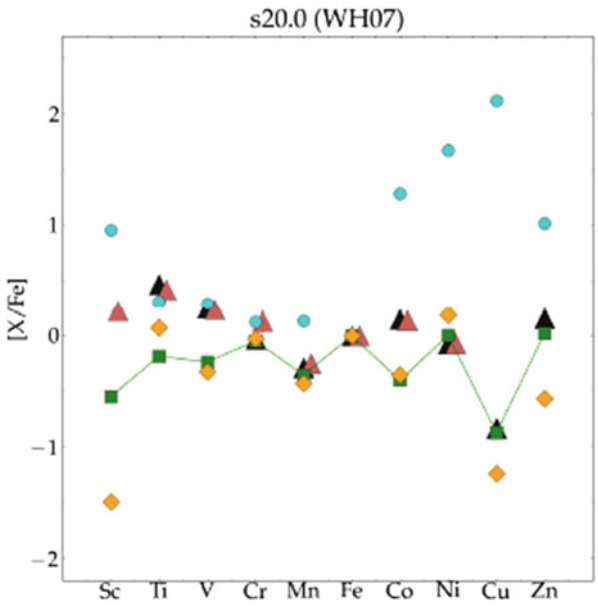

Fig. 4.32 Observed abundances of HD 84937 (Sneden et al. 2016) (black and magenta) compared with the yields obtained with progenitor models of a 20 $M_\odot$ star from the Woosley and Heger (2007) progenitor series. Shown are piston results (Woosley and Weaver 1995) (blue), thermal bomb results (Thielemann et al. 1996) (yellow), and the recent PUSH results (Sinha et al. 2017; Curtis et al. 2018) (green). Due to consistent explosion energies and Y_e-values based on neutrino interactions during the explosion, it can be recognized that especially Sc and Zn show highly improved values in comparison to these older approaches (a first improvement,when including neutrino interactions during the explosion was already obtained in Fröhlich et al. (2006a). Cu is mostly due to s-processing during stellar evolution, which is not part of the explosion calculation

After this discussion of the explosive conditions and their outcome in detail, plus referring the reader to presently available isotopic yields, we now summarize a few major aspects, related to dominant isotopes and those of specific interest. This includes a reflection about the radial-zone (or burning zone) origin of these species. This information can be found in Table 4.9. Especially the innermost alpha-rich freeze-out ejecta are influenced by neutrino interactions with matter during the explosion which determine Y_e (and the entropy).

The basic pattern given in Table 4.9 always applies. The abundances from incomplete Si-burning and explosive O-burning can explain galactic chemical evolution (see e.g. Nomoto et al. 2013; Mishenina et al. 2017), and it seems that the Fe-group elements also fit with the improved inner Y_e treatment of PUSH (see Fig. 4.32). A question is whether the Zn (from ^{64}Ge-decay) produced in regular supernovae is sufficient to explain Zn abundances in the very early Galaxy, or whether hypernovae have to be invoked as the main contributors in this early phase of the Galaxy. As mentioned in Sect. 4.4, the classical p-process takes place in

Table 4.9 Main products of explosive and hydrostatic burning

Burning type	(Main) products, major radioactivities
α-rich compl. Si-burning	He, ^{56}Ni, ^{60}Zn, ^{40}Ca, ^{44}Ti. ^{48}Cr, ^{52}Fe dependent on Y_e also ^{57,58}Ni, ^{61,62}Zn, ^{59}Cu and/or ^{64}Ge and νp-process or weak r-process?
Expl. incompl. Si-burning	^{56}Ni, ^{28}Si, ^{32}S, ^{36}Ar, ^{40}Ca, ^{54}Fe, ^{52}Fe, ^{55}Co, ^{57,58}Ni
Expl. O-burning	O, Si, S, Ar, Ca
Expl. Ne-burning	O, Mg, Si, Ne; ^{26}Al, p-process
Hydr. He-burning products in C/O-core	O, Ne, Mg, Si, s-process

explosive Ne-burning via photo-disintegrations of pre-existing heavy nuclei, but even with the best nuclear input the underproduction of light p-nuclei cannot be solved. The solution can be obtained by adding a *light (heavy) element primary process* (LEPP, Travaglio et al. 2004) where the best candidate is the νp-process, discussed briefly in Sect. 4.5 and further below. Thus, the classical p-process isotopes have possibly to be explained by a superposition of the innermost proton-rich complete Si-burning ejecta with those of explosive Ne-burning in outer zones.

The scheme indicated in Table 4.9 is too simplified when considering the ejecta of outer layers, whose composition was produced during stellar evolution and ejected essentially unaltered during the explosion. However, the *CO-core* scheme is not sufficient to describe massive-star yields. While it includes all matter which underwent He-burning, it does not differentiate between core He-burning and shell He-burning. The latter occurs at higher temperatures and has specific features different from core He-burning. In a similar way, the NeO-core contains all matter which underwent C-burning during stellar evolution, but also here, no difference is made between core C-burning and higher temperature shell C-burning. The same is true for Ne-burning.

4.6.2 *Production of Long-Lived Radioactivities ^{44}Ti, ^{26}Al and ^{60}Fe*

The radioactive isotopes ^{44}Ti, ^{26}Al and ^{60}Fe are sufficiently long-lived so that their decay occurs outside the star and its explosion. Hence they provide a messenger through characteristic decay gamma-rays of their nucleosynthesis environments, discussed in Sect. 4.7 below. ^{44}Ti probably originates from explosive burning in inner core-collapse regions, whereas the ^{26}Al and ^{60}Fe that is ejected by the explosion mostly is produced in pre-supernova burning stages, with some modifications by the explosion. Because of their special role for this book, their production is discussed in this subsection in more detail.

4.6.2.1 ^{44}Ti

The material which collapsed towards the proto-neutron star is decomposed into nucleons and α particles while being heated during the explosion, then reassembled during the expansion and cooling via the nuclear reactions in the complete Si-burning regime with alpha-rich freeze-out. This produce α-multiples and thus also ^{44}Ti, dependent on the entropy attained. Its total amount depends on the matter experiencing this burning and being ejected. In one-dimensional models only regions outside the mass cut contribute, and this mass cut was in principle unknown without successful explosion calculations. Its position was either derived based on total ^{56}Ni ejecta in thermal bombs (Thielemann et al. 1996; Nomoto et al. 2006) or on entropy jumps in the pre-collapse models in piston-induced explosions (Woosley and Weaver 1995). Depending on how the explosion is modelled, by (1) a thermal bomb or (2) a piston, ^{44}Ti productions are either larger or smaller than 5×10^{-5} M$_\odot$. This apparently leads to higher entropies in the first case and a more intense alpha-rich freeze-out. The values of Thielemann et al. (1996) range between 2×10^{-5} and 1.5×10^{-4} M$_\odot$. An interesting point here is that variations in the Y_e-structure can lead to changes up to a factor of 2. Rauscher et al. (2002) and Tur et al. (2010) find smaller values (either $1.5 - 5 \times 10^{-5}$ and $3.5 - 6 \times 10^{-5}$ M$_\odot$). The latter is based on a readjustment of the triple-alpha and ^{12}C$(\alpha, \gamma)^{16}$O-rates to most recent experimental values, which does not have a drastic influence, however. Indirectly, core sizes and other stellar properties, including explosion energies, can enter. Chieffi and Limongi (2017) discuss the effect of rotating (but still spherically symmetric) progenitor models and come to the conclusion that actually rotating models reduce the amount of alpha-rich to incomplete Si-burning ejecta, therefore also the ^{44}Ti/^{56}Ni ratio. Also the improved, but still spherically symmetric, PHOTB and PUSH approaches give results of this order (Sukhbold et al. 2016; Sinha et al. 2017; Curtis et al. 2018). Summing up the results of spherically symmetric investigations, whether from early piston or thermal bomb approaches or from improved approaches with adapted effective neutrino heating to mimic multi-D effects, all these result in too low ^{44}Ti yields. Also investigations on the reactions producing (^{40}Ca$(\alpha, \gamma)^{44}$Ti) and destroying (^{44}Ti$(\alpha, p)^{47}$V) ^{44}Ti could not change this result. The radioactive half-life of ^{44}Ti has also been re-measured with much better precision, after Cas A had been detected in ^{44}Ti γ-rays, to (59 ± 0.3) years (Ahmad et al. 1998). But as complete explosive Si-burning always results from a freeze-out from equilibrium, Hoffman et al. (1999), even a rate change by a factor of 6 changes the ^{44}Ti production only by a factor of 1.3.

Early, still artificially induced multi-D explosion models (Nagataki et al. 1998; Nagataki 2000), were able to obtain higher ^{44}Ti yields. In recent self-consistent 3D models with CHIMERA (Harris et al. 2017), an important finding is that due to filamentary inflow and ejection occurring simultaneously, the radioactive ejecta containing ^{44}Ti (the same argument holds for ^{56}Ni) may actually have rather high characteristic velocities, and the conceptual view of ^{44}Ti being slow because originating from near the mass cut may be considered obsolete (Harris et al. 2017);

in fact, the concept of a 'mass cut' is intrinsically a one-dimensional view, and probably misleading here. This intrinsic 3D effect, being highly important not only for the heating and explosion mechanism, but also for the total integrated ejecta from deeper layers, seems to be able to solve the ^{44}Ti puzzle.

4.6.2.2 ^{26}Al

Long-lived ^{26}Al ($\tau \sim 1.04 \times 10^6$ years) is produced in core and shell H-burning via the NaMgAl-cycle (see Chap. 3) through the ^{25}Mg$(p,\gamma)^{26}$Al reaction. Ejection into the interstellar medium may occur through the stellar wind during the Wolf-Rayet phase, and in the supernova. The amount of ^{26}Al ejected into the interstellar medium is very sensitive to metallicity, initial stellar mass, rotation and mass loss rate, related to one or more of the physical effects discussed above. Results of detailed calculations can be found in Langer et al. (1995), Meynet et al. (1997), Palacios et al. (2005), Limongi and Chieffi (2006b), Woosley and Heger (2007), Tur et al. (2010), Ekström et al. (2012), and Chieffi and Limongi (2013); see also Sect. 4.7 below. The dominant source of ^{26}Al production during stellar evolution is the ^{25}Mg$(p,\gamma)^{26}$Al reaction. Therefore the resulting ^{26}Al abundance depends (1) on this reaction rate converting ^{25}Mg into ^{26}Al, (2) on the amount of ^{25}Mg available, i.e. the total amount of matter in the NeNaMgAl-cycle (either in terms of the abundance/metallicity or in terms of the H-core size), and finally (3) on the amount of ^{26}Al destruction. In the part of the He-core which undergoes He-burning, (α, n)-reactions efficiently produce neutrons. These destroy the ^{26}Al produced earlier (in H burning) via ^{26}Al$(n, p)^{26}$Mg and ^{26}Al$(n, \alpha)^{23}$Na. A further reduction of the final ^{26}Al yield arises from β^+-decay with a half-life of 7.17×10^5 years between the time of its synthesis and the time when matter is ejected in winds (i.e. mass loss) during later stellar evolution. He-burning, with its neutrons released, is destructive for ^{26}Al, but shell C-burning is again a source of ^{26}Al, also via ^{25}Mg$(p,\gamma)^{26}$Al, which is effective due to protons released in ^{12}C$(^{12}$C$,p)^{23}$Na (see Table 4.2 in Sect. 4.2). Convection in the C-burning shell brings in fresh ^{12}C fuel and ^{25}Mg which has been also produced in prior He-burning in the ^{22}Ne$(\alpha, n)^{25}$Mg reaction. ^{26}Al production may be effective also in Ne-burning, based on ^{25}Mg left over from C-burning and protons released via ^{23}Na$(\alpha, p)^{26}$Mg (see Table 4.3). This ^{26}Al only survives if rapidly convected outwards to lower temperature environments (^{26}Al may decay rapidly in hot regions due to thermal population of its short-lived isomeric state; cmp. Fig. 1.3 in Chap. 1).

Some of the ^{26}Al produced during stellar evolution will again be destroyed, when a shock front is released in the supernova explosion and propagates through the stellar envelope. Such explosive post-processing will affect mainly the products from hydrostatic C and Ne-burning, being close to the Fe-core. But there are also source processes for explosive ^{26}Al production. The total yields, hydrostatic-evolution yields combined with the destruction and contribution from explosive burning are given in Fig. 4.36.

The explosive production of ^{26}Al occurs in the regions of explosive Ne/C-burning. Under these conditions ^{25}Mg is produced via ^{24}Mg$(n, \gamma)^{25}$Mg and the protons arise from ^{23}Na$(\alpha, p)^{26}$Mg, similar to the reaction pattern shown in Table 4.3 for hydrostatic Ne-burning (and partially also C-burning). Under explosive conditions at temperatures of the order 2.3×10^9 K, these reactions act in a combined way, and the temperatures are also sufficiently high to utilize the released protons for the ^{25}Mg$(p, \gamma)^{26}$Al reaction. However neutrons are also produced abundantly (see Table 4.3), and act as the main destructive species via (n, p) and (n, α) reactions. The mass involved in explosive Ne/C burning strongly depends on the progenitor mass. Thus, we expect a dramatic increase of ^{26}Al yields with increasing initial stellar mass. Limongi and Chieffi (2006b) have analyzed in detail the contributions from (1) wind ejecta during stellar evolution, (2) hydrostatic burning products ejected during the explosion, and (3) explosive Ne/C-burning. The latter dominates up to about 60 $M_\odot$ and increases from initially about 2×10^{-5} $M_\odot$ per event to $2-3 \times 10^{-4}$ $M_\odot$. Then wind ejecta start to take over and flatten out close to 10^{-3} $M_\odot$ at initial stellar masses of 120–140 $M_\odot$. The latter are subject to effects stimulated by stellar rotation (Langer et al. 1995; Meynet et al. 1997; Palacios et al. 2005), and increase with higher rotation rates (see Sect. 4.3). Tur et al. (2010) have confirmed this trend in the lower mass range from 15 to 25 $M_\odot$. They also found that the result does not depend much on the He-burning reaction rates of triple-alpha and ^{12}C$(\alpha, \gamma)^{16}$O. They show nicely how ^{26}Al production starts early, in H-burning, but the final explosion produces close to a factor of 10 more than the initial H-burning yields. Yields from different studies have been assembled in Fig. 4.36.

4.6.2.3 ^{60}Fe

^{60}Fe is produced by neutron captures on ^{59}Fe, and destroyed again via ^{60}Fe$(n, \gamma)^{61}$Fe, i.e. in an s-process. Generally, slow capture of neutrons released from the ^{22}Ne$(\alpha, n)^{25}$Mg reaction in core He-burning leads to the so-called *weak* s-process, producing nuclei up to nuclear mass numbers of around $A = 90$. ^{59}Fe is beta-unstable, thus requires a typical neutron density of about 3×10^{10} cm^{-3} in order for neutron capture rates to equate the beta-decay rates. These are relatively high neutron densities for an s-process, which then also make the destruction of ^{60}Fe via neutron captures dominate over its decay; the decay half-life is 2.6×10^6 years (Rugel et al. 2009, see also Chap. 7). Core He-burning will not provide sufficiently high-temperatures for the ^{22}Ne$(\alpha, n)^{25}$Mg reaction to produce such high neutron densities, whereas the conditions in shell He-burning could do so. Apparently, conditions are most favorable at late times during shell He-burning when central O-burning and a C-burning shell are both already active (see Woosley and Weaver 1995; Rauscher et al. 2002; Limongi and Chieffi 2006a,b; Tur et al. 2010). ^{60}Fe yields are very sensitive to uncertainties in He-destruction reactions (such as the 3α-rate and ^{12}C$(\alpha, \gamma)^{16}$O) which compete with the neutron source reaction ^{22}Ne$(\alpha, n)^{25}$Mg and neutron(-capture) *poisons*, which compete with the

production and destruction rates of ^{60}Fe via neutron captures (Rauscher et al. 2002; Tur et al. 2010; Giron et al. 2010; Uberseder et al. 2009). Such uncertainties add up to factors of up to 5, from individual rate uncertainties. Another possible uncertainty which has not been studied yet is the amount of ^{22}Ne available in He-burning. Here, an important effect in low metallicity stars is the production of primary ^{14}N (not inherited from CNO of previous stellar generations, but produced inside the star due to mixing of He-burning products with H); this causes the production of ^{22}Ne in He-burning and can permit sizable s-processing at low metallicities (with small seed abundances of Fe), thus affecting the abundance of ^{60}Fe.

The overall production ranges from 2×10^{-6} to 8×10^{-5} $M_\odot$ for initial stellar masses between 10 and 40 $M_\odot$. This result depends significantly on the He-burning reactions (triple-alpha and $^{12}C(\alpha, \gamma)^{16}O$), as they compete with the neutron producing reaction $^{22}Ne(\alpha, n)^{25}Mg$. Additional uncertainties in $^{59}Fe(n, \gamma)^{60}Fe$ and $^{60}Fe(n, \gamma)^{61}Fe$ cause yield uncertainties by a factor of up to 5. If the star experiences strong mass loss, the He-burning shell does not encounter the higher density conditions required for the high neutron density of 3×10^{10} cm^{-3}. Thus for initial stellar masses in excess of 40 $M_\odot$, the mass loss treatment can also lead to variations in predicted yields of more than a factor of 10.

4.6.3 Explosive Burning Off the Regime of Nuclear Stability

In Sect. 4.2 we introduced in a short way all hydrostatic and explosive burning processes (with the exception of the νp-process). In Sect. 4.4 we gave a specific example of the νp-process in combination with multi-D modeling of core-collapse supernovae, and in Sect. 4.5 we addressed already the r-process in simulations of MHD supernovae/magnetars as well as neutron star mergers. All those were given as short presentations of results with the focus on multi-D (magneto-)hydrodynamic modeling. In the present subsection we give a more in depth general presentation, which applies to the spherically symmetric simulations of the present section as well as the multi-D simulations of previous sections.

4.6.3.1 The p-Process

Up to now we discussed the production of heavy nuclei beyond the Fe-group only via slow neutron captures (the s-process) in hydrostatic stellar evolution. A number of proton-rich (p-)isotopes of naturally occurring stable heavy nuclei cannot be produced by neutron captures along the line of stability. The currently most favored production mechanism for those 35 p-isotopes between Se and Hg is photo-disintegration (γ-process) of intermediate and heavy elements at high temperatures in late (explosive) evolution stages of massive stars (Woosley and Howard 1978; Rayet et al. 1990). However, not all p-nuclides can be produced satisfactorily, yet. A well-known deficiency in the model is the underproduction of the Mo-Ru region,

but the region 151<A<167 is also underproduced, even in recent calculations (Rauscher et al. 2002, 2013; Arnould and Goriely 2003; Rapp et al. 2006; Dillmann et al. 2008). There exist deficiencies in astrophysical modeling and the employed nuclear physics. Recent investigations have shown that there are still considerable uncertainties in the description of nuclear properties governing the relevant photo-disintegration rates. This has triggered a number of experimental efforts to directly or indirectly determine reaction rates and nuclear properties for the p/γ-process (Rauscher 2006, 2013). Here it is important to investigate the sensitivity of the location of the γ-process path with respect to reaction rate uncertainties.

Concerning the astrophysical modeling, only a range of temperatures has to be considered which are related to the explosive Ne/O-burning zones of a supernova explosion (see Figs. 4.29 and 4.30), where partial (but not complete) photo-disintegration of pre-existing nuclei occurs (from prior hydrostatic evolution or inherited metallicity), i.e. at $\approx 2-3\times10^9$ K. The γ-process starts with the photo-disintegration of stable seed nuclei that are present in the stellar plasma. During the photo-disintegration period, neutron, proton, and alpha-emission channels compete with each other and with beta-decays further away from stability. In general, the process, acting like "spallation" of pre-existing nuclei, commences with a sequence of (γ, n)-reactions, moves the abundances to the proton-rich side. At some point in a chain of isotopes, (γ, p) and/or (γ, α)-reactions become faster than neutron emissions, and the flow branches and feeds other isotopic chains. At late times photo-disintegrations become less effective, when decreasing temperatures shift the branching points and make beta-decays more important. Finally the remaining unstable nuclei decay back to stability. The branchings established by the dominance of proton and/or alpha-emission over neutron emission are crucial in determining the radioactive progenitors of the stable p-nuclei and depend on the ratios of the involved reaction rates. Numerous experimental and theoretical efforts have been undertaken to improve the reaction input, especially with respect to open questions in optical potentials for alpha particles and protons (Gyürky et al. 2006; Kiss et al. 2007, 2008; Yalçın et al. 2009). One of the major open problems was the apparent alpha-potential mystery, leading to reduced (α, γ) cross sections in comparison to theoretical predictions. Rauscher (2013) could show that the consistent inclusion of Coulomb excitations solves this discrepancy.

Applications of p-process network calculations to the temperature profiles of initiated explosions have been performed by Rayet et al. (1995), Rapp et al. (2006), and Dillmann et al. (2008). Here, in Fig. 4.33 we present the results of a 25 $M_\odot$ mass model (Dillmann et al. 2008) with two reaction rate libraries without and with inclusion of all experimental improvements, existing at that point. It is noticed that the nuclear uncertainties cannot change the underproduction of especially the light p-nuclei. Another process seems to be required to supply these missing abundances.

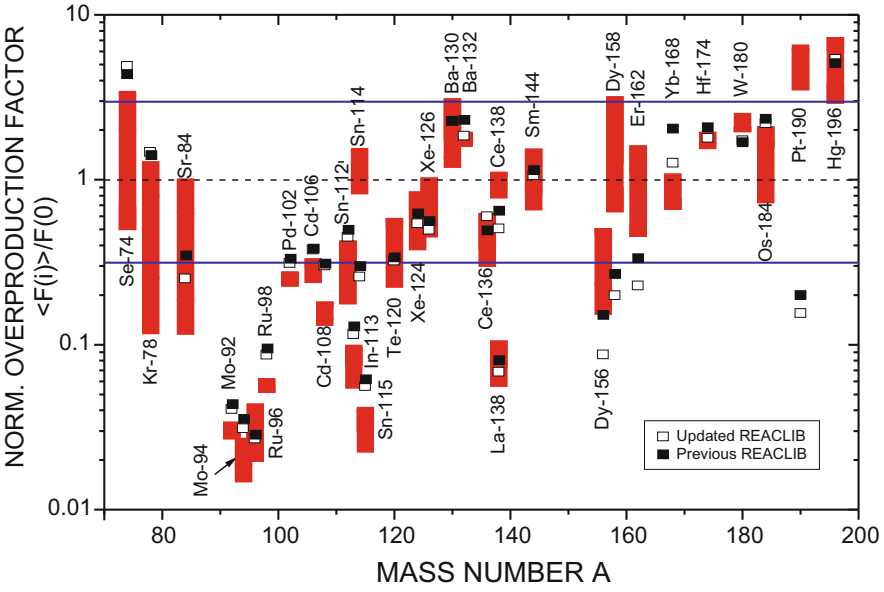

Fig. 4.33 Normalized overproduction factors of p-process nuclei derived with the Rapp et al. (2006) (open squares) and Dillmann et al. (2008) (full squares) reaction library. In addition, the results from a range of stellar models (10–25 $M_\odot$) from Rayet et al. (1995) are given for comparison. A value equal to unity corresponds to relative solar abundances

4.6.3.2 The ν p-Process

Neutron-deficient nuclei can also be produced by two other astrophysical nucleosynthesis processes: the rp-process in X-ray bursts (which, however, does not eject matter into the interstellar medium (Wallace and Woosley 1981; Schatz et al. 1998; Fisker et al. 2008; Cyburt et al. 2010) and the νp-process in core-collapse supernovae, discovered by Fröhlich et al. (2006a,b), Pruet et al. (2006), and Wanajo (2006). The νp-process occurs in explosive environments when proton-rich matter is ejected under the influence of strong neutrino fluxes. This includes the innermost ejecta of core-collapse supernova (see Sect. 4.4) and possibly also ejecta from black hole accretion disks (see Sect. 4.5). The discussion of these innermost ejected mass zones has been skipped above, presenting the results for explosive nucleosynthesis in a 20 $M_\odot$ star, but we mentioned already (together with the PUSH approach) the neutrino effects on Y_e, the effect on the composition of the Fe-group, and entered in Table 4.9 an entry νp-process for proton-rich conditions in the alpha-rich complete Si-burning. The PUSH treatment guaranteed a Y_e that is consistently determined by all weak interactions processes and led to a Y_e enhanced beyond 0.5 (see Fig. 4.17).

The matter in these ejecta is heated to temperatures well above 10^{10} and becomes fully dissociated into protons and neutrons. The ratio of protons to neutrons is mainly determined by neutrino and antineutrino absorptions on neutrons and

protons, respectively. Similar neutrino and antineutrino energy spectra and fluxes produce proton-dominated matter in the reactions $\nu_e + n \leftrightarrow p + e^-$ and $\bar{\nu}_e + p \leftrightarrow n + e^+$, due to the n-p mass difference. When the matter expands and cools, the free neutrons and protons combine into α-particles. Later, at temperatures around 5×10^9 K, alpha-particles assemble into heavier nuclei via unstable intermediate nuclei, e.g. the triple-α reaction via unstable ^{8}Be, but—depending on the entropy and the expansion of matter—only a fraction of those form iron-group nuclei (alpha-rich freeze-out). In case of a proton-rich environment, there are also still free protons available at the time of the alpha freeze-out. Once the temperature drops to about 2×10^9 K, the composition of the ejecta consists mostly of ^{4}He, protons, and iron group nuclei with N≈Z (mainly ^{56}Ni) in order of decreasing abundance. Without neutrinos, synthesis of nuclei beyond the iron peak becomes very inefficient due to bottleneck (mainly even-even $N = Z$) nuclei with long beta-decay half-lives and small proton-capture cross sections. Such a nucleus is ^{64}Ge. Thus, with the Y_e determined by neutrino interactions with free neutrons and protons in the early very hot phase of dissociated nuclei, the nucleosynthesis leads to an alpha- and proton-rich freeze-out which does not stop at ^{56}Ni but continues up to ^{64}Ge (which later decays to ^{64}Zn. This part of the story enables core collapse yields which produce Fe-group nuclei up to essentially ^{64}Zn. The effect is seen in the upper portion Fig. 4.34 from the original publications (Fröhlich et al. 2006a,b).

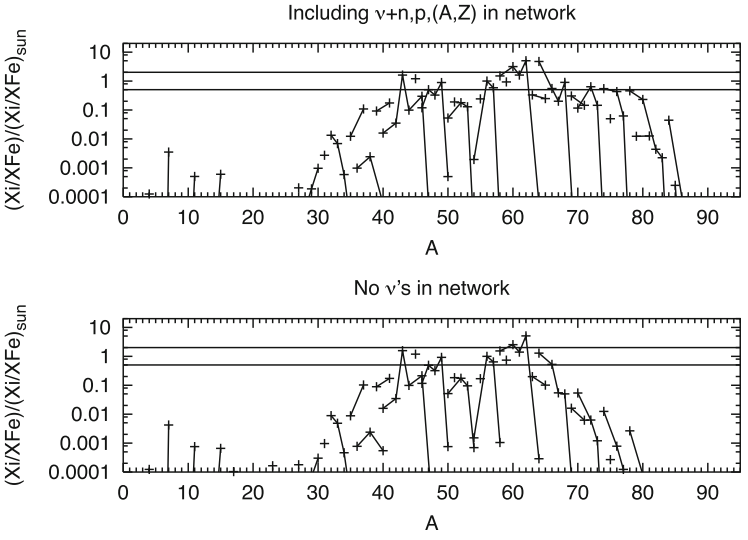

Fig. 4.34 Final abundances in mass zones in the innermost ejecta which experienced neutrino irradiation, leading to proton-rich conditions ($Y_e > 0.5$). The upper part of the figure shows the nucleosynthesis results in the innermost ejecta of explosive, after alpha-rich and proton-rich freeze-out from Si-burning, normalized to solar after decay. The bottom part of the figure also includes the interaction of anti-electron neutrinos with protons ($\bar{\nu}_e + p \rightarrow n + e^+$) which produces neutrons, permitting the late change of ^{64}Ge via ^{64}Ge$(n, p)^{64}$Ga. This feature permits further proton captures to produce heavier nuclei (the so-called νp-process. Here matter up to $A = 85$ is produced

However, the matter is subject to a large neutrino/antineutrino flux from the proto-neutron star. While neutrons are bound in neutron-deficient $N = Z$ nuclei and neutrino captures on these nuclei are negligible due to energetics, antineutrinos are readily captured both on free protons and on heavy nuclei on a timescale of a few seconds. As protons are more abundant than heavy nuclei, antineutrino captures occur predominantly on protons, leading to residual neutron densities of 10^{14}–$10^{15}\,\mathrm{cm}^{-3}$ for several seconds. These neutrons are easily captured by heavy neutron-deficient nuclei, for example ^{64}Ge, inducing (n, p) reactions with time scales much shorter than the beta-decay half-life. This permits further proton captures and allows the nucleosynthesis flow to continue to heavier nuclei (see lower part of Fig. 4.34). The νp-process (Fröhlich et al. 2006b) is this sequence of (p, γ)-reactions, followed by (n, p)-reactions or beta-decays, where the neutrons are supplied by antineutrino captures on free protons.

Similar effects were found by Weber et al. (2008) with improved experimental nuclear input on the proton-rich side of stability for the isotopes ^{87,88}Sr, ^{88}Tc, ^{89}Y, and ^{90,91}Zr. The recent PUSH results (Sinha et al. 2017; Curtis et al. 2018) find sizable abundances up to A = 120.

4.6.3.3 The r-Process

A rapid neutron-capture process (r-process) in an explosive environment is traditionally believed to be responsible for the nucleosynthesis of about half of the heavy elements above Fe. While in recent history the high entropy (neutrino) wind (HEW) of core-collapse supernovae had been considered to be one of the most promising sites, hydrodynamical simulations with the appropriate input physics (see Sect. 4.4.2) encounter difficulties to reproduce the astrophysical conditions under which this process occurs and more appropriate sites are probably MHD supernovae/magnetars or neutron star mergers (see Sect. 4.5 and Thielemann et al. 2017b).

For a pedagogical understanding the classical *waiting-point* approximation, with the basic assumptions of an Fe-group seed, an $(n, \gamma) - (\gamma, n)$-equilibrium for constant neutron densities n_n at a chosen temperature T, over a process duration τ, and an instantaneous freeze-out, has helped to gain improved insight into the systematics of an r-process in terms of its dependence on nuclear-physics input and astrophysical conditions (Cowan et al. 1991; Kratz et al. 1993, 2007). This corresponds to a set of quasi-equilibria with each QSE group being represented by an isotopic chain. Taking a specific seed nucleus, the solar r-process pattern peaks can be reproduced by a variation/superposition of neutron number densities n_n and durations τ. Whether the solar r-process abundances are fully reproduced in each astrophysical event, i.e., whether each such event encounters the full superposition of conditions required, is a matter of debate (Freiburghaus et al. 1999a; Farouqi et al. 2010). In realistic astrophysical environments with time variations in n_n and T, it has to be investigated whether at all and for which time duration τ the supposed $(n, \gamma) - (\gamma, n)$-equilibrium of the classical approach will hold and how freeze-out effects change this behavior. In general, late neutron captures may alter the final

abundance distribution. In this case neutron capture reactions will be important. Also β-delayed neutrons can play a role in forming and displacing the peaks after freeze-out.

There have been a number of suggestions for sites in which the strong r-process originates, being related (1) to the innermost ejecta of regular neutrino-driven core-collapse supernovae (Woosley et al. 1994; Takahashi et al. 1994; Hoffman et al. 1997; Qian and Wasserburg 2007; Farouqi et al. 2010; Roberts et al. 2010, 2012; Martínez-Pinedo et al. 2012; Arcones and Thielemann 2013; Mirizzi et al. 2015), (2) ejecta from binary neutron star mergers (Lattimer and Schramm 1976; Eichler et al. 1989, 2015; Freiburghaus et al. 1999b; Goriely et al. 2011, 2015; Bauswein et al. 2013; Rosswog et al. 2014; Wanajo et al. 2014; Just et al. 2015; Ramirez-Ruiz et al. 2015; Thielemann et al. 2017b), and (3) a special class of core collapse supernovae (MHD-jet supernovae) with fast rotation, high magnetic fields and neutron-rich jet ejecta along the poles (Fujimoto et al. 2008; Ono et al. 2012; Winteler et al. 2012; Mösta et al. 2014, 2015, 2017; Nishimura et al. 2015, 2017b).

Supernovae have been thought to be the origin of a strong r-process for many years, with the intrinsic expectation that the innermost ejecta, coming from regions close to the neutron star, should be neutron-rich (see e.g. Cowan et al. 1991; Sumiyoshi et al. 2001). Even when prompt explosion were realized to fail, early detailed and full-fledged r-process calculations in the neutrino wind, emerging from the hot proto neutron star, still underlined this expectation (Woosley and Hoffman 1992; Meyer et al. 1992; Woosley et al. 1994; Takahashi et al. 1994; Hoffman et al. 1997; Qian and Wasserburg 2007; Roberts et al. 2012; Arcones and Thielemann 2013) and parameterized simulations led to quite impressive results (Freiburghaus et al. 1999a; Farouqi et al. 2010; Kratz et al. 2014). Figure 4.35 is taken from the latter reference and shows a close to excellent fit to solar r-process abundances, especially when utilizing modern input from nuclear mass models.

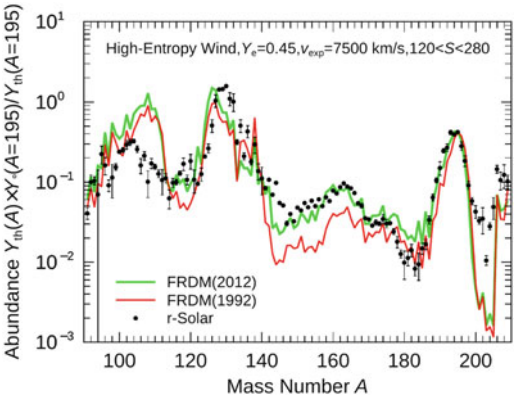

Fig. 4.35 Results from an r-process calculation, assuming an initial Y_e of 0.45, the adiabatic expansion of matter in a so-called neutrino wind with a given expansion speed v_{exp} of ejected mass shells, and that a superposition of entropies S between 120 and 280 k_B/baryon can be attained. The abundance plot assumes that similar amounts of matter are ejected per entropy interval and indicates the changes which occur due to utilizing an improved nuclear mass model (Möller et al. 2012, 2016)

However, in order to obtain this result, a superposition of entropies of up to 280 k_B per baryon is needed, which present simulations of neutrino-driven core collapse supernovae do not support, (see e.g. Fischer et al. 2010; Hüdepohl et al. 2010; Arcones and Thielemann 2013; Roberts et al. 2012; Mirizzi et al. 2016). Thus, while a real high-entropy wind would be able to lead to a strong r-process, presently there is no indication that the required entropies can be attained in realistic core-collapse supernova simulations. An exception might be so-called electron-capture supernovae in the stellar mass range 8–10 $M_\odot$, which could lead to a weak r-process (Kitaura et al. 2006; Janka et al. 2008; Wanajo et al. 2009, 2011), possibly producing nuclei up to Eu, but not up to and beyond the third r-process peak (for more details see Mirizzi et al. 2016).

4.7 The Aftermath of Explosions

In the preceding sections we have given an overview of hydrostatic and explosive burning processes in massive stars, including the individual phases of stellar evolution, and their final stages such as core collapse, and supernovae explosion. Variations in outcome will occur if core collapse ends in neutron star and black hole formation, related possibly to hypernovae or gamma-ray bursts. In the sections that follow we aim to (1) get a complete picture of how hydrostatic/wind and explosive contributions add up to the complete yields that could be observed, then (2) verify such models and simulations through specific types of observations, such as light-curves and spectroscopic signatures, and last (3) integrate all such events/stellar yields over a mass distribution and metallicity range as encountered in the evolution of galaxies, in order to discuss comparisons with observations which average over several/many stellar generations.

4.7.1 Overall Nucleosynthesis Yields

In Sect. 4.4 we have introduced in Eq. (4.7) a simplified rule which determined at which radius certain temperatures are attained in the explosion, assuming that the explosion energy is distributed at all times in a homogenous bubble within the radius of the present supernova shock position. If one knew the radial mass distribution $M(r)$ in pre-explosion models, which the shock front will traverse, one would know the amount of matter which encountered certain burning conditions. In Table 4.10 we put together a set of guiding information for different initial stellar masses at (up to) which radial mass position explosive (complete and incomplete) Si-burning, O-burning, Ne/C-burning would occur (upper portion), and on the size of these regions involved herein (in $M_\odot$; lower portion); still based on models from Nomoto and Hashimoto (1988). In addition, we give the size of the CO-core from prior He-burning in the stellar evolution. To first order, matter is ejected

Table 4.10 Mass zones and products in explosive and hydrostatic burning

$M(r)$	*Burning site*	$13\,M_\odot$	$15\,M_\odot$	$20\,M_\odot$	$25\,M_\odot$
Fe-core	Hydr. Si-burning	1.18	1.28	1.40	1.61
Mass cut	(Expl. mechanism)	?	?	?	?
Ex Si-c	Expl. compl. Si-burning	1.40	1.44	1.69	1.80
Ex Si-i	Expl. incompl. Si-burning	1.47	1.51	1.75	1.89
Ex O	Expl. O-burning	1.54	1.57	1.81	2.00
Ex C/Ne	Expl. Ne-burning	1.65	1.70	2.05	2.40
CO-core	Hydr. He-burning	1.75	2.02	3.70	5.75

unchanged from between the explosive C/Ne-burning region and the stellar surface. This simplified treatment ignores every detail of the explosion mechanism which produced the energy of the explosion, and also the separation between compact remnant and ejecta (the mass cut) is not known, and therefore also not the total amount of complete Si-burning material. The listed core sizes (e.g., CO-core after He-burning) also do not distinguish whether this matter resulted from initial core burning or subsequent outward propagating shell burning (e.g. shell He-burning or shell C-burning). Each of these produce specific isotopes of interest in this book, such as ^{26}Al, ^{60}Fe, as discussed in Sect. 4.3 and Chap. 3.

Initially we want to focus here on the explosive burning phases. We also want to add that the radial masses given in Table 4.10 show consistent values with (a) the simplified Eq.(4.7) applied to the appropriate stellar model ($M(r)$) and as well as with (b) results from an actual explosion calculation (initiated via a thermal bomb), as obtained in Thielemann et al. (1996). When comparing these numbers, we see a quite close agreement, except for the most massive stars where non-negligible deviations are encountered.

Based on this information we want to discuss complete nucleosynthesis yields, including explosive processing (also the νp-process, affected by neutrinos in the innermost ejecta, as well as the p-process in explosive Ne/O-burning), hydrostatic yields from the outer layers (including s-process) which are ejected unaltered, and prior wind yields lost during stellar evolution. Then we concentrate on the long-lived radioactivities ^{26}Al, ^{60}Fe, ^{44}Ti, other Fe-group and lightcurve-determining nuclei, including their origin which is e.g. important for ^{26}Al and ^{60}Fe, which have hydrostatic burning as well as explosive origins. The r-process in the neutrino wind or possibly polar jets has been presented qualitatively with entropy, Y_e and expansion timescale as free parameters or expansion timescale of neutron star matter as a free parameter. Presently no realistic explosion models are available to discuss this in sufficient detail for a link to observations, but a short discussion of long-lived radioactive chronometers is presented.

Table 4.10 leads to the following conclusions: The amount of ejected mass from the unaltered (essentially only hydrostatically processed) CO-core varies strongly over the progenitor mass range. The variation is still large for the ashes from explosive Ne/C-burning, while the amounts from explosive O- and Si-burning are

almost the same for all massive stars. Therefore, the ejecta mass from the unaltered CO-core and from explosive Ne/C-burning (C, O, Ne, Mg) varies strongly over the progenitor mass range, while the amount of ejecta from explosive O- and Si-burning (S, Ar, and Ca) is almost the same for all massive stars. Si has some contribution from hydrostatic burning and varies by a factor of 2–3. It should be mentioned that the present numbers are obtained, assuming for all progenitors the same explosion energy of 10^{51} erg. Thus, changing explosion energies, i.e. with the compactness of the progenitor will have an effect as well. Increasing compactness with progenitor mass would add (as correction) an additional progenitor mass dependence. The amount of ejecta with Fe-group nuclei depends directly on the explosion mechanism, which also affects the Y_e in these inner zones. These numbers are already available for the PHOTB simulations (Sukhbold et al. 2016) and will be soon available for the PUSH simulations (Ebinger et al. 2017, 2018; Sinha et al. 2017; Curtis et al. 2018).

Thus, we essentially have three types of nucleosynthesis products, which test different aspects of supernovae, when comparing with individual observations. The first set (C, O, Ne, Mg) tests the stellar progenitor models, the second (Si, S, Ar, Ca) the progenitor models and the explosion energy in the shock wave, and the Fe-group (beyond Ti) in addition probes the actual supernova mechanism. Thus, we require that all three aspects of the predicted abundance yields are based on secure modeling (stellar evolution, explosion energy, and explosion mechanism) in order to be secure for their application in lightcurve modeling, radioactivities in remnants as well as the in chemical evolution of galaxies (Nomoto et al. 2013; Mishenina et al. 2017).

As an example, we show in Fig. 4.36 the total yield of massive stars, versus their initial mass, and also the different components contributed from hydrostatic burning and ejected with stellar wind, and from the explosive release, which includes explosive nuclear burning contributions as well. Although over-all, different implementations of stellar evolution and explosion find yields which agree within factors of a few, there clearly are characteristic yield behaviors which depend on the implementation of the model. Unlike believed about 20 years ago, the wind contributions will likely not dominate the total ^{26}Al yields, although they remain a key contribution. Then, depending on the explodability of stars with masses above 25–40 $M_\odot$, the more-massive end of the stellar mass distribution may only contribute through their wind phases.

4.7.2 Spectroscopic Observations of Nucleosynthesis Products

The supernova explosion ejects freshly-produced nuclei, among those radioactive isotopes, which decay in and outside the expanding remnant. They can be observed rather directly through their nuclear and atomic lines, in X- and gamma-rays.

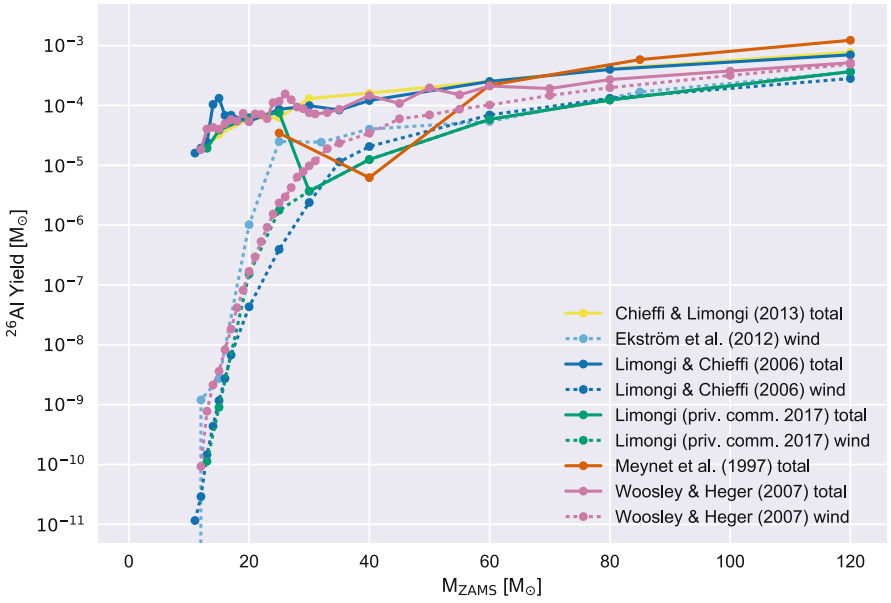

Fig. 4.36 The ^{26}Al yields from wind ejections and from the explosive release in the supernova, as a function of the initial mass of the star (from Meynet et al. 1997; Woosley and Heger 2007; Limongi and Chieffi 2006b; Ekström et al. 2012; Chieffi and Limongi 2013; Limongi, private communication)

4.7.2.1 SN1987A

The γ-ray line discovery only a few weeks after SN1987A had occurred in the Large Magellanic Cloud in February 1987 marks the first case to identify characteristic γ-rays from a single nucleosynthesis source and a specific isotope, through ^{56}Co decay lines at 847 and 1238 keV. These lines were seen in data of the Gamma-Ray Spectrometer on the Solar Maximum Mission (Matz et al. 1988; Leising and Share 1990). Their appearance was significantly earlier than expected from a spherically stratified distribution of elements, where the Fe-group nuclei are produced in the center. This is interpreted as due to deviations from spherical symmetry in the expanding remnant, bringing Ni-rich clumps to the surface earlier by convective instabilities, mixing ^{56}Ni/^{56}Co to outer layers at early times. Gamma-ray line profiles measured with high spectral resolution (a Ge detector balloon instrument launched quickly to exploit this unique opportunity, Tueller et al. 1990) indicated Doppler broadening of the lines from their ejecta motion. Several years later, after the Compton Gamma Ray Observatory (CGRO) was launched, the OSSE instrument on CGRO detected ^{57}Co (τ ~1.1 years) through its gamma-ray line at 122 keV, as another direct proof of iron group nuclei produced in the right amounts (Kurfess et al. 1992). A tentative detection of ^{44}Ti gamma-rays had been reported from INTEGRAL's two instruments (Grebenev et al. 2012); the flux inferred from

this observation seemed surprisingly high, and suggested some contamination may have contributed to this signal. But with NuSTAR, finally, also the fainter gamma-ray lines from decay of ^{44}Ti (τ ~89 years) could be clearly detected (Boggs et al. 2015), with an inferred ^{44}Ti amount of $(1.5 \pm 0.3) \times 10^{-4}$ $M_\odot$. SN1987A clearly is the best-observed core-collapse supernova, also in gamma rays that directly relate to a specific isotope.

4.7.2.2 Cas A

The discovery of the 1157 keV ^{44}Ti γ-ray line emission from the youngest Galactic SNR Cas A with COMPTEL indexsupernova!Cas A (Iyudin et al. 1994) was the first direct proof that this isotope is indeed produced in a supernova explosion from a massive star. Many follow-up observations were able to confirm this: With the two lines at 68 and 78 keV, respectively, from the initial stage of ^{44}Ti decay to ^{44}Sc, also X-ray instruments such as BeppoSAX/PDS and later NuSTAR were able to measure the in-situ decay of ^{44}Ti in this 350-year-old (or 'young') supernova remnant. By combining observations, Vink et al. (2001) deduced a ^{44}Ti yield of $(1.5 \pm 1.0) \times 10^{-4}$ $M_\odot$. This could later be refined, adding the high signal-to-noise NuSTAR measurement and the measurement of all 3 decay lines from ^{44*}Sc and also ^{44*}Ca de-excitations with INTEGRAL/SPI (Siegert et al. 2015). The consolidated value of ^{44}Ti yield of $(1.4 \pm 0.2) \times 10^{-4}$ $M_\odot$ seemed higher than the predictions of most models, and provides a constraint to be met by model variants.

The ^{44}Ti detection in Cas A stimulated several activities in related fields: The decay time was re-investigated in nuclear laboratories, through both measurements tracing the decay as well as the absolute radioactive activity, both challenging; the uncertainty of 10–20 % at the time of the Cas A detection could thus be reduced to below 1 % and a consolidated decay time of (85.12 ± 0.43) years (Ahmad et al. 2006). Then, nuclear reactions involved in ^{44}Ti production were re-investigated. The α-rich freeze-out from Si burning involves many reactions, and detailed nuclear network analysis is required (Magkotsios et al. 2010). Finally, the supernova explosion from the collapse of a massive star is a complex, 3-dimensional phenomenon, as discussed above. Simulations and models have begun to explore the impacts of deviations from spherical symmetry, which, as discussed above (Sect. 4.6), are probably very significant for ^{44}Ti ejection (Nagataki et al. 1998; Wongwathanarat et al. 2015, 2017; Harris et al. 2017), unlike many other supernova observables. From the three different γ-ray lines resulting from the ^{44}Ti decay chain, constraints for kinematic Doppler broadening can be derived: The Doppler broadening being a linear function of energy, it would broaden the 1157 keV line to values in the few to tens of keV range, which can be measured with Ge spectrometers; the lower-energy lines at 68 and 78 keV would not show significant kinematic broadening. INTEGRAL/SPI spectrometer data show that there is some tension among constraints from the different ^{44}Ti lines; but all confirm that the inner ejecta have velocities faster than 1500 km s^{-1}, clearly contradicting an earlier belief

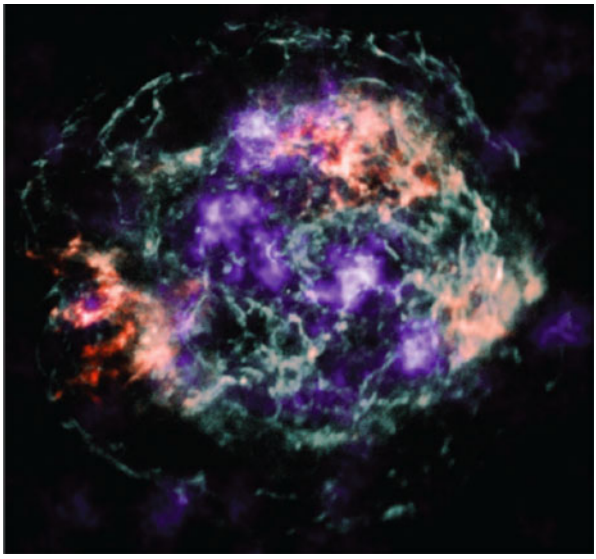

Fig. 4.37 The Cas A supernova remnant image in emission from ^{44}Ti decay (purple), superimposed on an X-ray image showing recombination lines (iron in red, silicon in green) (from Grefenstette et al. 2014)

that inner ejecta from close to the mass cut should be slow: The 'mass cut' concept over-simplifies the true 3D nature of the explosion.

The observations of the ^{44}Sc lines from ^{44}Ti decay with NuSTAR have obtained another important piece of information on the Cas A explosion: NuSTAR's X-ray mirror and field of view were just right to obtain an *image* of Cas A in line emission from ^{44}Ti decay, shown in Fig. 4.37 (Grefenstette et al. 2014). As emission from ^{44}Ti decay does not depend on thermodynamic variables nor ionisation state, the purple features in the image clearly show that these ejecta appear in clumps. Further analysis of spatial and velocity information leads to a picture where much of the ejected ^{44}Ti occurs away from our line of sight (Grefenstette et al. 2017), possibly in momentum balance with the motion of the remnant neutron star. Comparing with recombination emission that had been observed and imaged earlier with the Chandra X-ray satellite (red structures in Fig. 4.37), it appears that some of the iron that would be expected to be ejected with ^{44}Ti is not seen in X-rays, likely because the reverse shock has not reached those clumps to ionise the iron and thus make them shine in X-ray line emission. This demonstrates the complementary views of different observables, and also reminds us that observational bias could be severe and thus could have distorted our view of how supernovae explode and shed their ejecta.

Many supernova remnants show mixing in their ejecta (Vink 2005). There are theoretical indications that this could arise from instabilities as the propagating shock wave traverses the envelope; however, steep density gradients such as the H/He interface also have the opposite effect, as the shock is accelerated when passing such an interface. Also, the expansion of the supernova into an inhomogeneous medium such as, for example, structured by the pre-supernova wind phase, will lead

to deviations from spherical symmetry. SN1987A and its rings is a prominent such example (as reviewed in McCray and Fransson 2016). This illustrates the special role of ^{44}Ti and ^{56}Ni radioactive products, where 3D effects are much more directly related to the physics of the inner collapse and explosion.

4.7.2.3 Other Young Supernova Remnants

If ^{44}Ti ejection as seen in the Cas A event was typical for core-collapse events, the *gamma*-ray surveys made with COMPTEL (Dupraz et al. 1997; Iyudin et al. 1999) and with INTEGRAL (Renaud et al. 2006; Tsygankov et al. 2016) should have seen several objects along the plane of the Galaxy through their ^{44}Ti decay emission. But beyond Cas A, no firm detection of ^{44}Ti has been established since, though several candidates have been suggested: SNR RXJ0852.0-46.22 (Aschenbach 1998; Aschenbach et al. 1999; Slane et al. 2001), SNR G1.9+0.3 (Borkowski et al. 2010, 2013), and a source candidate in Perseus (Dupraz et al. 1997). None of these could be consolidated. From this, it had been concluded that ^{44}Ti ejection is rather a characteristic of a rare subclass of core-collapse supernovae (The et al. 2006; Dufour and Kaspi 2013).

The Vela region includes the Gum nebula and the Vela Supernova Remnant, two remnants from supernovae which are bright in X- and radio emissions. Both are relatively nearby, in the foreground of the Vela molecular ridge which is one of the nearest star-forming regions and located in about 700($\pm$200) kpc distance (Massi et al. 2007). At this distance, even for supernova remnants much older than the ^{44}Ti radioactive lifetime, a search for ^{26}Al seemed promising. With COMPTEL, diffuse and extended emission had been recognized from this direction (Diehl et al. 1995). But possibly-underlying extended ^{26}Al emission limits the interpretation of this measurement towards calibration of a single supernova in ^{26}Al; the ^{26}Al gamma-ray flux attributed to this supernova remnant is 0.5–2.7 10^{-5} ph cm^{-2} s^{-1}, well within expectations of an ^{26}Al yield of 10^{-4} M$_\odot$. Also for the much younger supernova remnant RXJ0852.0-46.22 or *Vela Junior*, no ^{26}Al emission was found. This is plausible, as the supernova remnant is probably older than 1000 y and more distant than 740 pc (Katsuda et al. 2009).

4.7.2.4 The ^{60}Fe to ^{26}Al Ratio

Cumulative emission from massive-star nucleosynthesis and its long-lived by-products ^{26}Al and ^{60}Fe has also been analysed. As pointed out from theorists (see, e.g. Woosley and Heger 2007), the same massive-star population likely is responsible for the bulk of these isotopes in the current Galaxy. As discussed above, ^{26}Al and ^{60}Fe originate, however, in very different zones and evolutionary phases of massive stars. ^{60}Fe only is ejected in the supernova, while ^{26}Al is both ejected in the supernova and in an earlier wind for very massive (Wolf Rayet) stars. The ratio measured from gamma rays is $\sim$ (15 $\pm$ 5) % (Wang et al. 2007).

Apparently a high mass loss rate is required to not overproduce ^{60}Fe in high mass stars $M > 40\ M_\odot$ (Limongi and Chieffi 2006b) with respect to these γ-ray line constraints (see discussion in Woosley and Heger 2007; Wang et al. 2007, and Chap. 7).

4.7.2.5 Fe-Group and Beyond, r-Process Ejecta

Matter close to the newly-forming neutron star is expected to be exposed to conditions ranging from nuclear statistical equilibrium, with Fe-group nuclei as major outcomes, to intense irradiation of available seed nuclei with free nucleons and α's, leading to an r-process or p-process, depending on the Y_e, and α captures in the nucleosynthesis and freeze-out phases.

In this picture, innermost matter which mainly experienced the shock only is thus ejected earlier. A typical example for the composition of such ejecta is shown in Fig. 4.28, which displays the zones of complete Si-burning with alpha-rich freeze-out. The change in abundances at mass coordinate $M = 1.63\,M_\odot$ is due to a change in Y_e in the underlying stellar-evolution model result, which was utilized for explosive nucleosynthesis predictions here, by introducing a simply thermal bomb of 10^{51} erg energy in the inner region. Early neutrino-wind models assumed neutron-rich material in the region behind those ejecta, shaped by the evaporising neutron star. But if one accounts correctly for the neutrino interactions during collapse and explosion, this matter even turns out to be slightly proton-rich ($Y_e > 0.5$). This leads to the νp-process discussed in Sect. 4.4 and Figs. 4.16 and 4.34 (Fröhlich et al. 2006a,b; Pruet et al. 2005, 2006; Wanajo 2006). This process then results also in a production of substantial fractions of ^{64}Ge (decaying to ^{64}Zn via ^{64}Ga. Both isotopes have a short half-life (minutes to seconds), and are therefore not of interest in terms of radioactivities which power an afterglow, or which may decay with characteristic gamma rays being observable. But in this νp-process also to the production of Sr and heavier nuclei can occur. The isotopic ratios ^{58}Ni, and ^{60,61,62}Zn are strongly modified by this process. Alpha-nuclei abundances such as ^{40}Ca, ^{44}Ti, ^{48}Cr, and ^{52}Fe are affected in characteristic ways as well. Higher entropies (such as expected in very energetic explosions and hypernovae) and higher Y_e-values, that is, close to 0.5, both increase the fraction of these alpha-nuclei, and this could proceed beyond ^{56}Ni up to radioactive ^{64}Ge that decays to the most-abundant Zn isotope ^{64}Zn, as discussed in Sects, 4.4 and 4.5. From observational constraints compared to chemical-evolution models, probably only a small fraction of black-hole producing events should lead to hypernovae, rather than ~50% as assumed in some cases (Nomoto et al. 2006; Kobayashi et al. 2006; Kobayashi and Nakasato 2011)). We caution, however: There are degeneracies, and a reduced ^{64}Ge production from hypernovae can well be balanced by a larger ^{64}Ge production in regular supernovae, which may follow with correct inclusion of neutrino-interactions and their effect on increasing Y_e to values larger than 0.5.

After the supernova shock has been launched, the neutrino wind evaporises the surface layers of the proto-neutron star, and also energises the shock from below to launch the explosion. This is an area of biggest uncertainty. It was believed that a neutron-rich wind which could trigger a rather complete, full r-process (Qian and Woosley 1996; Woosley et al. 1994). But after early questioning from other investigations (Takahashi et al. 1994; Liebendörfer et al. 2003), more-detailed calculations of neutrino physics and detailed transport modeling find the opposite behavior, i.e. proton-rich conditions for more than the first 10s after the explosion (Fischer et al. 2010). This is discussed above Sect. 4.6) together with the νp-process. A major question is if and how this environment might change again to be neutron-rich in late phases of the explosion, and what physics underlies this change (such as the nuclear equation-of-state, or neutrino interactions; see Fischer et al. 2016) a following question then is how the high entropies can be attained to produce also the heaviest nuclei. Observations of low metallicity stars show huge variations in heavy r-process content relative to iron. This indicates that in most supernova explosions no r-process is taking place, leaving the *full* r-process to a rare subclass with special settings. Typical supernovae might only provide an environment for a weak r-process. Whether either high entropies are only attained in exceptional cases or other origins of low entropy, highly neutron-rich matter (neutron star mergers or neutron-rich jets from rotating core collapse supernovae Freiburghaus et al. 1999a; Cameron 2003) cause the main r-process has to be explored, including the still-remaining challenges of nuclear physics far from stability.

In the preceding sections we have shown that a fundamental understanding about the nuclear working of the r-process is available, and that it is possible to reproduce solar system r-process elemental abundance pattern though superpositions of components with different environmental conditions. Yet, it seems impossible to clearly identify *the* responsible astrophysical site.

One can use radioactivity and nucleochronocosmology to advance (as also discussed in Chap. 2): Adopting such a composite, superimposed, r-process fit as setting *zero-age* abundances, that is, with production ratios for ^{232}Th/^{238}U or other actinide (chronometer) nuclei, one can evaluate how such ratios evolve as a function of decay time to later and present-age abundances. This allows to identify formation ages of very metal-poor stars, born with a fresh ingestion of an r-process pattern at that time (see, e.g., Cowan et al. 1991, 1999; Thielemann et al. 2002; Kratz et al. 2007, and references therein). A typical result of such studies is that these chronometers suggest an age of the oldest stars in our Galaxy of 14–15 Gyr, with an uncertainty of about 3–4 Gyr.

4.7.3 Radiogenic Luminosity and Late Lightcurves

Supernova light curves are powered by radioactive decays. Very early interpretations of supernova lightcurves related them to the radioactive decay of ^{254}Cf (Burbidge et al. 1957). In fact, a strong r-process (with fission-cycling) would cause observable

features based on the decay of heavy radioactive nuclei. This question re-appeared, as a potential optical transient (macronova) was predicted from a neutron star merger and its r-process radioactivities (see Metzger et al. 2010, and below). Supernova lightcurves, however, are dominated by Fe-group ejecta. In addition to abundant ^{56}Ni, there are a number of radioactive nuclei which will decay on time scales of ms up to 10^7y. Here we only want to concentrate on a few nuclei, which by a combination of their abundances and half-lives, can be of importance. These nuclei are ^{56}Co (^{56}Ni), ^{57}Co (^{57}Ni), ^{55}Fe (^{55}Co), ^{44}Ti, and ^{22}Na. For a 20 $M_\odot$ star like SN 1987A they were predicted with total masses of 0.07, 3.12×10^{-3}, 3.03×10^{-4}, 1.53×10^{-4}, and 1.33×10^{-7} $M_\odot$ (Thielemann et al. 1990, 1996).

Observations of light curves in radiation which reflects the thermalized energy of this radioactivity constrained these values to $M(^{56}\text{Ni})\approx 0.071\,M_\odot$ (e.g., Suntzeff and Bouchet 1990) and $M(^{57}\text{Ni})\approx 3.3\times10^3\,M_\odot$ (Fransson and Kozma 1993, and references therein). A very careful analysis extracted an upper limit on ^{44}Ti of the order $1.1\times10^{-4}\,M_\odot$ (Lundqvist et al. 2001). A recent re-assessment, including radioactivity inputs from gamma-rays, positrons, as well as electron captures (Auger electrons) (Seitenzahl et al. 2012) finds a ^{44}Ti amount of $(0.55\pm0.2)\times10^{-4}\,M_\odot$ to best fit the detailed late light curve constraints up to more than 4000 days. This is significantly below the value derived from the hard X-ray lines of ^{44}Ti decay directly. Uncertainties from the radioactive energy deposit in the expanding remnant exist, and certainly it is important to have calibrations from more than a few objects with measurements of direct radioactivity as well as its re-radiated energy deposit.

Let us discuss the various steps of radioactive energy deposition in more detail: Generally, after beta-decay or electron capture, a daughter nucleus is produced in an excited state (^{55}Fe is a notable exception, see below). The ground state is reached by one or several gamma transitions, observable by current gamma-ray detectors for nearby sources (see Sect. 10.1). Photons, positron-electron annihilations following β^+-decays, and the kinetic energy given to the decay products can contribute to the light curve at later times. The number of photons released for each of the transitions, occurring in the daughter nucleus after beta-decay, is equal to the number of decays N_d, multiplied with the appropriate percentage of the occurrence (*branching ratio*) for the specific transition. The total energy released corresponds to the product of the number of decays with the decay Q-value:

$$N_d(t) = -\frac{dN}{dt}(t) = \lambda N_o \exp(-\lambda t) \quad \frac{dE}{dt}(t) = Q N_d(t) = Q\lambda N_o \exp(-\lambda t), \quad (4.8)$$

where $\lambda = \ln 2/t_{1/2}$ is the decay rate of the nucleus. The initial number of radioactive nuclei can be calculated from their total mass by $N_o = M/Am_u$, with A being the nucleon number of the nucleus, m_u the atomic mass unit, and M the mass given above. When using the radioactivity half-lives of relevant isotopes expected in supernova ejecta (i.e., 78.76d, 271.3d, 2.7y, 54.2y, and 2.602y, and atomic Q-values of 4.566, 0.835, 0.232, 3.919, and 2.842 MeV) we can estimate radioactive-energy generation rates in erg s^{-1} and the total number of decays per sec. The Q-value used for ^{44}Ti combines the subsequent decays of ^{44}Ti and ^{44}Sc.

Q-values include all available energies, i.e. the kinetic energy of the decay products, the energy in photons, the annihilation energy of positron-electron pairs in β^+-decays, and the neutrino energy. At densities prevailing in the expanding remnant, neutrinos will escape freely and their energy has to be subtracted, which leaves corrected values for the appropriate energy deposits of 3.695, 0.136, 0.0, 2.966, and 2.444 MeV. Because the electron capture on ^{55}Fe does only lead to an energetic neutrino, there is no local energy deposition from this isotope.[10] Gamma transitions following the decays of the other isotopes under consideration obtain candidate γ-rays at (rounded to full percent values): ^{56}Co, 847 keV (100%), 1038 keV (14%), 1238 keV (68%), 1772 keV (16%), 2599 keV (17%); ^{57}Co, 122 keV (86%), 136 keV (11%); ^{44}Ti, 78 keV (93%), 68 keV (88%), 147 keV (9%), 1157 keV (100%); ^{22}Na, 1275 keV (100%; branching ratios given as percentages per decay). If positrons from β^+-decay slow down and annihilate with electrons locally within the supernova envelope, the full neutrino-loss corrected energy corresponding to the reaction Q-value will be deposited in the envelope. Observable signatures include high energy photons such as the ones from the gamma transitions, and their Compton scattered and completely thermalized descendants.[11]

Then the sum of all individual contributions discussed above would make up the bolometric lightcurve of the supernova (see Fig. 4.38). The *light curve*, i.e. the brightness as a function of time, will be dominated first by the decay of ^{56}Co, and then ^{57}Co and ^{44}Ti, if one neglects possible radiation from a pulsar. ^{22}Na never plays a significant role. At lower densities (and later times), escaping high energy photons or positrons lead to a reduction of the brightness of *bolometric* emission. This can be seen towards the later-time observations, as shown e.g. in Leibundgut and Suntzeff (2003) (see Fig. 4.38). An important consistency check is to compare this bolometric light curve (which includes only optical, UV and IR emission, hence thermalized gas and dust components) to the high-energy photons more directly reflecting radioactive decays. At late times, those high energy photons escape freely.

Other indications came from the modeling of the optical light curve. The best agreement between calculated and observed light curves were obtained for a composition which mixed a small fraction of Ni all the way into the 10 $M_\odot$ hydrogen envelope and hydrogen into the deeper layers, containing mostly heavy elements (see, e.g., Benz and Thielemann 1990).

[10]This contribution was recently re-evaluated by Seitenzahl et al. (2009). The electron capture occurs from an electron in an atomic orbit, leaving a hole which can be filled by other electrons cascading down to fill this hole, thus emitting photons—X-rays— or depositing the energy in ejecting outer electrons—Auger electrons. Thus, in cases where only ground-state to ground-state electron capture occurs and the energy is emitted in an escaping neutrino only Auger electrons or X-rays can contribute to local energy deposition.

[11]Deposition of energy from radioactive decay involves absorption of high-energy photons, slowing down of ∼MeV-type energy electrons and positrons, and proper treatment of temporary energy reservoirs such as ionization and inhibited radioactive decay from completely-ionized nuclei (see, e.g., Sim et al. 2009; Mochizuki et al. 1999; Kerzendorf and Sim 2014).

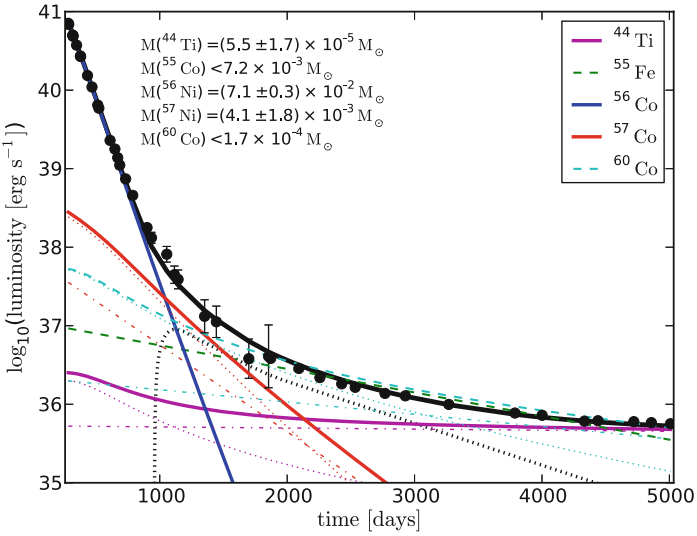

Fig. 4.38 Reconstructed bolometric lightcurve of SN1987A for 5000 days past explosion, using observational data from different bands, cross calibrated and merged (Seitenzahl et al. 2012). The model with its different radioactivity components is shown to provide a satisfactory fit

The lightcurve from SN1987A could be reproduced with theoretical modelling, including the effects of X-ray and γ-ray escape, as well as mixing of ^{56}Ni (see Fig. 4.38). SNe Ib and Ic events, believed to be core collapse events without an overlying hydrogen envelope have to be treated accordingly. The combination of small masses involved (only He-cores or C-cores without H-envelope) and the assumption of mixing can reproduce the steeper decline than found in massive SNe II. A typical case of a type Ic supernova is SN 1998bw, associated with GRB 980425. The straight-forward modeling of the observed lightcurve (Sollerman et al. 2002) led to interpretations of a largely non-solar ^{56}Ni/Fe to ^{56}Ni/Fe ratio. The inclusion of internal conversion and Auger electrons, as suggested by Seitenzahl et al. (2009) could naturally explain the observed slowdown of the lightcurve without invoking such extreme abundance ratios.

We note that in recent years photon transport calculations have reached major improvements, and are now able to consistently reproduce both light curves and spectra from SNIa, and also from core collapse supernovae (e.g. Kerzendorf and Sim 2014; Kasen et al. 2008; Dessart et al. 2015, 2017, for descriptions of the method). Presently, systematic uncertainties of the method are being investigated, and appear rather well understood (at least for SNIa (see, e.g., Woosley et al. 2007). As optical-to-IR light curves and spectra will be collected in abundance through large telescope survey programs for cosmological studies, it is likely that those (more indirect) measurements of core-collapse supernova nucleosynthesis will generate the tightest constraints to learn more about these events and their internal nuclear processes.

We have shown how supernova lightcurves reflect explosion properties and ejecta, though indirectly. More detailed information is contained in the evolution of spectra following an explosion, as the cooling of initially ionised gas and its dilution from expansion provides a characteristic spectral evolution, sometimes called 'tomography'. The receding photosphere in terms of radial mass in an expanding, radiation-filled bubble can give clear indications of the element composition (as a function of time equivalent to declining Lagrangian mass). The problem of type II supernovae is that the huge H-envelope does not really contain much information in terms of nucleosynthesis. Type Ib and Ic supernovae, which lost their H- and possibly He-envelope, reveal much more information of the compact inner part, which experienced explosive processing (e.g., Matheson et al. 2001; Sauer et al. 2006; Branch et al. 2002). This is similar to type Ia supernovae, originating from exploding white dwarfs, which have been extensively utilized for abundance diagnostics.

4.7.3.1 Macronovae from Neutron Star Mergers

Energy deposition from radioactive decays are understood to power the light seen at UV to optical to IR wavelengths from a supernova (see Fig. 4.38 for SN1987A). Such radiation transport is complex, starting from MeV gamma-rays and particles, which have a significant path length until they interact with envelope material to lose their energy, and multiple such interactions then deposit thermal energy. In the case of supernovae, the composition of the envelope is rather well known, as is the expected radioactivity, dominated by ^{56}Ni and ^{44}Ti, as shown above. In the case of neutron star mergers, the situation is much less clear (Kasen et al. 2015). First, the r-process may proceed into the A$\sim$130 region, or may proceed up to the third r-process peak at A$\sim$195 from efficient fission cycling see above). Then, the composition of the envelope where radioactive energy is deposited is unclear as well: Ejecta are expected from the dynamical interaction as the neutron stars approach each other, then from an accretion disk around the newly-forming black hole, and here a wind may be launched for even more complex envelope structure. Hence, it is not straightforward how to learn about those various unknowns; light curves in re-radiated light result from atomic-line multitudes that are largely unknown. Unless such an event would come fortunately-close to measure its radioactivity more directly in nuclear lines (which would require distances below a Mpc), modeling and cross-calibrations of radiogenic luminosities are the tedious way forward.

4.7.4 Material Deposits on Earth and Moon

Ejecta from massive stars are predominant drivers of chemical evolution, as they cool and are incorporated into next generations of stars forming from material

enriched by products of nucleosynthesis (see Chapter on Chemical Evolution). Tracing the flow of ejected plasma as it cools and propagates into the star-forming dense cores of molecular clouds is difficult, as it occurs over times of scale 100 million years, and phase changes from plasma to atoms and molecules add complexity, as do accompanying physical and chemical reactions under varying environmental conditions. However, dust grains formed near the exploding nucleosynthesis site can propagate in different ways, ballistic trajectories and the solid-state form simplifying some of the processing along its journey. Analysing interstellar material which can reach us for example through cosmic rays and meteorites thus provides a valuable 'material astronomy'.

'Stardust' is a major messenger from nucleosynthesis sources (see Chap. 1, Fig. 1.7 and Table 1.1, Chap. 2 for stardust science history, and Chap. 10 on instrumentation). The formation of dust in a supernova envelope is driven by the cooling properties of expanding gas and by nucleation initiating the formation of dust grains from molecules. The composition of such a dust grain then reflects the extent of mixing in the expanding and cooling remnant when chemical reactions and dust formation set in. Clayton and Nittler (2004) review what has been learned from stardust. But, as one example, Liu et al. (2017) discuss the issues as ambiguities among nova or supernova origins remain, while abundances of C, N, and Si isotopes indicate characteristic signatures.

^{60}Fe has been discovered through accelerator-mass spectroscopy (AMS) analyses of ocean crust and lunar material (Knie et al. 2004) (Fig. 10.7 in Chap. 10). If taken from places on Earth which are remote from any antropogeneous contamination, such as in deep parts of the Pacific ocean, they provide a record of past composition of ocean water. Manganese crusts grow very slowly from sedimentation. Therefore, a rather small sample will cover tens of My of sedimentation history within a few cm of depth. ^{60}Fe production from cosmic ray irradiation in the atmosphere is unlikely, other systematic contaminations also seem low. The age of each depth layer can be determined from Be isotopes produced by cosmic rays in the atmosphere of the Earth, also ingested into ocean water with other atmospheric gas and dust. The AMS method is one of the most-sensitive techniques to detect small amounts of specific isotopes, reaching a sensitivity of 10^{-16}.

Meanwhile, ^{60}Fe has been measured in a variety of ocean crust and sediment samples from different deep-sea locations around Earth, and also in lunar material probes; see Sect. 7.3.3 for discussion of how this might relate to nearby supernovae, or to sweeping up by the interstellar shell bounding the Local Bubble cavity of cumulative nucleosynthesis ejecta (Schulreich et al. 2017).

Such terrestrial samples also have been investigated for signs from r-process material, specifically ^{244}Pu, also using the sensitive AMS analysis method. Recently, a positive detection of ^{244}Pu was achieved (Wallner et al. 2015). From the detected amount of nuclei, knowing its age sampling, and estimating transport from interstellar dust to ocean crust settling using cosmic-ray produced trace materials, Wallner et al. (2015) find that their number of nuclei should have been two orders of magnitude larger if r process nucleosynthesis occurred at the same rate as the synthesis of iron group or lighter nuclei. From this, either r-process ejecta are

produced by rare events only, such as neutron star mergers (see Sect. 4.5 and Thielemann et al. 2017b, for a review), or else their transport in interstellar medium is very different from how ejecta from normal massive-star nucleosynthesis is transported to reach Earth.

References

Abbott BP, Abbott R, Abbott TD, Acernese F, Ackley K, Adams C, Adams T, Addesso P, Adhikari RX, Adya VB et al (2017) Multi-messenger observations of a binary neutron star merger. Astrophys J 848:L12. https://doi.org/10.3847/2041-8213/aa91c9. arXiv:1710.05833

Adelberger EG, García A, Robertson RGH, Snover KA, Balantekin AB, Heeger K, Ramsey-Musolf MJ, Bemmerer D, Junghans A, Bertulani CA, Chen JW, Costantini H, Prati P, Couder M, Uberseder E, Wiescher M, Cyburt R, Davids B, Freedman SJ, Gai M, Gazit D, Gialanella L, Imbriani G, Greife U, Hass M, Haxton WC, Itahashi T, Kubodera K, Langanke K, Leitner D, Leitner M, Vetter P, Winslow L, Marcucci LE, Motobayashi T, Mukhamedzhanov A, Tribble RE, Nollett KM, Nunes FM, Park TS, Parker PD, Schiavilla R, Simpson EC, Spitaleri C, Strieder F, Trautvetter HP, Suemmerer K, Typel S (2011) Solar fusion cross sections. II. The pp chain and CNO cycles. Rev Mod Phys 83:195–246. https://doi.org/10.1103/RevModPhys.83.195. arXiv:1004.2318

Ahmad I, Bonino G, Castagnoli GC, Fischer SM, Kutschera W, Paul M (1998) Three-laboratory measurement of the ^{44}Ti half-life. Phys Rev Lett 80:2550–2553. https://doi.org/10.1103/PhysRevLett.80.2550

Ahmad I, Greene JP, Moore EF, Ghelberg S, Ofan A, Paul M, Kutschera W (2006) Improved measurement of the Ti44 half-life from a 14-year long study. Phys Rev C 74(6):065803. https://doi.org/10.1103/PhysRevC.74.065803

Arcones A, Thielemann FK (2013) Neutrino-driven wind simulations and nucleosynthesis of heavy elements. J Phys G Nucl Phys 40(1):013201. https://doi.org/10.1088/0954-3899/40/1/013201. arXiv:1207.2527

Arlandini C, Käppeler F, Wisshak K, Gallino R, Lugaro M, Busso M, Straniero O (1999) Neutron capture in low-mass asymptotic giant branch stars: cross sections and abundance signatures. Astrophys J 525:886–900. https://doi.org/10.1086/307938. arXiv:astro-ph/9906266

Arnett D (1996) 2D simulations of supernovae. In: IAU Colloquium. Supernovae and supernova remnants, vol 145, pp 91–+

Arnett D, Meakin C, Young PA (2009) Turbulent convection in stellar interiors. II. The velocity field. Astrophys J 690:1715–1729. https://doi.org/10.1088/0004-637X/690/2/1715. arXiv:0809.1625

Arnould M, Goriely S (2003) The p-process of stellar nucleosynthesis: astrophysics and nuclear physics status. Phys Rep 384:1–84. https://doi.org/10.1016/S0370-1573(03)00242-4

Aschenbach B (1998) Discovery of a young nearby supernova remnant. Nature 396:141–142. https://doi.org/10.1038/24103

Aschenbach B, Iyudin AF, Schönfelder V (1999) Constraints of age, distance and progenitor of the supernova remnant RX J0852.0-4622/GRO J0852-4642. Astron Astrophys 350:997–1006. arXiv:astro-ph/9909415

Aufderheide MB, Fushiki I, Woosley SE, Hartmann DH (1994) Search for important weak interaction nuclei in presupernova evolution. Astrophys J Suppl 91:389–417. https://doi.org/10.1086/191942

Balasi KG, Langanke K, Martínez-Pinedo G (2015) Neutrino-nucleus reactions and their role for supernova dynamics and nucleosynthesis. Prog Part Nucl Phys 85:33–81. https://doi.org/10.1016/j.ppnp.2015.08.001. arXiv:1503.08095

Bao ZY, Beer H, Käppeler F, Voss F, Wisshak K, Rauscher T (2000) Neutron cross sections for nucleosynthesis studies. At Data Nucl Data Tables 76:70–154. https://doi.org/10.1006/adnd.2000.0838

Barnes J, Kasen D, Wu MR, Martínez-Pinedo G (2016) Radioactivity and thermalization in the ejecta of compact object mergers and their impact on kilonova light curves. Astrophys J 829:110. https://doi.org/10.3847/0004-637X/829/2/110. arXiv:1605.07218

Bauswein A, Goriely S, Janka HT (2013) Systematics of dynamical mass ejection, nucleosynthesis, and radioactively powered electromagnetic signals from neutron-star mergers. Astrophys J 773:78. https://doi.org/10.1088/0004-637X/773/1/78. arXiv:1302.6530

Benz W, Thielemann F (1990) Convective instabilities in SN 1987A. Astrophys J 348:L17–L20. https://doi.org/10.1086/185620

Bernardini MG (2015) Gamma-ray bursts and magnetars: observational signatures and predictions. J High Energy Astrophys 7:64–72. https://doi.org/10.1016/j.jheap.2015.05.003

Bethe HA (1990) Supernova mechanisms. Rev Mod Phys 62:801–866. https://doi.org/10.1103/RevModPhys.62.801

Bethe HA, Brown GE, Applegate J, Lattimer JM (1979) Equation of state in the gravitational collapse of stars. Nucl Phys A 324:487–533. https://doi.org/10.1016/0375-9474(79)90596-7

Blondin JM, Mezzacappa A, DeMarino C (2003) Stability of standing accretion shocks, with an eye toward core-collapse supernovae. Astrophys J 584:971–980. https://doi.org/10.1086/345812. arXiv:astro-ph/0210634

Boggs SE, Harrison FA, Miyasaka H, Grefenstette BW, Zoglauer A, Fryer CL, Reynolds SP, Alexander DM, An H, Barret D, Christensen FE, Craig WW, Forster K, Giommi P, Hailey CJ, Hornstrup A, Kitaguchi T, Koglin JE, Madsen KK, Mao PH, Mori K, Perri M, Pivovaroff MJ, Puccetti S, Rana V, Stern D, Westergaard NJ, Zhang WW (2015) ^{44}Ti gamma-ray emission lines from SN1987A reveal an asymmetric explosion. Science 348:670–671. https://doi.org/10.1126/science.aaa2259

Borkowski KJ, Reynolds SP, Green DA, Hwang U, Petre R, Krishnamurthy K, Willett R (2010) Radioactive scandium in the youngest galactic supernova remnant G1.9+0.3. Astrophys J 724:L161–L165. https://doi.org/10.1088/2041-8205/724/2/L161. arXiv:1006.3552

Borkowski KJ, Reynolds SP, Hwang U, Green DA, Petre R, Krishnamurthy K, Willett R (2013) Supernova ejecta in the youngest galactic supernova remnant G1.9+0.3. Astrophys J 771:L9. https://doi.org/10.1088/2041-8205/771/1/L9. arXiv:1305.7399

Branch D, Wheeler JC (2017) Supernova explosions. https://doi.org/10.1007/978-3-662-55054-0

Branch D, Benetti S, Kasen D, Baron E, Jeffery DJ, Hatano K, Stathakis RA, Filippenko AV, Matheson T, Pastorello A, Altavilla G, Cappellaro E, Rizzi L, Turatto M, Li W, Leonard DC, Shields JC (2002) Direct analysis of spectra of type Ib supernovae. Astrophys J 566:1005–1017. https://doi.org/10.1086/338127. arXiv:astro-ph/0106367

Bruenn SW, Haxton WC (1991) Neutrino-nucleus interactions in core-collapse supernovae. Astrophys J 376:678–700. https://doi.org/10.1086/170316

Bruenn SW, Lentz EJ, Hix WR, Mezzacappa A, Harris JA, Messer OEB, Endeve E, Blondin JM, Chertkow MA, Lingerfelt EJ, Marronetti P, Yakunin KN (2016) The development of explosions in axisymmetric ab initio core-collapse supernova simulations of 12–25 M stars. Astrophys J 818:123. https://doi.org/10.3847/0004-637X/818/2/123. arXiv:1409.5779

Buchmann LR, Barnes CA (2006) Nuclear reactions in stellar helium burning and later hydrostatic burning stages. Nucl Phys A 777:254–290. https://doi.org/10.1016/j.nuclphysa.2005.01.005

Buras R, Rampp M, Janka H, Kifonidis K (2003) Improved models of stellar core collapse and still no explosions: what is missing? Phys Rev Lett 90(24):241, 101–+. https://doi.org/10.1103/PhysRevLett.90.241101. arXiv:astro-ph/0303171

Burbidge EM, Burbidge GR, Fowler WA, Hoyle F (1957) Synthesis of the elements in stars. Rev Mod Phys 29:547–650. https://doi.org/10.1103/RevModPhys.29.547

Burrows A (2013) Colloquium: perspectives on core-collapse supernova theory. Rev Mod Phys 85:245–261. https://doi.org/10.1103/RevModPhys.85.245. arXiv:1210.4921

Burrows A, Livne E, Dessart L, Ott CD, Murphy J (2006a) A new mechanism for core-collapse supernova explosions. Astrophys J 640:878–890. https://doi.org/10.1086/500174. arXiv:astro-ph/0510687

Burrows A, Reddy S, Thompson TA (2006b) Neutrino opacities in nuclear matter. Nucl Phys A 777:356–394. https://doi.org/10.1016/j.nuclphysa.2004.06.012. arXiv:astro-ph/0404432

Burrows A, Vartanyan D, Dolence JC, Skinner MA, Radice D (2018) Crucial physical dependencies of the core-collapse supernova mechanism. Space Sci Rev 214:33. https://doi.org/10.1007/s11214-017-0450-9

Cameron AGW (2003) Some nucleosynthesis effects associated with r-process jets. Astrophys J 587:327–340. https://doi.org/10.1086/368110

Cayrel R, Hill V, Beers TC, Barbuy B, Spite M, Spite F, Plez B, Andersen J, Bonifacio P, François P, Molaro P, Nordström B, Primas F (2001) Measurement of stellar age from uranium decay. Nature 409:691–692. https://doi.org/10.1038/35055507. arXiv:astro-ph/0104357

Chandrasekhar S (1957) An introduction to the study of stellar structure

Chiappini C, Hirschi R, Meynet G, Ekström S, Maeder A, Matteucci F (2006) A strong case for fast stellar rotation at very low metallicities. Astron Astrophys 449:L27–L30. https://doi.org/10.1051/0004-6361:20064866. arXiv:astro-ph/0602459

Chieffi A, Limongi M (2004) Explosive yields of massive stars from Z = 0 to Z = Z_{solar}. Astrophys J 608:405–410. https://doi.org/10.1086/392523. arXiv:astro-ph/0402625

Chieffi A, Limongi M (2013) Pre-supernova evolution of rotating solar metallicity stars in the mass range 13-120 M$_{Ł}$ and their explosive yields. Astrophys J 764:21. https://doi.org/10.1088/0004-637X/764/1/21

Chieffi A, Limongi M (2017) The synthesis of ^{44}Ti and ^{56}Ni in massive stars. Astrophys J 836:79. https://doi.org/10.3847/1538-4357/836/1/79. arXiv:1701.02914

Clayton DD (1968) Principles of stellar evolution and nucleosynthesis. McGraw-Hill, New York, 1968

Clayton DD, Nittler LR (2004) Astrophysics with presolar stardust. Annu Rev Astron Astrophys 42:39–78. https://doi.org/10.1146/annurev.astro.42.053102.134022

Costantini H, Formicola A, Imbriani G, Junker M, Rolfs C, Strieder F (2009) LUNA: a laboratory for underground nuclear astrophysics. Rep Prog Phys 72(8):086,301–+. https://doi.org/10.1088/0034-4885/72/8/086301. arXiv:0906.1097

Cowan JJ, Thielemann F, Truran JW (1991) The R-process and nucleochronology. Phys Rep 208:267–394. https://doi.org/10.1016/0370-1573(91)90070-3

Cowan JJ, Pfeiffer B, Kratz K, Thielemann F, Sneden C, Burles S, Tytler D, Beers TC (1999) R-process abundances and chronometers in metal-poor stars. Astrophys J 521:194–205. https://doi.org/10.1086/307512. arXiv:astro-ph/9808272

Cristini A, Hirschi R, Georgy C, Meakin C, Arnett D, Viallet M (2015) Linking 1D stellar evolution to 3D hydrodynamic simulations. In: Meynet G, Georgy C, Groh J, Stee P (eds) New windows on massive stars. IAU symposium, vol 307, pp 98–99. https://doi.org/10.1017/S1743921314006371. arXiv:1410.7672

Curtis S, Ebinger K, Fröhlich C, Hempel M, Perego A, Liebendörfer M, Thielemann F-K (2018) PUSHing core-collapse supernovae to explosions in spherical symmetry III: nucleosynthesis yields. arXiv:1805.00498

Cyburt RH, Amthor AM, Ferguson R, Meisel Z, Smith K, Warren S, Heger A, Hoffman RD, Rauscher T, Sakharuk A, Schatz H, Thielemann FK, Wiescher M (2010) The JINA REACLIB database: its recent updates and impact on type-I X-ray bursts. Astrophys J Suppl 189:240–252. https://doi.org/10.1088/0067-0049/189/1/240

De Marco O, Izzard RG (2017) Dawes review 6: the impact of companions on stellar evolution. Publ Astron Soc Aust 34:e001. https://doi.org/10.1017/pasa.2016.52. arXiv:1611.03542

deBoer RJ, Görres J, Wiescher M, Azuma RE, Best A, Brune CR, Fields CE, Jones S, Pignatari M, Sayre D, Smith K, Timmes FX, Uberseder E (2017) The ^{12}C(α,γ)^{16}O reaction and its implications for stellar helium burning. Rev Mod Phys 89(3):035007. https://doi.org/10.1103/RevModPhys.89.035007. arXiv:1709.03144

Dessart L, Hillier DJ, Woosley S, Livne E, Waldman R, Yoon SC, Langer N (2015) Radiative-transfer models for supernovae IIb/Ib/Ic from binary-star progenitors. Mon Not R Astron Soc 453:2189–2213. https://doi.org/10.1093/mnras/stv1747. arXiv:1507.07783

Dessart L, John Hillier D, Yoon SC, Waldman R, Livne E (2017) Radiative-transfer models for explosions from rotating and non-rotating single WC stars. Implications for SN 1998bw and LGRB/SNe. Astron Astrophys 603:A51. https://doi.org/10.1051/0004-6361/201730873. arXiv:1703.08932

Diehl R, Bennett K, Bloemen H, Dupraz C, Hermsen W, Knoedlseder J, Lichti G, Morris D, Oberlack U, Ryan J, Schoenfelder V, Steinle H, Varendorff M, Winkler C (1995) 1.809 MeV gamma-rays from the VELA region. Astron Astrophys 298:L25+

Diehl R, Wessolowski U, Oberlack U, Bloemen H, Georgii R, Iyudin A, Knodlseder J, Lichti G, Hermsen W, Morris D, Ryan J, Schonfelder V, Strong A, von Ballmoos P, Winkler C (1997) 26Al and the COMPTEL 60Fe data. In: Dermer CD, Strickman MS, Kurfess JD (eds) Proceedings of the fourth compton symposium. American institute of physics conference series, vol 410, pp 1109–+. https://doi.org/10.1063/1.54176

Diehl R, Halloin H, Kretschmer K, Lichti GG, Schönfelder V, Strong AW, von Kienlin A, Wang W, Jean P, Knödlseder J, Roques JP, Weidenspointner G, Schanne S, Hartmann DH, Winkler C, Wunderer C (2006a) Radioactive ^{26}Al from massive stars in the galaxy. Nature 439:45–47. https://doi.org/10.1038/nature04364. arXiv:astro-ph/0601015

Diehl R, Prantzos N, von Ballmoos P (2006b) Astrophysical constraints from gamma-ray spectroscopy. Nucl Phys A 777:70–97. https://doi.org/10.1016/j.nuclphysa.2005.02.155. arXiv:astro-ph/0502324

Dillmann I, Heil M, Käppeler F, Plag R, Rauscher T, Thielemann FK (2006) KADoNiS- the Karlsruhe astrophysical database of nucleosynthesis in stars. In: Woehr A, Aprahamian A (eds) Capture gamma-ray spectroscopy and related topics. American institute of physics conference series, vol 819, pp 123–127. https://doi.org/10.1063/1.2187846

Dillmann I, Rauscher T, Heil M, Käppeler F, Rapp W, Thielemann F (2008) p-Process simulations with a modified reaction library. J Phys G Nucl Phys 35(1):014,029–+. https://doi.org/10.1088/0954-3899/35/1/014029. arXiv:0805.4756

Dillmann I, Szücs T, Plag R, Fülöp Z, Käppeler F, Mengoni A, Rauscher T (2014) The Karlsruhe astrophysical database of nucleosynthesis in stars project - status and prospects. Nucl Data Sheets 120:171–174. https://doi.org/10.1016/j.nds.2014.07.038. arXiv:1408.3688

Duan H, Fuller GM, Qian Y (2006) Collective neutrino flavor transformation in supernovae. Phys Rev D 74(12):123,004–+. https://doi.org/10.1103/PhysRevD.74.123004. arXiv:astro-ph/0511275

Duan H, Fuller GM, Carlson J, Qian Y (2007) Neutrino mass hierarchy and stepwise spectral swapping of supernova neutrino flavors. Phys Rev Lett 99(24):241,802–+. https://doi.org/10.1103/PhysRevLett.99.241802. arXiv:0707.0290

Duflo J, Zuker AP (1995) Microscopic mass formulas. Phys Rev C 52:R23–R27. https://doi.org/10.1103/PhysRevC.52.R23. arXiv:nucl-th/9505011

Dufour F, Kaspi VM (2013) Limits on the number of galactic young supernova remnants emitting in the decay lines of ^{44}Ti. Astrophys J 775:52. https://doi.org/10.1088/0004-637X/775/1/52. arXiv:1308.4859

Dupraz C, Bloemen H, Bennett K, Diehl R, Hermsen W, Iyudin AF, Ryan J, Schoenfelder V (1997) COMPTEL three-year search for galactic sources of ˆ44ˆTi gamma-ray line emission at 1.157MeV. Astron Astrophys 324:683–689

Ebinger K, Sinha S, Fröhlich C, Perego A, Hempel M, Eichler M, Casanova J, Liebendörfer M, Thielemann FK (2017) Explosion dynamics of parametrized spherically symmetric core-collapse supernova simulations. In: Kubono S, Kajino T, Nishimura S, Isobe T, Nagataki S, Shima T, Takeda Y (eds) 14th international symposium on nuclei in the cosmos (NIC2016), p 020611. https://doi.org/10.7566/JPSCP.14.020611. arXiv:1610.05629

Ebinger K, Curtis S, Fröhlich C, Hempel M, Perego A, Liebendörfer M, Thielemann F-K (2018) PUSHing core-collapse supernovae to explosions in spherical symmetry II: explodability and global properties. arXiv:1804.03182

Edelmann PVF, Röpke FK, Hirschi R, Georgy C, Jones S (2017) Testing a one-dimensional prescription of dynamical shear mixing with a two-dimensional hydrodynamic simulation. Astron Astrophys 604:A25. https://doi.org/10.1051/0004-6361/201629873. arXiv:1704.06261

Eggenberger P, Meynet G, Maeder A, Hirschi R, Charbonnel C, Talon S, Ekström S (2008) The Geneva stellar evolution code. Astrophys Space Sci 316:43–54. https://doi.org/10.1007/s10509-007-9511-y

Eichler D, Livio M, Piran T, Schramm DN (1989) Nucleosynthesis, neutrino bursts and gamma-rays from coalescing neutron stars. Nature 340:126–128. https://doi.org/10.1038/340126a0

Eichler M, Arcones A, Kelic A, Korobkin O, Langanke K, Marketin T, Martinez-Pinedo G, Panov I, Rauscher T, Rosswog S, Winteler C, Zinner NT, Thielemann FK (2015) The role of fission in neutron star mergers and its impact on the r-process peaks. Astrophys J 808:30. https://doi.org/10.1088/0004-637X/808/1/30. arXiv:1411.0974

Eichler M, Nakamura K, Takiwaki T, Kuroda T, Kotake K, Hempel M, Cabezón R, Liebendörfer M, Thielemann F (2018) Nucleosynthesis in 2D core-collapse supernovae of 11.2 and 17.0 M_⊙ progenitors: implications for Mo and Ru production. J Phys G Nucl Phys 48(1):014001. https://doi.org/10.1088/1361-6471/aa8891. arXiv:1708.08393

Ekström S, Meynet G, Chiappini C, Hirschi R, Maeder A (2008) Effects of rotation on the evolution of primordial stars. Astron Astrophys 489:685–698. https://doi.org/10.1051/0004-6361:200809633. arXiv:0807.0573

Ekström S, Georgy C, Eggenberger P, Meynet G, Mowlavi N, Wyttenbach A, Granada A, Decressin T, Hirschi R, Frischknecht U, Charbonnel C, Maeder A (2012) Grids of stellar models with rotation. I. Models from 0.8 to 120 M_⊙ at solar metallicity (Z = 0.014). Astron Astrophys 537:A146. https://doi.org/10.1051/0004-6361/201117751. arXiv:1110.5049

El Eid MF, The L, Meyer BS (2009) Massive stars: input physics and stellar models. Space Sci Rev 147:1–29. https://doi.org/10.1007/s11214-009-9517-6

Eldridge JJ, Izzard RG, Tout CA (2008) The effect of massive binaries on stellar populations and supernova progenitors. Mon Not R Astron Soc 384:1109–1118. https://doi.org/10.1111/j.1365-2966.2007.12738.x. arXiv:0711.3079

Ertl T, Janka HT, Woosley SE, Sukhbold T, Ugliano M (2016) A Two-parameter criterion for classifying the explodability of massive stars by the neutrino-driven mechanism. Astrophys J 818:124. https://doi.org/10.3847/0004-637X/818/2/124. arXiv:1503.07522

Fabbian D, Nissen PE, Asplund M, Pettini M, Akerman C (2009) The C/O ratio at low metallicity: constraints on early chemical evolution from observations of galactic halo stars. Astron Astrophys 500:1143–1155. https://doi.org/10.1051/0004-6361/200810095. arXiv:0810.0281

Farouqi K, Kratz KL, Pfeiffer B, Rauscher T, Thielemann FK, Truran JW (2010) Charged-particle and neutron-capture processes in the high-entropy wind of core-collapse supernovae. Astrophys J 712:1359–1377. https://doi.org/10.1088/0004-637X/712/2/1359. arXiv:1002.2346

Fischer T, Whitehouse SC, Mezzacappa A, Thielemann F, Liebendörfer M (2009) The neutrino signal from protoneutron star accretion and black hole formation. Astron Astrophys 499:1–15. https://doi.org/10.1051/0004-6361/200811055. arXiv:0809.5129

Fischer T, Whitehouse SC, Mezzacappa A, Thielemann FK, Liebendörfer M (2010) Protoneutron star evolution and the neutrino-driven wind in general relativistic neutrino radiation hydrodynamics simulations. Astron Astrophys 517:A80. https://doi.org/10.1051/0004-6361/200913106. arXiv:0908.1871

Fischer T, Sagert I, Pagliara G, Hempel M, Schaffner-Bielich J, Rauscher T, Thielemann FK, Käppeli R, Martínez-Pinedo G, Liebendörfer M (2011) Core-collapse supernova explosions triggered by a Quark-Hadron phase transition during the early post-bounce phase. Astrophys J Suppl 194:39. https://doi.org/10.1088/0067-0049/194/2/39. arXiv:1011.3409

Fischer T, Huther L, Lohs A, Martínez-Pinedo G (2016) Early protoneutron star deleptonization - consistent modeling of weak processes and equation of state. J Phys Conf Ser 665:012069. https://doi.org/10.1088/1742-6596/665/1/012069

Fisker JL, Schatz H, Thielemann F (2008) Explosive hydrogen burning during type I X-ray bursts. Astrophys J Suppl 174:261–276. https://doi.org/10.1086/521104

Fogli G, Lisi E, Marrone A, Mirizzi A (2007) Collective neutrino flavor transitions in supernovae and the role of trajectory averaging. J Cosmol Astropart Phys 12:10–+. https://doi.org/10.1088/1475-7516/2007/12/010. arXiv:0707.1998

Foglizzo T (2009) A simple toy model of the advective-acoustic instability. I. Perturbative approach. Astrophys J 694:820–832. https://doi.org/10.1088/0004-637X/694/2/820. arXiv:0809.2302

Fransson C, Kozma C (1993) The freeze-out phase of SN 1987A - implications for the light curve. Astrophys J 408:L25–L28. https://doi.org/10.1086/186822

Freiburghaus C, Rembges J, Rauscher T, Kolbe E, Thielemann F, Kratz K, Pfeiffer B, Cowan JJ (1999a) The astrophysical r-process: a comparison of calculations following adiabatic expansion with classical calculations based on neutron densities and temperatures. Astrophys J 516:381–398. https://doi.org/10.1086/307072

Freiburghaus C, Rosswog S, Thielemann FK (1999b) R-process in neutron star mergers. Astrophys J 525:L121–L124. https://doi.org/10.1086/312343

Frischknecht U, Hirschi R, Pignatari M, Maeder A, Meynet G, Chiappini C, Thielemann FK, Rauscher T, Georgy C, Ekström S (2016) s-Process production in rotating massive stars at solar and low metallicities. Mon Not R Astron Soc 456:1803–1825. https://doi.org/10.1093/mnras/stv2723. arXiv:1511.05730

Fröhlich C, Hauser P, Liebendörfer M, Martínez-Pinedo G, Thielemann F, Bravo E, Zinner NT, Hix WR, Langanke K, Mezzacappa A, Nomoto K (2006a) Composition of the innermost core-collapse supernova ejecta. Astrophys J 637:415–426. https://doi.org/10.1086/498224. arXiv:astro-ph/0410208

Fröhlich C, Martínez-Pinedo G, Liebendörfer M, Thielemann F, Bravo E, Hix WR, Langanke K, Zinner NT (2006b) Neutrino-induced nucleosynthesis of a greater 64 nuclei: the νp process. Phys Rev Lett 96(14):142502. https://doi.org/10.1103/PhysRevLett.96.142502. arXiv:astro-ph/0511376

Fryxell B, Olson K, Ricker P, Timmes FX, Zingale M, Lamb DQ, MacNeice P, Rosner R, Truran JW, Tufo H (2000) FLASH: an adaptive mesh hydrodynamics code for modeling astrophysical thermonuclear flashes. Astrophys J Suppl 131:273–334. https://doi.org/10.1086/317361

Fujimoto Si, Hashimoto Ma, Kotake K, Yamada S (2007) Heavy-element nucleosynthesis in a collapsar. Astrophys J 656:382–392. https://doi.org/10.1086/509908. arXiv:astro-ph/0602460

Fujimoto Si, Nishimura N, Hashimoto Ma (2008) Nucleosynthesis in magnetically driven jets from collapsars. Astrophys J 680:1350–1358. https://doi.org/10.1086/529416. arXiv:0804.0969

Fukuda I (1982) A statistical study of rotational velocities of the stars. Publ Astron Soc Pac 94:271–284. https://doi.org/10.1086/130977

Fuller GM, Fowler WA, Newman MJ (1980) Stellar weak-interaction rates for sd-shell nuclei. I - nuclear matrix element systematics with application to Al-26 and selected nuclei of importance to the supernova problem. Astrophys J Suppl 42:447–473. https://doi.org/10.1086/190657

Fuller GM, Fowler WA, Newman MJ (1982) Stellar weak interaction rates for intermediate-mass nuclei. II - A = 21 to A = 60. Astrophys J 252:715–740. https://doi.org/10.1086/159597

Fuller GM, Fowler WA, Newman MJ (1985) Stellar weak interaction rates for intermediate-mass nuclei. IV - interpolation procedures for rapidly varying lepton capture rates using effective log (ft)-values. Astrophys J 293:1–16. https://doi.org/10.1086/163208

Georgy C, Meynet G, Walder R, Folini D, Maeder A (2009) The different progenitors of type Ib, Ic SNe, and of GRB. Astron Astrophys 502:611–622. https://doi.org/10.1051/0004-6361/200811339. arXiv:0906.2284

Georgy C, Ekström S, Meynet G, Massey P, Levesque EM, Hirschi R, Eggenberger P, Maeder A (2012) Grids of stellar models with rotation. II. WR populations and supernovae/GRB progenitors at Z = 0.014. Astron Astrophys 542:A29. https://doi.org/10.1051/0004-6361/201118340. arXiv:1203.5243

Georgy C, Ekström S, Eggenberger P, Meynet G, Haemmerlé L, Maeder A, Granada A, Groh JH, Hirschi R, Mowlavi N, Yusof N, Charbonnel C, Decressin T, Barblan F (2013) Grids of stellar models with rotation. III. Models from 0.8 to 120 $M_\odot$ at a metallicity Z = 0.002. Astron Astrophys 558:A103. https://doi.org/10.1051/0004-6361/201322178. arXiv:1308.2914

Georgy C, Meynet G, Ekström S, Wade GA, Petit V, Keszthelyi Z, Hirschi R (2017) Possible pair-instability supernovae at solar metallicity from magnetic stellar progenitors. Astron Astrophys 599:L5. https://doi.org/10.1051/0004-6361/201730401. arXiv:1702.02340

Giron S, Hammache F, de Séréville N, Beaumel D, Burgunder J, Caceres L, Clement E, Duchene G, Flavigny F, de France G, Franchoo S, Fernandez B, Galaviz-Redondo D, Gasques L, Gibelin J, Gillibert A, Grevy S, Guillot J, Heil M, Kiener J, Lapoux V, Maréchal F, Matta A, Matea Y, Moukaddam M, Nalpas L, Obertelli A, Perrot L, Raabe R, Scarpaci JA, Sorlin O, Stefan I, Stoedel C, Takechi M, Thomas JC, Togano Y (2010) Study of ^{60}Fe(n,γ)^{61}Fe reaction of astrophysical interest via d(^{60}Fe,pγ) indirect reaction. In: Spitaleri C, Rolfs C, Pizzone RG (ed) American institute of physics conference series, vol 1213, pp 201–204. https://doi.org/10.1063/1.3362577

Goldreich P, Weber SV (1980) Homologously collapsing stellar cores. Astrophys J 238:991–997. https://doi.org/10.1086/158065

Goriely S (2015) Towards more accurate and reliable predictions for nuclear applications. Eur Phys J A 51:172. https://doi.org/10.1140/epja/i2015-15172-2

Goriely S, Bauswein A, Janka HT (2011) r-process nucleosynthesis in dynamically ejected matter of neutron star mergers. Astrophys J 738:L32. https://doi.org/10.1088/2041-8205/738/2/L32. arXiv:1107.0899

Goriely S, Bauswein A, Just O, Pllumbi E, Janka HT (2015) Impact of weak interactions of free nucleons on the r-process in dynamical ejecta from neutron star mergers. Mon Not R Astron Soc 452:3894–3904. https://doi.org/10.1093/mnras/stv1526. arXiv:1504.04377

Grebenev SA, Lutovinov AA, Tsygankov S, Winkler C (2012) Hard-X-ray emission lines from the decay of ^{44}ti in the remnant of supernova 1987A. Nature 490:373–375. https://doi.org/10.1038/nature11473. arXiv:1211.2656

Grefenstette BW, Harrison FA, Boggs SE, Reynolds SP, Fryer CL, Madsen KK, Wik DR, Zoglauer A, Ellinger CI, Alexander DM, An H, Barret D, Christensen FE, Craig WW, Forster K, Giommi P, Hailey CJ, Hornstrup A, Kaspi VM, Kitaguchi T, Koglin JE, Mao PH, Miyasaka H, Mori K, Perri M, Pivovaroff MJ, Puccetti S, Rana V, Stern D, Westergaard NJ, Zhang WW (2014) Asymmetries in core-collapse supernovae from maps of radioactive ^{44}Ti in CassiopeiaA. Nature 506:339–342. https://doi.org/10.1038/nature12997. arXiv:1403.4978

Grefenstette BW, Fryer CL, Harrison FA, Boggs SE, DeLaney T, Laming JM, Reynolds SP, Alexander DM, Barret D, Christensen FE, Craig WW, Forster K, Giommi P, Hailey CJ, Hornstrup A, Kitaguchi T, Koglin JE, Lopez L, Mao PH, Madsen KK, Miyasaka H, Mori K, Perri M, Pivovaroff MJ, Puccetti S, Rana V, Stern D, Westergaard NJ, Wik DR, Zhang WW, Zoglauer A (2017) The distribution of radioactive ^{44}Ti in Cassiopeia A. Astrophys J 834:19. https://doi.org/10.3847/1538-4357/834/1/19. arXiv:1612.02774

Greiner J, Mazzali PA, Kann DA, Krühler T, Pian E, Prentice S, Olivares E F, Rossi A, Klose S, Taubenberger S, Knust F, Afonso PMJ, Ashall C, Bolmer J, Delvaux C, Diehl R, Elliott J, Filgas R, Fynbo JPU, Graham JF, Guelbenzu AN, Kobayashi S, Leloudas G, Savaglio S, Schady P, Schmidl S, Schweyer T, Sudilovsky V, Tanga M, Updike AC, van Eerten H, Varela K (2015) A very luminous magnetar-powered supernova associated with an ultra-long γ-ray burst. Nature 523:189–192. https://doi.org/10.1038/nature14579. arXiv:1509.03279

Gyürky G, Kiss GG, Elekes Z, Fülöp Z, Somorjai E, Palumbo A, Görres J, Lee HY, Rapp W, Wiescher M, Özkan N, Güray RT, Efe G, Rauscher T (2006) α-induced cross sections of Cd106 for the astrophysical p process. Phys Rev C 74(2):025,805–+. https://doi.org/10.1103/PhysRevC.74.025805. arXiv:nucl-ex/0605034

Halevi G, Mösta P (2018) r-Process nucleosynthesis from three-dimensional jet-driven core-collapse supernovae with magnetic misalignments. Mon Not R Astron Soc 477:2366–2375. https://doi.org/10.1093/mnras/sty797. arXiv:1801.08943

Hamuy M (2003) Observed and physical properties of core-collapse supernovae. Astrophys J 582:905–914. https://doi.org/10.1086/344689. arXiv:astro-ph/0209174

Harris JA, Hix WR, Chertkow MA, Lee CT, Lentz EJ, Messer OEB (2017) Implications for post-processing nucleosynthesis of core-collapse supernova models with lagrangian particles. Astrophys J 843:2. https://doi.org/10.3847/1538-4357/aa76de. arXiv:1701.08876

Haxton WC, Parker PD, Rolfs CE (2006) Solar hydrogen burning and neutrinos. Nucl Phys A 777:226–253. https://doi.org/10.1016/j.nuclphysa.2005.02.088. arXiv:nucl-th/0501020
Heger A (2018) Private communication
Heger A, Langer N (2000) Presupernova evolution of rotating massive stars. II. Evolution of the surface properties. Astrophys J 544:1016–1035. https://doi.org/10.1086/317239. arXiv:astro-ph/0005110
Heger A, Woosley SE (2002) The nucleosynthetic signature of population III. Astrophys J 567:532–543. https://doi.org/10.1086/338487. arXiv:astro-ph/0107037
Heger A, Woosley SE (2010) Nucleosynthesis and evolution of massive metal-free stars. Astrophys J 724:341–373. https://doi.org/10.1088/0004-637X/724/1/341. arXiv:0803.3161
Heger A, Langer N, Woosley SE (2000) Presupernova evolution of rotating massive stars. I. Numerical method and evolution of the internal stellar structure. Astrophys J 528:368–396. https://doi.org/10.1086/308158. arXiv:astro-ph/9904132
Heger A, Langanke K, Martínez-Pinedo G, Woosley SE (2001a) Presupernova collapse models with improved weak-interaction rates. Phys Rev Lett 86:1678–1681. https://doi.org/10.1103/PhysRevLett.86.1678. arXiv:astro-ph/0007412
Heger A, Woosley SE, Martínez-Pinedo G, Langanke K (2001b) Presupernova evolution with improved rates for weak interactions. Astrophys J 560:307–325. https://doi.org/10.1086/324092. arXiv:astro-ph/0011507
Heger A, Fryer CL, Woosley SE, Langer N, Hartmann DH (2003) How massive single stars end their life. Astrophys J 591:288–300. https://doi.org/10.1086/375341. arXiv:astro-ph/0212469
Heger A, Woosley SE, Spruit HC (2005) Presupernova evolution of differentially rotating massive stars including magnetic fields. Astrophys J 626:350–363. https://doi.org/10.1086/429868. arXiv:astro-ph/0409422
Hempel M, Schaffner-Bielich J (2010) A statistical model for a complete supernova equation of state. Nucl Phys A 837:210–254. https://doi.org/10.1016/j.nuclphysa.2010.02.010. arXiv:0911.4073
Hempel M, Heinimann O, Yudin A, Iosilevskiy I, Liebendörfer M, Thielemann FK (2016) Hot third family of compact stars and the possibility of core-collapse supernova explosions. Phys Rev D 94(10):103001. https://doi.org/10.1103/PhysRevD.94.103001. arXiv:1511.06551
Herant M, Benz W, Hix WR, Fryer CL, Colgate SA (1994) Inside the supernova: a powerful convective engine. Astrophys J 435:339–361. https://doi.org/10.1086/174817. arXiv:astro-ph/9404024
Hirschi R (2007) Very low-metallicity massive stars: pre-SN evolution models and primary nitrogen production. Astron Astrophys 461:571–583. https://doi.org/10.1051/0004-6361:20065356. arXiv:astro-ph/0608170
Hirschi R, Meynet G, Maeder A (2004) Stellar evolution with rotation. XII. Pre-supernova models. Astron Astrophys 425:649–670. https://doi.org/10.1051/0004-6361:20041095. arXiv:astro-ph/0406552
Hirschi R, Meynet G, Maeder A (2005) Stellar evolution with rotation. XIII. Predicted GRB rates at various Z. Astron Astrophys 443:581–591. https://doi.org/10.1051/0004-6361:20053329. arXiv:astro-ph/0507343
Hirschi R, Frischknecht U, Thielemann F, Pignatari M, Chiappini C, Ekström S, Meynet G, Maeder A (2008) Stellar evolution in the early universe. In: Hunt LK, Madden S, Schneider R (ed) IAU symposium, vol 255, pp 297–304. https://doi.org/10.1017/S1743921308024976
Hix WR, Meyer BS (2006) Thermonuclear kinetics in astrophysics. Nucl Phys A 777:188–207. https://doi.org/10.1016/j.nuclphysa.2004.10.009. arXiv:astro-ph/0509698
Hix WR, Thielemann F (1996) Silicon burning. I. Neutronization and the physics of quasi-equilibrium. Astrophys J 460:869–+. https://doi.org/10.1086/177016. arXiv:astro-ph/9511088
Hix WR, Thielemann F (1999a) Computational methods for nucleosynthesis and nuclear energy generation. J Comput Appl Math 109:321–351. arXiv:astro-ph/9906478
Hix WR, Thielemann F (1999b) Silicon burning. II. Quasi-equilibrium and explosive burning. Astrophys J 511:862–875. https://doi.org/10.1086/306692. arXiv:astro-ph/9808203

Hix WR, Messer OE, Mezzacappa A, Liebendörfer M, Sampaio J, Langanke K, Dean DJ, Martínez-Pinedo G (2003) Consequences of nuclear electron capture in core collapse supernovae. Phys Rev Lett 91(20):201,102–+. https://doi.org/10.1103/PhysRevLett.91.201102. arXiv:astro-ph/0310883

Hix WR, Parete-Koon ST, Freiburghaus C, Thielemann F (2007) The QSE-reduced nuclear reaction network for silicon burning. Astrophys J 667:476–488. https://doi.org/10.1086/520672

Hix WR, Lentz EJ, Bruenn SW, Mezzacappa A, Messer OEB, Endeve E, Blondin JM, Harris JA, Marronetti P, Yakunin KN (2016) The multi-dimensional character of core-collapse supernovae. Acta Phys Pol B 47:645. https://doi.org/10.5506/APhysPolB.47.645. arXiv:1602.05553

Hoffman RD, Woosley SE, Qian Y (1997) Nucleosynthesis in neutrino-driven winds. II. Implications for heavy element synthesis. Astrophys J 482:951–+. https://doi.org/10.1086/304181. arXiv:astro-ph/9611097

Hoffman RD, Woosley SE, Weaver TA, Rauscher T, Thielemann FK (1999) The reaction rate sensitivity of nucleosynthesis in type II supernovae. Astrophys J 521:735–752. https://doi.org/10.1086/307568. arXiv:astro-ph/9809240

Honda S, Aoki W, Ishimaru Y, Wanajo S, Ryan SG (2006) Neutron-capture elements in the very metal poor star HD 122563. Astrophys J 643:1180–1189. https://doi.org/10.1086/503195. arXiv:astro-ph/0602107

Hüdepohl L, Müller B, Janka H, Marek A, Raffelt GG (2010) Neutrino signal of electron-capture supernovae from core collapse to cooling. Phys Rev Lett 104(25):251,101–+. https://doi.org/10.1103/PhysRevLett.104.251101. arXiv:0912.0260

Iliadis C (2007) Nuclear physics of stars. Wiley-VCH Verlag, Weinheim. ISBN 978-3-527-40602-9

Iwakami W, Kotake K, Ohnishi N, Yamada S, Sawada K (2008) Three-dimensional simulations of standing accretion shock instability in core-collapse supernovae. Astrophys J 678:1207–1222. https://doi.org/10.1086/533582. arXiv:0710.2191

Iyudin AF, Diehl R, Bloemen H, Hermsen W, Lichti GG, Morris D, Ryan J, Schoenfelder V, Steinle H, Varendorff M, de Vries C, Winkler C (1994) COMPTEL observations of Ti-44 gamma-ray line emission from CAS A. Astron Astrophys 284:L1–L4

Iyudin AF, Schönfelder V, Bennett K, Bloemen H, Diehl R, Hermsen W, Knödlseder J, Lichti GG, Oberlack U, Ryan J, Strong AW, Winkler C (1999) COMPTEL all-sky survey in ^{44}Ti line emission. Astrophys Lett Commun 38:383–+

Janiuk A (2014) Nucleosynthesis of elements in gamma-ray burst engines. Astron Astrophys 568:A105. https://doi.org/10.1051/0004-6361/201423822. arXiv:1406.4440

Janka HT (2012) Explosion mechanisms of core-collapse supernovae. Annu Rev Nucl Part Sci 62:407–451. https://doi.org/10.1146/annurev-nucl-102711-094901. arXiv:1206.2503

Janka HT, Müller B, Kitaura FS, Buras R (2008) Dynamics of shock propagation and nucleosynthesis conditions in O-Ne-Mg core supernovae. Astron Astrophys 485:199–208. https://doi.org/10.1051/0004-6361:20079334. arXiv:0712.4237

Janka HT, Melson T, Summa A (2016) Physics of core-collapse supernovae in three dimensions: a sneak preview. Annu Rev Nucl Part Sci 66:341–375. https://doi.org/10.1146/annurev-nucl-102115-044747. arXiv:1602.05576

Jones S, Hirschi R, Nomoto K, Fischer T, Timmes FX, Herwig F, Paxton B, Toki H, Suzuki T, Martínez-Pinedo G, Lam YH, Bertolli MG (2013) Advanced burning stages and fate of 8-10 $M_\odot$ stars. Astrophys J 772:150. https://doi.org/10.1088/0004-637X/772/2/150. arXiv:1306.2030

Jones S, Hirschi R, Pignatari M, Heger A, Georgy C, Nishimura N, Fryer C, Herwig F (2015) Code dependencies of pre-supernova evolution and nucleosynthesis in massive stars: evolution to the end of core helium burning. Mon Not R Astron Soc 447:3115–3129. https://doi.org/10.1093/mnras/stu2657. arXiv:1412.6518

Jones S, Ritter C, Herwig F, Fryer C, Pignatari M, Bertolli MG, Paxton B (2016) H ingestion into He-burning convection zones in super-AGB stellar models as a potential site for intermediate neutron-density nucleosynthesis. Mon Not R Astron Soc 455:3848–3863. https://doi.org/10.1093/mnras/stv2488. arXiv:1510.07417

Jose J (2016) Stellar explosions: hydrodynamics and nucleosynthesis. CRC Press, Boca Raton. https://doi.org/10.1201/b19165

Juodagalvis A, Langanke K, Hix WR, Martínez-Pinedo G, Sampaio JM (2010) Improved estimate of electron capture rates on nuclei during stellar core collapse. Nucl Phys A 848:454–478. https://doi.org/10.1016/j.nuclphysa.2010.09.012. arXiv:0909.0179

Just O, Bauswein A, Pulpillo RA, Goriely S, Janka HT (2015) Comprehensive nucleosynthesis analysis for ejecta of compact binary mergers. Mon Not R Astron Soc 448:541–567. https://doi.org/10.1093/mnras/stv009. arXiv:1406.2687

Käppeler F, Gallino R, Bisterzo S, Aoki W (2011) The s process: Nuclear physics, stellar models, and observations. Rev Mod Phys 83:157–194. https://doi.org/10.1103/RevModPhys.83.157. arXiv:1012.5218

Karakas AI, Lattanzio JC (2014) The Dawes review 2: nucleosynthesis and stellar yields of low- and intermediate-mass single stars. Publ Astron Soc Aust 31:e030. https://doi.org/10.1017/pasa.2014.21. arXiv:1405.0062

Karlsson T, Bromm V, Bland-Hawthorn J (2013) Pregalactic metal enrichment: the chemical signatures of the first stars. Rev Mod Phys 85:809–848. https://doi.org/10.1103/RevModPhys.85.809. arXiv:1101.4024

Kasen D, Thomas RC, Röpke F, Woosley SE (2008) Multidimensional radiative transfer calculations of the light curves and spectra of type Ia supernovae. J Phys Conf Ser 125:012007. https://doi.org/10.1088/1742-6596/125/1/012007

Kasen D, Woosley SE, Heger A (2011) Pair instability supernovae: light curves, spectra, and shock breakout. Astrophys J 734:102. https://doi.org/10.1088/0004-637X/734/2/102. arXiv:1101.3336

Kasen D, Fernández R, Metzger BD (2015) Kilonova light curves from the disc wind outflows of compact object mergers. Mon Not R Astron Soc 450:1777–1786. https://doi.org/10.1093/mnras/stv721. arXiv:1411.3726

Katsuda S, Tsunemi H, Mori K (2009) Is Vela Jr. a young supernova remnant? Adv Space Res 43:895–899. https://doi.org/10.1016/j.asr.2009.01.004

Kelic A, Ricciardi MV, Schmidt KH (2008) New insight into the fission process from experiments with relativistic heavy-ion beams. In: Kliman J, Itkis MG, Gmuca Š (eds) Dynamical aspects of nuclear fission, pp 203–215. https://doi.org/10.1142/9789812837530_0016

Kerzendorf WE, Sim SA (2014) A spectral synthesis code for rapid modelling of supernovae. Mon Not R Astron Soc 440:387–404. https://doi.org/10.1093/mnras/stu055. arXiv:1401.5469

Kippenhahn R, Weigert A (1994) Stellar structure and evolution. Springer, Berlin

Kiss GG, Gyürky G, Elekes Z, Fülöp Z, Somorjai E, Rauscher T, Wiescher M (2007) Ge70(p,γ)As71 and Ge76(p,n)As76 cross sections for the astrophysical p process: sensitivity of the optical proton potential at low energies. Phys Rev C 76(5):055,807–+. https://doi.org/10.1103/PhysRevC.76.055807. arXiv:0711.1079

Kiss GG, Rauscher T, Gyürky G, Simon A, Fülöp Z, Somorjai E (2008) Coulomb suppression of the stellar enhancement factor. Phys Rev Lett 101(19):191,101–+. https://doi.org/10.1103/PhysRevLett.101.191101. arXiv:0809.2676

Kitaura FS, Janka H, Hillebrandt W (2006) Explosions of O-Ne-Mg cores, the crab supernova, and subluminous type II-P supernovae. Astron Astrophys 450:345–350. https://doi.org/10.1051/0004-6361:20054703. arXiv:astro-ph/0512065

Knie K, Korschinek G, Faestermann T, Dorfi EA, Rugel G, Wallner A (2004) ^{60}Fe anomaly in a deep-sea manganese crust and implications for a nearby supernova source. Phys Rev Lett 93(17):171,103–+. https://doi.org/10.1103/PhysRevLett.93.171103

Kobayashi C, Nakasato N (2011) Chemodynamical simulations of the milky way galaxy. Astrophys J 729:16. https://doi.org/10.1088/0004-637X/729/1/16. arXiv:1012.5144

Kobayashi C, Umeda H, Nomoto K, Tominaga N, Ohkubo T (2006) Galactic chemical evolution: carbon through zinc. Astrophys J 653:1145–1171. https://doi.org/10.1086/508914. arXiv:astro-ph/0608688

Kolbe E, Langanke K, Martínez-Pinedo G, Vogel P (2003) Neutrino nucleus reactions and nuclear structure. J Phys G Nucl Phys 29:2569–2596. https://doi.org/10.1088/0954-3899/29/11/010. arXiv:nucl-th/0311022

Korobkin O, Rosswog S, Arcones A, Winteler C (2012) On the astrophysical robustness of the neutron star merger r-process. Mon Not R Astron Soc 426:1940–1949. https://doi.org/10.1111/j.1365-2966.2012.21859.x. arXiv:1206.2379

Kotake K, Sato K, Takahashi K (2006) Explosion mechanism, neutrino burst and gravitational wave in core-collapse supernovae. Rep Prog Phys 69:971–1143. https://doi.org/10.1088/0034-4885/69/4/R03. arXiv:astro-ph/0509456

Kratz K, Bitouzet J, Thielemann F, Moeller P, Pfeiffer B (1993) Isotopic r-process abundances and nuclear structure far from stability - implications for the r-process mechanism. Astrophys J 403:216–238. https://doi.org/10.1086/172196

Kratz K, Farouqi K, Pfeiffer B, Truran JW, Sneden C, Cowan JJ (2007) Explorations of the r-processes: comparisons between calculations and observations of low-metallicity stars. Astrophys J 662:39–52. https://doi.org/10.1086/517495. arXiv:astro-ph/0703091

Kratz KL, Farouqi K, Möller P (2014) A high-entropy-wind r-process study based on nuclear-structure quantities from the new finite-range droplet model FRDM(2012). Astrophys J 792:6. https://doi.org/10.1088/0004-637X/792/1/6. arXiv:1406.2529

Kurfess JD, Johnson WN, Kinzer RL, Kroeger RA, Strickman MS, Grove JE, Leising MD, Clayton DD, Grabelsky DA, Purcell WR, Ulmer MP, Cameron RA, Jung GV (1992) Oriented scintillation spectrometer experiment observations of Co-57 in SN 1987A. Astrophys J 399:L137–L140. https://doi.org/10.1086/186626

Kuroda T, Kotake K, Takiwaki T, Thielemann FK (2018) A full general relativistic neutrino radiation-hydrodynamics simulation of a collapsing very massive star and the formation of a black hole. ArXiv e-prints 1801.01293

Langanke K, Martínez-Pinedo G (2000) Shell-model calculations of stellar weak interaction rates: II. Weak rates for nuclei in the mass range/A=45-65 in supernovae environments. Nucl Phys A 673:481–508. https://doi.org/10.1016/S0375-9474(00)00131-7. arXiv:nucl-th/0001018

Langanke K, Martínez-Pinedo G (2001) Rate tables for the weak processes of pf-SHELL nuclei in stellar environments. At Data Nucl Data Tables 79:1–46. https://doi.org/10.1006/adnd.2001.0865

Langanke K, Martínez-Pinedo G (2003) Nuclear weak-interaction processes in stars. Rev Mod Phys 75:819–862. https://doi.org/10.1103/RevModPhys.75.819. arXiv:nucl-th/0203071

Langanke K, Martínez-Pinedo G, Sampaio JM, Dean DJ, Hix WR, Messer OE, Mezzacappa A, Liebendörfer M, Janka H, Rampp M (2003) Electron capture rates on nuclei and implications for stellar core collapse. Phys Rev Lett 90(24):241,102–+. https://doi.org/10.1103/PhysRevLett.90.241102. arXiv:astro-ph/0302459

Langanke K, Martínez-Pinedo G, Müller B, Janka H, Marek A, Hix WR, Juodagalvis A, Sampaio JM (2008) Effects of inelastic neutrino-nucleus scattering on supernova dynamics and radiated neutrino spectra. Phys Rev Lett 100(1):011,101–+. https://doi.org/10.1103/PhysRevLett.100.011101. arXiv:0706.1687

Langer N (2012) Presupernova evolution of massive single and binary stars. Annu Rev Astron Astrophys 50:107–164. https://doi.org/10.1146/annurev-astro-081811-125534. arXiv:1206.5443

Langer N, Braun H, Fliegner J (1995) The production of circumstellar ^{26}Al by massive stars. Astrophys Space Sci 224:275–278. https://doi.org/10.1007/BF00667858

Lattimer JM, Douglas Swesty F (1991) A generalized equation of state for hot, dense matter. Nucl Phys A 535:331–376. https://doi.org/10.1016/0375-9474(91)90452-C

Lattimer JM, Schramm DN (1974) Black-hole-neutron-star collisions. Astrophys J 192:L145–L147. https://doi.org/10.1086/181612

Lattimer JM, Schramm DN (1976) The tidal disruption of neutron stars by black holes in close binaries. Astrophys J 210:549–567. https://doi.org/10.1086/154860

Leibundgut B, Suntzeff NB (2003) Optical light curves of supernovae. In: Weiler K (ed) Supernovae and gamma-ray bursters. Lecture notes in physics, vol 598. Springer, Berlin, pp 77–90

Leising MD, Share GH (1990) The gamma-ray light curves of SN 1987A. Astrophys J 357:638–648. https://doi.org/10.1086/168952

Lentz EJ, Bruenn SW, Hix WR, Mezzacappa A, Messer OEB, Endeve E, Blondin JM, Harris JA, Marronetti P, Yakunin KN (2015) Three-dimensional core-collapse supernova simulated using a 15 $M_\odot$ Progenitor. Astrophys J 807:L31. https://doi.org/10.1088/2041-8205/807/2/L31. arXiv:1505.05110

Liebendörfer M (2005) A simple parameterization of the consequences of deleptonization for simulations of stellar core collapse. Astrophys J 633:1042–1051. https://doi.org/10.1086/466517. arXiv:astro-ph/0504072

Liebendörfer M, Mezzacappa A, Thielemann FK (2001) Conservative general relativistic radiation hydrodynamics in spherical symmetry and comoving coordinates. Phys Rev D 63(10):104,003–+. https://doi.org/10.1103/PhysRevD.63.104003. arXiv:astro-ph/0012201

Liebendörfer M, Mezzacappa A, Messer OEB, Martinez-Pinedo G, Hix WR, Thielemann F (2003) The neutrino signal in stellar core collapse and postbounce evolution. Nucl Phys A 719:144–+. https://doi.org/10.1016/S0375-9474(03)00984-9. arXiv:astro-ph/0211329

Liebendörfer M, Messer OEB, Mezzacappa A, Bruenn SW, Cardall CY, Thielemann F (2004) A finite difference representation of neutrino radiation hydrodynamics in spherically symmetric general relativistic spacetime. Astrophys J Suppl 150:263–316. https://doi.org/10.1086/380191. arXiv:astro-ph/0207036

Liebendörfer M, Rampp M, Janka H, Mezzacappa A (2005) Supernova simulations with Boltzmann neutrino transport: a comparison of methods. Astrophys J 620:840–860. https://doi.org/10.1086/427203. arXiv:astro-ph/0310662

Liebendörfer M, Fischer T, Fröhlich C, Thielemann F, Whitehouse S (2008) Nuclear physics with spherically symmetric supernova models. J Phys G Nucl Phys 35(1):014,056–+. https://doi.org/10.1088/0954-3899/35/1/014056. arXiv:0708.4296

Liebendörfer M, Whitehouse SC, Fischer T (2009) The isotropic diffusion source approximation for supernova neutrino transport. Astrophys J 698:1174–1190. https://doi.org/10.1088/0004-637X/698/2/1174. arXiv:0711.2929

Liebendörfer M, Fischer T, Hempel M, Käppeli R, Pagliara G, Perego A, Sagert I, Schaffner-Bielich J, Scheidegger S, Thielemann F, Whitehouse SC (2010) Neutrino radiation-hydrodynamics: general relativistic versus multidimensional supernova simulations. Prog Theor Phys Suppl 186:87–92. https://doi.org/10.1143/PTPS.186.87

Limongi M, Chieffi A (2003) Evolution, explosion, and nucleosynthesis of core-collapse supernovae. Astrophys J 592:404–433. https://doi.org/10.1086/375703. arXiv:astro-ph/0304185

Limongi M, Chieffi A (2006a) Nucleosynthesis of ^{60}Fe in massive stars. New Astron Rev 50:474–476. https://doi.org/10.1016/j.newar.2006.06.005. arXiv:astro-ph/0512598

Limongi M, Chieffi A (2006b) The nucleosynthesis of ^{26}Al and ^{60}Fe in solar metallicity stars extending in mass from 11 to 120 $M_\odot$: the hydrostatic and explosive contributions. Astrophys J 647:483–500. https://doi.org/10.1086/505164. arXiv:astro-ph/0604297

Limongi M, Chieffi A (2009) Presupernova evolution and explosion of massive stars: the role of mass loss during the Wolf-Rayet stage. Mem Soc Astron Ital 80:151

Limongi M, Chieffi A (2012) Presupernova evolution and explosive nucleosynthesis of zero metal massive stars. Astrophys J Suppl 199:38. https://doi.org/10.1088/0067-0049/199/2/38. arXiv:1202.4581

Limongi M, Straniero O, Chieffi A (2000) Massive stars in the range 13-25 M_{solar}: evolution and nucleosynthesis. II. The solar metallicity models. Astrophys J Suppl 129:625–664. https://doi.org/10.1086/313424. arXiv:astro-ph/0003401

Lippuner J, Roberts LF (2017) SkyNet: A modular nuclear reaction network library. Astrophys J Suppl 233:18. https://doi.org/10.3847/1538-4365/aa94cb. arXiv:1706.06198

Liu N, Nittler LR, Pignatari M, O'D Alexander CM, Wang J (2017) Stellar origin of ^{15}N-rich presolar SiC grains of type AB: supernovae with explosive hydrogen burning. Astrophys J 842:L1. https://doi.org/10.3847/2041-8213/aa74e5. arXiv:1705.08222

Lodders K, Palme H (2009) Solar system elemental abundances in 2009. Meteor Planet Sci Suppl 72:5154

Lundqvist P, Kozma C, Sollerman J, Fransson C (2001) ISO/SWS observations of SN 1987A. II. A refined upper limit on the mass of ^{44}Ti in the ejecta of SN 1987A. Astron Astrophys 374:629–637. https://doi.org/10.1051/0004-6361:20010725. arXiv:astro-ph/0105402

MacFadyen AI, Woosley SE (1999) Collapsars: gamma-ray bursts and explosions in "Failed supernovae". Astrophys J 524:262–289. https://doi.org/10.1086/307790. arXiv:astro-ph/9810274

MacFadyen AI, Woosley SE, Heger A (2001) Supernovae, jets, and collapsars. Astrophys J 550:410–425. https://doi.org/10.1086/319698. arXiv:astro-ph/9910034

Maeder A (2009) Physics, formation and evolution of rotating stars. Springer, Berlin. https://doi.org/10.1007/978-3-540-76949-1

Maeder A, Meynet G (2012) Rotating massive stars: from first stars to gamma ray bursts. Rev Mod Phys 84:25–63. https://doi.org/10.1103/RevModPhys.84.25

Maeder A, Grebel EK, Mermilliod J (1999) Differences in the fractions of Be stars in galaxies. Astron Astrophys 346:459–464. arXiv:astro-ph/9904008

Maeder A, Przybilla N, Nieva MF, Georgy C, Meynet G, Ekström S, Eggenberger P (2014) Evolution of surface CNO abundances in massive stars. Astron Astrophys 565:A39. https://doi.org/10.1051/0004-6361/201220602. arXiv:1404.1020

Magkotsios G, Timmes FX, Hungerford AL, Fryer CL, Young PA, Wiescher M (2010) Trends in ^{44}Ti and ^{56}Ni from core-collapse supernovae. Astrophys J Suppl 191:66–95. https://doi.org/10.1088/0067-0049/191/1/66. arXiv:1009.3175

Marek A, Janka H (2009) Delayed neutrino-driven supernova explosions aided by the standing accretion-shock instability. Astrophys J 694:664–696. https://doi.org/10.1088/0004-637X/694/1/664. arXiv:0708.3372

Marek A, Janka H, Buras R, Liebendörfer M, Rampp M (2005) On ion-ion correlation effects during stellar core collapse. Astron Astrophys 443:201–210. https://doi.org/10.1051/0004-6361:20053236. arXiv:astro-ph/0504291

Marketin T, Huther L, Martínez-Pinedo G (2016) Large-scale evaluation of β -decay rates of r -process nuclei with the inclusion of first-forbidden transitions. Phys Rev C 93(2):025805. https://doi.org/10.1103/PhysRevC.93.025805. arXiv:1507.07442

Martayan C, Frémat Y, Hubert A, Floquet M, Zorec J, Neiner C (2007) Effects of metallicity, star-formation conditions, and evolution in B and Be stars. II. Small magellanic cloud, field of NGC330. Astron Astrophys 462:683–694. https://doi.org/10.1051/0004-6361:20065076. arXiv:astro-ph/0609677

Martin D, Perego A, Arcones A, Thielemann FK, Korobkin O, Rosswog S (2015) Neutrino-driven winds in the aftermath of a neutron star merger: nucleosynthesis and electromagnetic transients. Astrophys J 813:2. https://doi.org/10.1088/0004-637X/813/1/2. arXiv:1506.05048

Martin D, Perego A, Kastaun W, Arcones A (2017) The role of weak interactions in dynamic ejecta from binary neutron star mergers. ArXiv e-prints 1710.04900

Martínez-Pinedo G, Liebendörfer M, Frekers D (2006) Nuclear input for core-collapse models. Nucl Phys A 777:395–423. https://doi.org/10.1016/j.nuclphysa.2006.02.014. arXiv:astro-ph/0412091

Martínez-Pinedo G, Fischer T, Lohs A, Huther L (2012) Charged-Current weak interaction processes in hot and dense matter and its impact on the spectra of neutrinos emitted from protoneutron star cooling. Phys Rev Lett 109(25):251104. https://doi.org/10.1103/PhysRevLett.109.251104. arXiv:1205.2793

Martins F, Palacios A (2013) A comparison of evolutionary tracks for single galactic massive stars. Astron Astrophys 560:A16. https://doi.org/10.1051/0004-6361/201322480. arXiv:1310.7218

Mashonkina L, Christlieb N, Eriksson K (2014) The hamburg/ESO R-process enhanced star survey (HERES). X. HE 2252-4225, one more r-process enhanced and actinide-boost halo star. Astron Astrophys 569:A43. https://doi.org/10.1051/0004-6361/201424017. arXiv:1407.5379

Massi F, de Luca M, Elia D, Giannini T, Lorenzetti D, Nisini B (2007) Star formation in the Vela molecular ridge. Large scale mapping of cloud D in the mm continuum. Astron Astrophys 466:1013–1023. https://doi.org/10.1051/0004-6361:20066438. arXiv:astro-ph/0702687

Matheson T, Filippenko AV, Li W, Leonard DC, Shields JC (2001) Optical spectroscopy of type IB/C supernovae. Astron J 121:1648–1675. https://doi.org/10.1086/319390. arXiv:astro-ph/0101119

Matz SM, Share GH, Leising MD, Chupp EL, Vestrand WT (1988) Gamma-ray line emission from SN1987A. Nature 331:416–418. https://doi.org/10.1038/331416a0

McCray R, Fransson C (2016) The remnant of supernova 1987A. Annu Rev Astron Astrophys 54:19–52. https://doi.org/10.1146/annurev-astro-082615-105405

McKinney JC, Tchekhovskoy A, Blandford RD (2013) Alignment of magnetized accretion disks and relativistic jets with spinning black holes. Science 339:49. https://doi.org/10.1126/science.1230811. arXiv:1211.3651

Meakin CA, Arnett D (2007) Turbulent convection in stellar interiors. I. Hydrodynamic simulation. Astrophys J 667:448–475. https://doi.org/10.1086/520318. arXiv:astro-ph/0611315

Melson T, Janka HT, Bollig R, Hanke F, Marek A, Müller B (2015) Neutrino-driven explosion of a 20 solar-mass star in three dimensions enabled by strange-quark contributions to neutrino-nucleon scattering. Astrophys J 808:L42. https://doi.org/10.1088/2041-8205/808/2/L42. arXiv:1504.07631

Mendoza-Temis JdJ, Wu MR, Langanke K, Martínez-Pinedo G, Bauswein A, Janka HT (2015) Nuclear robustness of the r process in neutron-star mergers. Phys Rev C 92(5):055805. https://doi.org/10.1103/PhysRevC.92.055805

Metzger BD (2017a) Kilonovae. Living Rev Relat 20:3. https://doi.org/10.1007/s41114-017-0006-z. arXiv:1610.09381

Metzger BD (2017b) Welcome to the multi-messenger era! lessons from a neutron star merger and the landscape ahead. arXiv:1710.05931

Metzger BD, Martínez-Pinedo G, Darbha S, Quataert E, Arcones A, Kasen D, Thomas R, Nugent P, Panov IV, Zinner NT (2010) Electromagnetic counterparts of compact object mergers powered by the radioactive decay of r-process nuclei. Mon Not R Astron Soc 406:2650–2662. https://doi.org/10.1111/j.1365-2966.2010.16864.x. arXiv:1001.5029

Meyer BS, Mathews GJ, Howard WM, Woosley SE, Hoffman RD (1992) R-process nucleosynthesis in the high-entropy supernova bubble. Astrophys J 399:656–664. https://doi.org/10.1086/171957

Meynet G, Maeder A (2000) Stellar evolution with rotation. V. Changes in all the outputs of massive star models. Astron Astrophys 361:101–120. arXiv:astro-ph/0006404

Meynet G, Maeder A (2005) Stellar evolution with rotation. XI. Wolf-Rayet star populations at different metallicities. Astron Astrophys 429:581–598. https://doi.org/10.1051/0004-6361:20047106. arXiv:astro-ph/0408319

Meynet G, Maeder A (2017) Supernovae from rotating stars. ArXiv e-prints 1711.07740

Meynet G, Arnould M, Prantzos N, Paulus G (1997) Contribution of Wolf-Rayet stars to the synthesis of ^{26}Al. I. The γ-ray connection. Astron Astrophys 320:460–468

Meynet G, Ekström S, Maeder A (2006) The early star generations: the dominant effect of rotation on the CNO yields. Astron Astrophys 447:623–639. https://doi.org/10.1051/0004-6361:20053070. arXiv:astro-ph/0510560

Meynet G, Ekström S, Georgy C, Maeder A, Hirschi R (2008) Massive star evolution: from the early to the present day universe. In: Deng L, Chan KL (ed) IAU symposium, vol 252, pp 317–327. https://doi.org/10.1017/S1743921308023119

Meynet G, Maeder A, Eggenberger P, Ekstrom S, Georgy C, Chiappini C, Privitera G, Choplin A (2016) Impact of rotation on stellar models. Astron Nachr 337:827. https://doi.org/10.1002/asna.201612380. arXiv:1512.00767

Mikheyev SP, Smirnov AY (1985) Resonance enhancement of oscillations in matter and solar neutrino spectroscopy. Yad Fiz Sov J Nucl Phys 42:1441–1448, 913

Mirizzi A, Mangano G, Saviano N (2015) Self-induced flavor instabilities of a dense neutrino stream in a two-dimensional model. Phys Rev D 92(2):021702. https://doi.org/10.1103/PhysRevD.92.021702. arXiv:1503.03485

Mirizzi A, Tamborra I, Janka HT, Saviano N, Scholberg K, Bollig R, Hüdepohl L, Chakraborty S (2016) Supernova neutrinos: production, oscillations and detection. Nuovo Cimento Rivista Serie 39:1–112. https://doi.org/10.1393/ncr/i2016-10120-8. arXiv:1508.00785

Mishenina T, Pignatari M, Côté B, Thielemann FK, Soubiran C, Basak N, Gorbaneva T, Korotin SA, Kovtyukh VV, Wehmeyer B, Bisterzo S, Travaglio C, Gibson BK, Jordan C, Paul A, Ritter C, Herwig F, NuGrid Collaboration (2017) Observing the metal-poor solar neighbourhood: a comparison of galactic chemical evolution predictions. Mon Not R Astron Soc 469:4378–4399. https://doi.org/10.1093/mnras/stx1145. arXiv:1705.03642

Mochizuki Y, Takahashi K, Janka HT, Hillebrandt W, Diehl R (1999) 44Ti: its effective decay rate in young supernova remnants, and its abundance in Cassiopeia A. Astron Astrophys 346:831–842. arXiv:astro-ph/9904378

Moe M, Di Stefano R (2017) Mind your Ps and Qs: the interrelation between period (P) and mass-ratio (Q) distributions of binary stars. Astrophys J Suppl 230:15. https://doi.org/10.3847/1538-4365/aa6fb6. arXiv:1606.05347

Möller P, Pfeiffer B, Kratz KL (2003) New calculations of gross β-decay properties for astrophysical applications: speeding-up the classical r process. Phys Rev C 67(5):055802. https://doi.org/10.1103/PhysRevC.67.055802

Möller P, Myers WD, Sagawa H, Yoshida S (2012) New finite-range droplet mass model and equation-of-state parameters. Phys Rev Lett 108(5):052501. https://doi.org/10.1103/PhysRevLett.108.052501

Möller P, Sierk AJ, Ichikawa T, Sagawa H (2016) Nuclear ground-state masses and deformations: FRDM(2012). At Data Nucl Data Tables 109:1–204. https://doi.org/10.1016/j.adt.2015.10.002. arXiv:1508.06294

Moriya TJ, Tominaga N, Langer N, Nomoto K, Blinnikov SI, Sorokina EI (2014) Electron-capture supernovae exploding within their progenitor wind. Astron Astrophys 569:A57. https://doi.org/10.1051/0004-6361/201424264. arXiv:1407.4563

Mösta P, Richers S, Ott CD, Haas R, Piro AL, Boydstun K, Abdikamalov E, Reisswig C, Schnetter E (2014) Magnetorotational core-collapse supernovae in three dimensions. Astrophys J 785:L29. https://doi.org/10.1088/2041-8205/785/2/L29. arXiv:1403.1230

Mösta P, Ott CD, Radice D, Roberts LF, Schnetter E, Haas R (2015) A large-scale dynamo and magnetoturbulence in rapidly rotating core-collapse supernovae. Nature 528:376–379. https://doi.org/10.1038/nature15755. arXiv:1512.00838

Mösta P, Roberts LF, Halevi G, Ott CD, Lippuner J, Haas R, Schnetter E (2017) R-process nucleosynthesis from three-dimensional magnetorotational core-collapse supernovae. ArXiv e-prints 1712.09370

Müller B, Heger A, Liptai D, Cameron JB (2016a) A simple approach to the supernova progenitor-explosion connection. Mon Not R Astron Soc 460:742–764. https://doi.org/10.1093/mnras/stw1083. arXiv:1602.05956

Müller B, Viallet M, Heger A, Janka HT (2016b) The last minutes of oxygen shell burning in a massive star. Astrophys J 833:124. https://doi.org/10.3847/1538-4357/833/1/124. arXiv:1605.01393

Müller B, Wanajo S, Janka HT, Heger A, Gay D, Sim SA (2017) Simulations of electron capture and low-mass iron core supernovae. ArXiv e-prints 1710.02641

Nagataki S (2000) Effects of jetlike explosion in SN 1987A. Astrophys J Suppl 127:141–157. https://doi.org/10.1086/313317. arXiv:astro-ph/9907109

Nagataki S (2011) Grb-Sn connection:. central engine of long GRBs and explosive nucleosynthesis. Int J Mod Phys D 20:1975–1978. https://doi.org/10.1142/S0218271811020032

Nagataki S, Hashimoto MA, Sato K, Yamada S, Mochizuki YS (1998) The high ratio of 44Ti/56Ni in Cassiopeia A and the axisymmetric collapse-driven supernova explosion. Astrophys J 492:L45+. https://doi.org/10.1086/311089. arXiv:astro-ph/9807015

Nagataki S, Takahashi R, Mizuta A, Takiwaki T (2007) Numerical study of gamma-ray burst jet formation in collapsars. Astrophys J 659:512–529. https://doi.org/10.1086/512057. arXiv:astro-ph/0608233

Nakamura K, Takiwaki T, Kuroda T, Kotake K (2015) Systematic features of axisymmetric neutrino-driven core-collapse supernova models in multiple progenitors. Publ Astron Soc Jpn 67:107. https://doi.org/10.1093/pasj/psv073. arXiv:1406.2415

Nakamura T, Umeda H, Nomoto K, Thielemann F, Burrows A (1999) Nucleosynthesis in type II supernovae and the abundances in metal-poor stars. Astrophys J 517:193–208. https://doi.org/10.1086/307167. arXiv:astro-ph/9809307

Nakamura T, Umeda H, Iwamoto K, Nomoto K, Hashimoto M, Hix WR, Thielemann F (2001) Explosive nucleosynthesis in hypernovae. Astrophys J 555:880–899. https://doi.org/10.1086/321495. arXiv:astro-ph/0011184

Nakar E, Piran T (2017) The observable signatures of GRB cocoons. Astrophys J 834:28. https://doi.org/10.3847/1538-4357/834/1/28. arXiv:1610.05362

Nishimura N, Takiwaki T, Thielemann FK (2015) The r-process nucleosynthesis in the various jet-like explosions of magnetorotational core-collapse supernovae. Astrophys J 810:109. https://doi.org/10.1088/0004-637X/810/2/109. arXiv:1501.06567

Nishimura N, Hirschi R, Rauscher T, St J Murphy A, Cescutti G (2017a) Uncertainties in s-process nucleosynthesis in massive stars determined by Monte Carlo variations. Mon Not R Astron Soc 469:1752–1767. https://doi.org/10.1093/mnras/stx696. arXiv:1701.00489

Nishimura N, Sawai H, Takiwaki T, Yamada S, Thielemann FK (2017b) The Intermediate r-process in core-collapse supernovae driven by the magneto-rotational instability. Astrophys J 836:L21. https://doi.org/10.3847/2041-8213/aa5dee. arXiv:1611.02280

Nomoto K (1987) Evolution of 8-10 solar mass stars toward electron capture supernovae. II - collapse of an O + NE + MG core. Astrophys J 322:206–214. https://doi.org/10.1086/165716

Nomoto K (2017) Nucleosynthesis in hypernovae associated with gamma ray bursts. In: Alsabti AW, Murdin P (eds) Handbook of supernovae. Springer, Berlin. https://doi.org/10.1007/978-3-319-20794-0_86-1

Nomoto K, Hashimoto M (1988) Presupernova evolution of massive stars. Phys Rep 163:13–36. https://doi.org/10.1016/0370-1573(88)90032-4

Nomoto K, Thielemann F, Miyaji S (1985) The triple alpha reaction at low temperatures in accreting white dwarfs and neutron stars. Astron Astrophys 149:239–245

Nomoto K, Mazzali PA, Nakamura T, Iwamoto K, Danziger IJ, Patat F (2001) The properties of hypernovae: SNe Ic 1998bw, 1997ef, and SN IIn 1997cy. In: Livio M, Panagia N, Sahu (eds) Supernovae and gamma-ray bursts: the greatest explosions since the big bang, pp 144–170

Nomoto K, Tominaga N, Umeda H, Kobayashi C, Maeda K (2006) Nucleosynthesis yields of core-collapse supernovae and hypernovae, and galactic chemical evolution. Nucl Phys A 777:424–458. https://doi.org/10.1016/j.nuclphysa.2006.05.008. arXiv:astro-ph/0605725

Nomoto K, Tanaka M, Tominaga N, Maeda K (2010) Hypernovae, gamma-ray bursts, and first stars. New A Rev 54:191–200. https://doi.org/10.1016/j.newar.2010.09.022

Nomoto K, Kobayashi C, Tominaga N (2013) Nucleosynthesis in stars and the chemical enrichment of galaxies. Annu Rev Astron Astrophys 51:457–509. https://doi.org/10.1146/annurev-astro-082812-140956

O'Connor E, Ott CD (2011) Black hole formation in failing core-collapse supernovae. Astrophys J 730:70. https://doi.org/10.1088/0004-637X/730/2/70. arXiv:1010.5550

O'Connor E, Ott CD (2013) The progenitor dependence of the pre-explosion neutrino emission in core-collapse supernovae. Astrophys J 762:126. https://doi.org/10.1088/0004-637X/762/2/126. arXiv:1207.1100

Oda T, Hino M, Muto K, Takahara M, Sato K (1994) Rate tables for the weak processes of sd-shell nuclei in stellar matter. At Data Nucl Data Tables 56:231–403. https://doi.org/10.1006/adnd.1994.1007

Oertel M, Hempel M, Klähn T, Typel S (2017) Equations of state for supernovae and compact stars. Rev Mod Phys 89(1):015007. https://doi.org/10.1103/RevModPhys.89.015007. arXiv:1610.03361

Ohkubo T, Umeda H, Maeda K, Nomoto K, Suzuki T, Tsuruta S, Rees MJ (2008) Evolution of core-collapse very massive population III stars. In: O'Shea BW, Heger A (eds) First stars III. American institute of physics conference series, vol 990, pp 244–246. https://doi.org/10.1063/1.2905553

Ono M, Hashimoto M, Fujimoto S, Kotake K, Yamada S (2012) Explosive nucleosynthesis in magnetohydrodynamical jets from collapsars. II — heavy-element nucleosynthesis of s, p, r-processes. Prog Theor Phys 128:741–765. arXiv:1203.6488

Palacios A, Meynet G, Vuissoz C, Knödlseder J, Schaerer D, Cerviño M, Mowlavi N (2005) New estimates of the contribution of Wolf-Rayet stellar winds to the galactic ^{26}Al. Astron Astrophys 429:613–624. https://doi.org/10.1051/0004-6361:20041757. arXiv:astro-ph/0409580

Pan KC, Liebendörfer M, Hempel M, Thielemann FK (2016) Two-dimensional core-collapse supernova simulations with the isotropic diffusion source approximation for neutrino transport. Astrophys J 817:72. https://doi.org/10.3847/0004-637X/817/1/72. arXiv:1505.02513

Pan KC, Liebendörfer M, Couch SM, Thielemann FK (2017) Equation of state dependent dynamics and multimessenger signals from stellar-mass black hole formation. arXiv:1710.01690

Panov IV, Korneev IY, Thielemann FK (2008) The r-Process in the region of transuranium elements and the contribution of fission products to the nucleosynthesis of nuclei with A $\leq$ 130. Astron Lett 34:189–197. https://doi.org/10.1007/s11443-008-3006-1

Paxton B, Bildsten L, Dotter A, Herwig F, Lesaffre P, Timmes F (2011) Modules for experiments in stellar astrophysics (MESA). Astrophys J Suppl 192:3. https://doi.org/10.1088/0067-0049/192/1/3. arXiv:1009.1622

Perego A, Rosswog S, Cabezón RM, Korobkin O, Käppeli R, Arcones A, Liebendörfer M (2014) Neutrino-driven winds from neutron star merger remnants. Mon Not R Astron Soc 443:3134–3156. https://doi.org/10.1093/mnras/stu1352. arXiv:1405.6730

Perego A, Hempel M, Fröhlich C, Ebinger K, Eichler M, Casanova J, Liebendörfer M, Thielemann FK (2015) PUSHing core-collapse supernovae to explosions in spherical symmetry i: the model and the case of SN 1987A. Astrophys J 806:275. https://doi.org/10.1088/0004-637X/806/2/275. arXiv:1501.02845

Perego A, Cabezón RM, Käppeli R (2016) An advanced leakage scheme for neutrino treatment in astrophysical simulations. Astrophys J Suppl 223:22. https://doi.org/10.3847/0067-0049/223/2/22. arXiv:1511.08519

Pettini M, Zych BJ, Steidel CC, Chaffee FH (2008) C, N, O abundances in the most metal-poor damped Lyman alpha systems. Mon Not R Astron Soc 385:2011–2024. https://doi.org/10.1111/j.1365-2966.2008.12951.x. arXiv:0712.1829

Pignatari M, Gallino R, Meynet G, Hirschi R, Herwig F, Wiescher M (2008) The s-process in massive stars at low metallicity: the effect of primary ^{14}N from fast rotating stars. Astrophys J 687:L95–L98. https://doi.org/10.1086/593350. arXiv:0810.0182

Pignatari M, Herwig F, Hirschi R, Bennett M, Rockefeller G, Fryer C, Timmes FX, Ritter C, Heger A, Jones S, Battino U, Dotter A, Trappitsch R, Diehl S, Frischknecht U, Hungerford A, Magkotsios G, Travaglio C, Young P (2016) NuGrid stellar data set. I.Stellar yields from H to Bi for stars with metallicities Z = 0.02 and Z = 0.01. Astrophys J Suppl 225:24. https://doi.org/10.3847/0067-0049/225/2/24. arXiv:1307.6961

Piran T (2004) The physics of gamma-ray bursts. Rev Mod Phys 76:1143–1210. https://doi.org/10.1103/RevModPhys.76.1143. arXiv:astro-ph/0405503

Pruet J, Woosley SE, Buras R, Janka H, Hoffman RD (2005) Nucleosynthesis in the hot convective bubble in core-collapse supernovae. Astrophys J 623:325–336. https://doi.org/10.1086/428281. arXiv:astro-ph/0409446

Pruet J, Hoffman RD, Woosley SE, Janka H, Buras R (2006) Nucleosynthesis in early supernova winds. II. The role of neutrinos. Astrophys J 644:1028–1039. https://doi.org/10.1086/503891. arXiv:astro-ph/0511194

Qian YZ, Wasserburg GJ (2007) Where, oh where has the r-process gone? Phys Rep 442:237–268. https://doi.org/10.1016/j.physrep.2007.02.006. arXiv:0708.1767

Qian YZ, Woosley SE (1996) Nucleosynthesis in neutrino-driven winds. I. The physical conditions. Astrophys J 471:331–+. https://doi.org/10.1086/177973. arXiv:astro-ph/9611094

Ramirez-Ruiz E, Trenti M, MacLeod M, Roberts LF, Lee WH, Saladino-Rosas MI (2015) Compact stellar binary assembly in the first nuclear star clusters and r-process synthesis in the early universe. Astrophys J 802:L22. https://doi.org/10.1088/2041-8205/802/2/L22. arXiv:1410.3467

Rapp W, Görres J, Wiescher M, Schatz H, Käppeler F (2006) Sensitivity of p-process nucleosynthesis to nuclear reaction rates in a 25 M_{solar} supernova model. Astrophys J 653:474–489. https://doi.org/10.1086/508402. arXiv:astro-ph/0608341

Rauscher T (2006) Branchings in the γ process path revisited. Phys Rev C 73(1):015,804–+. https://doi.org/10.1103/PhysRevC.73.015804. arXiv:astro-ph/0510710

Rauscher T (2013) Solution of the α-potential mystery in the γ process and its impact on the Nd/Sm ratio in meteorites. Phys Rev Lett 111(6):061104. https://doi.org/10.1103/PhysRevLett.111.061104. arXiv:1307.4921

Rauscher T, Heger A, Hoffman RD, Woosley SE (2002) Nucleosynthesis in massive stars with improved nuclear and stellar physics. Astrophys J 576:323–348. https://doi.org/10.1086/341728. arXiv:astro-ph/0112478

Rauscher T, Dauphas N, Dillmann I, Fröhlich C, Fülöp Z, Gyürky G (2013) Constraining the astrophysical origin of the p-nuclei through nuclear physics and meteoritic data. Rep Prog Phys 76(6):066201. https://doi.org/10.1088/0034-4885/76/6/066201. arXiv:1303.2666

Rayet M, Arnould M, Prantzos N (1990) The p-process revisited. Astron Astrophys 227:271–281

Rayet M, Arnould M, Hashimoto M, Prantzos N, Nomoto K (1995) The p-process in type II supernovae. Astron Astrophys 298:517–+

Renaud M, Vink J, Decourchelle A, Lebrun F, Terrier R, Ballet J (2006) An INTEGRAL/IBIS view of young galactic SNRs through the ^{44}Ti gamma-ray lines. New Astron Rev 50:540–543. https://doi.org/10.1016/j.newar.2006.06.061. arXiv:astro-ph/0602304

Roberts LF, Woosley SE, Hoffman RD (2010) Integrated nucleosynthesis in neutrino-driven winds. Astrophys J 722:954–967. https://doi.org/10.1088/0004-637X/722/1/954. arXiv:1004.4916

Roberts LF, Reddy S, Shen G (2012) Medium modification of the charged-current neutrino opacity and its implications. Phys Rev C 86(6):065803. https://doi.org/10.1103/PhysRevC.86.065803. arXiv:1205.4066

Rosswog S, Korobkin O, Arcones A, Thielemann FK, Piran T (2014) The long-term evolution of neutron star merger remnants - I. The impact of r-process nucleosynthesis. Mon Not R Astron Soc 439:744–756. https://doi.org/10.1093/mnras/stt2502. arXiv:1307.2939

Rugel G, Faestermann T, Knie K, Korschinek G, Poutivtsev M, Schumann D, Kivel N, Günther-Leopold I, Weinreich R, Wohlmuther M (2009) New measurement of the Fe60 half-life. Phys Rev Lett 103(7):072,502–+. https://doi.org/10.1103/PhysRevLett.103.072502

Sagert I, Fischer T, Hempel M, Pagliara G, Schaffner-Bielich J, Mezzacappa A, Thielemann F, Liebendörfer M (2009) Signals of the QCD phase transition in core-collapse supernovae. Phys Rev Lett 102(8):081101. https://doi.org/10.1103/PhysRevLett.102.081101. arXiv:0809.4225

Sallaska AL, Iliadis C, Champange AE, Goriely S, Starrfield S, Timmes FX (2013) STARLIB: A next-generation reaction-rate library for nuclear astrophysics. Astrophys J Suppl 207:18. https://doi.org/10.1088/0067-0049/207/1/18. arXiv:1304.7811

Sampaio JM, Langanke K, Martínez-Pinedo G, Kolbe E, Dean DJ (2003) Electron capture rates for core collapse supernovae. Nucl Phys A 718:440–442. https://doi.org/10.1016/S0375-9474(03)00832-7. arXiv:nucl-th/0209057

Sauer DN, Mazzali PA, Deng J, Valenti S, Nomoto K, Filippenko AV (2006) The properties of the 'standard' type Ic supernova 1994I from spectral models. Mon Not R Astron Soc 369:1939–1948. https://doi.org/10.1111/j.1365-2966.2006.10438.x. arXiv:astro-ph/0604293

Sawyer RF (2005) Effects of ion and electron correlations on neutrino scattering in the infall phase of a supernova. Phys Lett B 630:1–6. https://doi.org/10.1016/j.physletb.2005.09.032. arXiv:astro-ph/0505520

Schatz H, Aprahamian A, Goerres J, Wiescher M, Rauscher T, Rembges JF, Thielemann F, Pfeiffer B, Moeller P, Kratz K, Herndl H, Brown BA, Rebel H (1998) rp-Process nucleosynthesis at extreme temperature and density conditions. Phys Rep 294:167–264. https://doi.org/10.1016/S0370-1573(97)00048-3

Schulreich MM, Breitschwerdt D, Feige J, Dettbarn C (2017) Numerical studies on the link between radioisotopic signatures on Earth and the formation of the local bubble. I. ^{60}Fe transport to the solar system by turbulent mixing of ejecta from nearby supernovae into a locally homogeneous interstellar medium. Astron Astrophys 604:A81. https://doi.org/10.1051/0004-6361/201629837. arXiv:1704.08221

Seitenzahl IR, Taubenberger S, Sim SA (2009) Late-time supernova light curves: the effect of internal conversion and Auger electrons. Mon Not R Astron Soc 400:531–535. https://doi.org/10.1111/j.1365-2966.2009.15478.x. arXiv:0908.0247

Seitenzahl I, Timmes F, Magkotsios G (2012) Sn87a late lightcurve analysis. Astrophys J 792(1):7

Sekiguchi Y, Shibata M (2011) Formation of black hole and accretion disk in a massive high-entropy stellar core collapse. Astrophys J 737:6. https://doi.org/10.1088/0004-637X/737/1/6. arXiv:1009.5303

Shibagaki S, Kajino T, Mathews GJ, Chiba S, Nishimura S, Lorusso G (2016) Relative contributions of the weak, main, and fission-recycling r-process. Astrophys J 816:79. https://doi.org/10.3847/0004-637X/816/2/79. arXiv:1505.02257

Siegert T, Diehl R, Krause MGH, Greiner J (2015) Revisiting INTEGRAL/SPI observations of ^{44}Ti from Cassiopeia A. Astron Astrophys 579:A124. https://doi.org/10.1051/0004-6361/201525877. arXiv:1505.05999

Sim SA, Kromer M, Roepke FK, Sorokina EI, Blinnikov SI, Kasen D, Hillebrandt W (2009) Monte Carlo radiative transfer simulations: applications to astrophysical outflows and explosions. ArXiv e-prints 0911.1549

Sinha S, Fröhlich C, Ebinger K, Perego A, Hempel M, Eichler M, Liebendörfer M, Thielemann FK (2017) PUSHing core-collapse supernovae to explosions in spherical symmetry: nucleosynthesis yields. In: Kubono S, Kajino T, Nishimura S, Isobe T, Nagataki S, Shima T, Takeda Y (eds) 14th international symposium on nuclei in the cosmos (NIC2016), p 020608. https://doi.org/10.7566/JPSCP.14.020608. arXiv:1701.05203

Slane P, Hughes JP, Edgar RJ, Plucinsky PP, Miyata E, Tsunemi H, Aschenbach B (2001) RX J0852.0-4622: another nonthermal shell-type supernova remnant (G266.2-1.2). Astrophys J 548:814–819. https://doi.org/10.1086/319033. arXiv:astro-ph/0010510

Sneden C, McWilliam A, Preston GW, Cowan JJ, Burris DL, Armosky BJ (1996) The ultra–metal-poor, neutron-capture–rich giant star CS 22892-052. Astrophys J 467:819. https://doi.org/10.1086/177656

Sneden C, Cowan JJ, Gallino R (2008) Neutron-capture elements in the early galaxy. Annu Rev Astron Astrophys 46:241–288. https://doi.org/10.1146/annurev.astro.46.060407.145207

Sneden C, Cowan JJ, Kobayashi C, Pignatari M, Lawler JE, Den Hartog EA, Wood MP (2016) Iron-group abundances in the metal-poor main-sequence turnoff star HD˜84937. Astrophys J 817:53. https://doi.org/10.3847/0004-637X/817/1/53. arXiv:1511.05985

Sollerman J, Holland ST, Challis P, Fransson C, Garnavich P, Kirshner RP, Kozma C, Leibundgut B, Lundqvist P, Patat F, Filippenko AV, Panagia N, Wheeler JC (2002) Supernova 1998bw - the final phases. Astron Astrophys 386:944–956. https://doi.org/10.1051/0004-6361:20020326. arXiv:astro-ph/0204498

Spite M, Cayrel R, Plez B, Hill V, Spite F, Depagne E, François P, Bonifacio P, Barbuy B, Beers T, Andersen J, Molaro P, Nordström B, Primas F (2005) First stars VI - abundances of C, N, O, Li, and mixing in extremely metal-poor giants. Galactic evolution of the light elements. Astron Astrophys 430:655–668. https://doi.org/10.1051/0004-6361:20041274. arXiv:astro-ph/0409536

Sukhbold T, Ertl T, Woosley SE, Brown JM, Janka HT (2016) Core-collapse supernovae from 9 to 120 solar masses based on neutrino-powered explosions. Astrophys J 821:38. https://doi.org/10.3847/0004-637X/821/1/38. arXiv:1510.04643

Sukhbold T, Woosley S, Heger A (2017) High resolution study of presupernova compactness. arXiv:1710.03243

Sullivan C, O'Connor E, Zegers RGT, Grubb T, Austin SM (2016) The sensitivity of core-collapse supernovae to nuclear electron capture. Astrophys J 816:44. https://doi.org/10.3847/0004-637X/816/1/44. arXiv:1508.07348

Sumiyoshi K, Terasawa M, Mathews GJ, Kajino T, Yamada S, Suzuki H (2001) r-Process in prompt supernova explosions revisited. Astrophys J 562:880–886. https://doi.org/10.1086/323524. arXiv:astro-ph/0106407

Sumiyoshi K, Yamada S, Suzuki H (2007) Dynamics and neutrino signal of black hole formation in nonrotating failed supernovae. I. Equation of state dependence. Astrophys J 667:382–394. https://doi.org/10.1086/520876. arXiv:0706.3762

Suntzeff NB, Bouchet P (1990) The bolometric light curve of SN 1987A. I - Results from ESO and CTIO U to Q0 photometry. Astron J 99:650–663. https://doi.org/10.1086/115358

Surman R, McLaughlin GC, Hix WR (2006) Nucleosynthesis in the outflow from gamma-ray burst accretion disks. Astrophys J 643:1057–1064. https://doi.org/10.1086/501116. arXiv:astro-ph/0509365

Takahashi K, Witti J, Janka H (1994) Nucleosynthesis in neutrino-driven winds from protoneutron stars II. The r-process. Astron Astrophys 286:857–869

Takiwaki T, Kotake K, Suwa Y (2014) A comparison of two- and three-dimensional neutrino-hydrodynamics simulations of core-collapse supernovae. Astrophys J 786:83. https://doi.org/10.1088/0004-637X/786/2/83. arXiv:1308.5755

Tanvir NR, Levan AJ, Fruchter AS, Hjorth J, Hounsell RA, Wiersema K, Tunnicliffe RL (2013) A 'kilonova' associated with the short-duration γ-ray burst GRB 130603B. Nature 500:547–549. https://doi.org/10.1038/nature12505. arXiv:1306.4971

The L, El Eid MF, Meyer BS (2007) s-Process nucleosynthesis in advanced burning phases of massive stars. Astrophys J 655:1058–1078. https://doi.org/10.1086/509753. arXiv:astro-ph/0609788

The LS, Clayton DD, Diehl R, Hartmann DH, Iyudin AF, Leising MD, Meyer BS, Motizuki Y, Schönfelder V (2006) Are ^{44}Ti-producing supernovae exceptional? Astron Astrophys 450:1037–1050. https://doi.org/10.1051/0004-6361:20054626. arXiv:astro-ph/0601039

Thielemann FK, Arnett WD (1985) Hydrostatic nucleosynthesis - part two - core neon to silicon burning and presupernova abundance yields of massive stars. Astrophys J 295:604–+. https://doi.org/10.1086/163403

Thielemann FK, Nomoto K, Yokoi K (1986) Explosive nucleosynthesis in carbon deflagration models of Type I supernovae. Astron Astrophys 158:17–33

Thielemann F, Hashimoto M, Nomoto K (1990) Explosive nucleosynthesis in SN 1987A. II - composition, radioactivities, and the neutron star mass. Astrophys J 349:222–240. https://doi.org/10.1086/168308

Thielemann FK, Nomoto K, Hashimoto MA (1996) Core-collapse supernovae and their ejecta. Astrophys J 460:408–+. https://doi.org/10.1086/176980

Thielemann F, Hauser P, Kolbe E, Martinez-Pinedo G, Panov I, Rauscher T, Kratz K, Pfeiffer B, Rosswog S, Liebendörfer M, Mezzacappa A (2002) Heavy elements and age determinations. Space Sci Rev 100:277–296

Thielemann FK, Eichler M, Panov IV, Pignatrari M, Wehmeyer B (2017a) Making the heaviest elements in a rare class of supernovae. In: Alsabti AW, Murdin P (eds) Handbook of supernovae. Springer, Berlin. https://doi.org/10.1007/978-3-319-20794-0_81-1

Thielemann FK, Eichler M, Panov IV, Wehmeyer B (2017b) Neutron star mergers and nucleosynthesis of heavy elements. Annu Rev Nucl Part Sci 67. https://doi.org/10.1146/annurev-nucl-101916-123246. arXiv:1710.02142

Timmes FX (1999) Integration of nuclear reaction networks for stellar hydrodynamics. Astrophys J Suppl 124:241–263. https://doi.org/10.1086/313257

Tominaga N, Umeda H, Nomoto K (2007) Supernova nucleosynthesis in population III 13-50 M_{solar} stars and abundance patterns of extremely metal-poor stars. Astrophys J 660:516–540. https://doi.org/10.1086/513063

Travaglio C, Gallino R, Arnone E, Cowan J, Jordan F, Sneden C (2004) Galactic evolution of Sr, Y, and Zr: a multiplicity of nucleosynthetic processes. Astrophys J 601:864–884. https://doi.org/10.1086/380507. arXiv:astro-ph/0310189

Tsygankov SS, Krivonos RA, Lutovinov AA, Revnivtsev MG, Churazov EM, Sunyaev RA, Grebenev SA (2016) Galactic survey of ^{44}Ti sources with the IBIS telescope onboard INTEGRAL. Mon Not R Astron Soc 458:3411–3419. https://doi.org/10.1093/mnras/stw549. arXiv:1603.01264

Tueller J, Barthelmy S, Gehrels N, Teegarden BJ, Leventhal M, MacCallum CJ (1990) Observations of gamma-ray line profiles from SN 1987A. Astrophys J 351:L41–L44. https://doi.org/10.1086/185675

Tur C, Heger A, Austin SM (2010) Production of ^{26}Al, ^{44}Ti, and ^{60}Fe in core-collapse supernovae: sensitivity to the rates of the triple alpha and ^{12}C(α, γ)^{16}O reactions. Astrophys J 718:357–367. https://doi.org/10.1088/0004-637X/718/1/357. arXiv:0908.4283

Uberseder E, Reifarth R, Schumann D, Dillmann I, Pardo CD, Görres J, Heil M, Käppeler F, Marganiec J, Neuhausen J, Pignatari M, Voss F, Walter S, Wiescher M (2009) Measurement of the Fe60(n,γ)^{61}Fe cross section at stellar temperatures. Phys Rev Lett 102(15):151,101–+. https://doi.org/10.1103/PhysRevLett.102.151101

Ugliano M, Janka HT, Marek A, Arcones A (2012) Progenitor-explosion connection and remnant birth masses for neutrino-driven supernovae of iron-core progenitors. Astrophys J 757:69. https://doi.org/10.1088/0004-637X/757/1/69. arXiv:1205.3657

Umeda H, Nomoto K (2005) Variations in the abundance pattern of extremely metal-poor stars and nucleosynthesis in population III supernovae. Astrophys J 619:427–445. https://doi.org/10.1086/426097. arXiv:astro-ph/0308029

Umeda H, Nomoto K (2008) How much ^{56}Ni can be produced in core-collapse supernovae? Evolution and explosions of 30-100 M_{solar} stars. Astrophys J 673:1014–1022. https://doi.org/10.1086/524767. arXiv:0707.2598

Vink J (2005) Gamma-ray observations of explosive nucleosynthesis products. Adv Space Res 35:976–986. https://doi.org/10.1016/j.asr.2005.01.097. arXiv:astro-ph/0501645

Vink J, Laming JM, Kaastra JS, Bleeker JAM, Bloemen H, Oberlack U (2001) Detection of the 67.9 and 78.4 keV lines associated with the radioactive decay of ^{44}Ti in Cassiopeia A. Astrophys J 560:L79–L82. https://doi.org/10.1086/324172. arXiv:astro-ph/0107468

Walder R, Burrows A, Ott CD, Livne E, Lichtenstadt I, Jarrah M (2005) Anisotropies in the neutrino fluxes and heating profiles in two-dimensional, time-dependent, multigroup radiation hydrodynamics simulations of rotating core-collapse supernovae. Astrophys J 626:317–332. https://doi.org/10.1086/429816. arXiv:astro-ph/0412187

Wallace RK, Woosley SE (1981) Explosive hydrogen burning. Astrophys J Suppl 45:389–420. https://doi.org/10.1086/190717

Wallner A, Faestermann T, Feige J, Feldstein C, Knie K, Korschinek G, Kutschera W, Ofan A, Paul M, Quinto F, Rugel G, Steier P (2015) Abundance of live ^{244}Pu in deep-sea reservoirs on earth points to rarity of actinide nucleosynthesis. Nat Commun 6:5956. https://doi.org/10.1038/ncomms6956. arXiv:1509.08054

Wanajo S (2006) The rp-process in neutrino-driven winds. Astrophys J 647:1323–1340. https://doi.org/10.1086/505483. arXiv:astro-ph/0602488

Wanajo S, Nomoto K, Janka H, Kitaura FS, Müller B (2009) Nucleosynthesis in electron capture supernovae of asymptotic giant branch stars. Astrophys J 695:208–220. https://doi.org/10.1088/0004-637X/695/1/208. arXiv:0810.3999

Wanajo S, Janka HT, Müller B (2011) Electron-capture supernovae as the origin of elements beyond iron. Astrophys J 726:L15. https://doi.org/10.1088/2041-8205/726/2/L15. arXiv:1009.1000

Wanajo S, Sekiguchi Y, Nishimura N, Kiuchi K, Kyutoku K, Shibata M (2014) Production of all the r-process nuclides in the dynamical ejecta of neutron star mergers. Astrophys J 789:L39. https://doi.org/10.1088/2041-8205/789/2/L39. arXiv:1402.7317

Wang W, Harris MJ, Diehl R, Halloin H, Cordier B, Strong AW, Kretschmer K, Knödlseder J, Jean P, Lichti GG, Roques JP, Schanne S, von Kienlin A, Weidenspointner G, Wunderer C (2007) SPI observations of the diffuse ^{60}Fe emission in the galaxy. Astron Astrophys 469:1005–1012. https://doi.org/10.1051/0004-6361:20066982. arXiv:0704.3895

Wang W, Lang MG, Diehl R, Halloin H, Jean P, Knödlseder J, Kretschmer K, Martin P, Roques JP, Strong AW, Winkler C, Zhang XL (2009) Spectral and intensity variations of Galactic ^{26}Al emission. Astron Astrophys 496:713–724. https://doi.org/10.1051/0004-6361/200811175. arXiv:0902.0211

Weaver TA, Woosley SE (1980) Evolution and explosion of massive stars. In: Ehlers J, Perry JJ, Walker M (ed) Ninth texas symposium on relativistic astrophysics. N Y Acad Sci Ann, 336:335–357. https://doi.org/10.1111/j.1749-6632.1980.tb15942.x

Weber C, Elomaa V, Ferrer R, Fröhlich C, Ackermann D, Äystö J, Audi G, Batist L, Blaum K, Block M, Chaudhuri A, Dworschak M, Eliseev S, Eronen T, Hager U, Hakala J, Herfurth F, Heßberger FP, Hofmann S, Jokinen A, Kankainen A, Kluge H, Langanke K, Martín A, Martínez-Pinedo G, Mazzocco M, Moore ID, Neumayr JB, Novikov YN, Penttilä H, Plaß WR, Popov AV, Rahaman S, Rauscher T, Rauth C, Rissanen J, Rodríguez D, Saastamoinen A, Scheidenberger C, Schweikhard L, Seliverstov DM, Sonoda T, Thielemann F, Thirolf PG, Vorobjev GK (2008) Mass measurements in the vicinity of the rp-process and the νp-process paths with the penning trap facilities JYFLTRAP and SHIPTRAP. Phys Rev C 78(5):054,310–+. https://doi.org/10.1103/PhysRevC.78.054310. arXiv:0808.4065

Wehmeyer B, Pignatari M, Thielemann FK (2015) Galactic evolution of rapid neutron capture process abundances: the inhomogeneous approach. Mon Not R Astron Soc 452:1970–1981. https://doi.org/10.1093/mnras/stv1352. arXiv:1501.07749

West C, Heger A (2018, in preparation)

Wiescher M, Görres J, Pignatari M (2010) Experimental status of reactions in H- and He-burning. Annu Rev Nucl Part Sci 60:175–251. https://doi.org/10.1146/annurev.nucl.60.1.175

Wiescher M, Käppeler F, Langanke K (2012) Critical reactions in contemporary nuclear astrophysics. Annu Rev Astron Astrophys 50:165–210. https://doi.org/10.1146/annurev-astro-081811-125543

Wilson JR, Mayle RW (1993) Report on the progress of supernova research by the Livermore group. Phys Rep 227:97–111. https://doi.org/10.1016/0370-1573(93)90059-M

Winteler C, Käppeli R, Perego A, Arcones A, Vasset N, Nishimura N, Liebendörfer M, Thielemann FK (2012) Magnetorotationally driven supernovae as the origin of early galaxy r-process elements? Astrophys J 750:L22. https://doi.org/10.1088/2041-8205/750/1/L22. arXiv:1203.0616

Wolfenstein L (1978) Neutrino oscillations in matter. Phys Rev D 17:2369–2374. https://doi.org/10.1103/PhysRevD.17.2369

Wongwathanarat A, Müller E, Janka HT (2015) Three-dimensional simulations of core-collapse supernovae: from shock revival to shock breakout. Astron Astrophys 577:A48. https://doi.org/10.1051/0004-6361/201425025. arXiv:1409.5431

Wongwathanarat A, Janka HT, Müller E, Pllumbi E, Wanajo S (2017) Production and distribution of ^{44}Ti and ^{56}Ni in a three-dimensional supernova model resembling Cassiopeia A. Astrophys J 842:13. https://doi.org/10.3847/1538-4357/aa72de. arXiv:1610.05643

Woosley SE, Bloom JS (2006) The supernova gamma-ray burst connection. Annu Rev Astron Astrophys 44:507–556. https://doi.org/10.1146/annurev.astro.43.072103.150558. arXiv:astro-ph/0609142

Woosley SE, Heger A (2007) Nucleosynthesis and remnants in massive stars of solar metallicity. Phys Rep 442:269–283. https://doi.org/10.1016/j.physrep.2007.02.009. arXiv:astro-ph/0702176

Woosley SE, Heger A (2015a) The deaths of very massive stars. In: Vink JS (ed) Very massive stars in the local universe. Astrophysics and space science library, vol 412, p 199. https://doi.org/10.1007/978-3-319-09596-7_7. arXiv:1406.5657

Woosley SE, Heger A (2015b) The remarkable deaths of 9-11 solar mass stars. Astrophys J 810:34. https://doi.org/10.1088/0004-637X/810/1/34. arXiv:1505.06712

Woosley SE, Hoffman RD (1992) The alpha-process and the r-process. Astrophys J 395:202–239. https://doi.org/10.1086/171644

Woosley SE, Howard WM (1978) The p-process in supernovae. Astrophys J Suppl 36:285–304. https://doi.org/10.1086/190501

Woosley SE, Weaver TA (1994) Sub-Chandrasekhar mass models for type IA supernovae. Astrophys J 423:371–379. https://doi.org/10.1086/173813

Woosley SE, Weaver TA (1995) The evolution and explosion of massive stars. II. Explosive hydrodynamics and nucleosynthesis. Astrophys J Suppl 101:181–+. https://doi.org/10.1086/192237

Woosley SE, Arnett WD, Clayton DD (1973) The explosive burning of oxygen and silicon. Astrophys J Suppl 26:231–+. https://doi.org/10.1086/190282

Woosley SE, Wilson JR, Mathews GJ, Hoffman RD, Meyer BS (1994) The r-process and neutrino-heated supernova ejecta. Astrophys J 433:229–246. https://doi.org/10.1086/174638

Woosley SE, Heger A, Weaver TA (2002) The evolution and explosion of massive stars. Rev Mod Phys 74:1015–1071. https://doi.org/10.1103/RevModPhys.74.1015

Woosley SE, Kasen D, Blinnikov S, Sorokina E (2007) Type Ia supernova light curves. Astrophys J 662:487–503. https://doi.org/10.1086/513732. arXiv:astro-ph/0609562

Wu MR, Fischer T, Huther L, Martínez-Pinedo G, Qian YZ (2014) Impact of active-sterile neutrino mixing on supernova explosion and nucleosynthesis. Phys Rev D 89(6):061303. https://doi.org/10.1103/PhysRevD.89.061303. arXiv:1305.2382

Wu MR, Qian YZ, Martínez-Pinedo G, Fischer T, Huther L (2015) Effects of neutrino oscillations on nucleosynthesis and neutrino signals for an 18 $M_?$ supernova model. Phys Rev D 91(6):065016. https://doi.org/10.1103/PhysRevD.91.065016. arXiv:1412.8587

Wu MR, Fernández R, Martínez-Pinedo G, Metzger BD (2016a) Production of the entire range of r-process nuclides by black hole accretion disc outflows from neutron star mergers. Mon Not R Astron Soc 463:2323–2334. https://doi.org/10.1093/mnras/stw2156. arXiv:1607.05290

Wu MR, Martínez-Pinedo G, Qian YZ (2016b) Linking neutrino oscillations to the nucleosynthesis of elements. Eur Phys J Web Conf 109, 06005. https://doi.org/10.1051/epjconf/201610906005. arXiv:1512.03630

Xu Y, Takahashi K, Goriely S, Arnould M, Ohta M, Utsunomiya H (2013) NACRE II: an update of the NACRE compilation of charged-particle-induced thermonuclear reaction rates for nuclei with mass number A<16. Nucl Phys A 918:61–169. https://doi.org/10.1016/j.nuclphysa.2013.09.007. arXiv:1310.7099

Yalçın C, Güray RT, Özkan N, Kutlu S, Gyürky G, Farkas J, Kiss GG, Fülöp Z, Simon A, Somorjai E, Rauscher T (2009) Odd p isotope In113: measurement of α-induced reactions. Phys Rev C 79(6):065,801–+. https://doi.org/10.1103/PhysRevC.79.065801. arXiv:0906.4041

Yamamoto Y, Fujimoto Si, Nagakura H, Yamada S (2013) Post-shock-revival evolution in the neutrino-heating mechanism of core-collapse supernovae. Astrophys J 771:27. https://doi.org/10.1088/0004-637X/771/1/27. arXiv:1209.4824

Yamasaki T, Yamada S (2005) Effects of rotation on the revival of a stalled shock in supernova explosions. Astrophys J 623:1000–1010. https://doi.org/10.1086/428496. arXiv:astro-ph/0412625

Yoon SC (2015) Evolutionary models for type Ib/c supernova progenitors. Publ Astron Soc Aust 32:e015. https://doi.org/10.1017/pasa.2015.16. arXiv:1504.01205

Yoshida T, Suwa Y, Umeda H, Shibata M, Takahashi K (2017) Explosive nucleosynthesis of ultra-stripped Type Ic supernovae: application to light trans-iron elements. Mon Not R Astron Soc 471:4275–4285. https://doi.org/10.1093/mnras/stx1738. arXiv:1707.02685

Yusof N, Hirschi R, Meynet G, Crowther PA, Ekström S, Frischknecht U, Georgy C, Abu Kassim H, Schnurr O (2013) Evolution and fate of very massive stars. Mon Not R Astron Soc 433:1114–1132. https://doi.org/10.1093/mnras/stt794. arXiv:1305.2099